PHYSICAL SCI. LIB.

PHYSICAL SCIENCES LIBRARY
S

VERTICAL DEFORMATION, STRESS ACCUMULATION, AND SECONDARY FAULTING IN THE VICINITY OF THE TRANSVERSE RANGES OF SOUTHERN CALIFORNIA

BULLETIN 203
California Division of Mines and Geology
Sacramento, California 1979

U.C.D. LIBRARY

STATE OF CALIFORNIA
EDMUND G. BROWN JR.
GOVERNOR

THE RESOURCES AGENCY
HUEY D. JOHNSON
SECRETARY FOR RESOURCES

DEPARTMENT OF CONSERVATION
PRISCILLA C. GREW
DIRECTOR

DIVISION OF MINES AND GEOLOGY
JAMES F. DAVIS
STATE GEOLOGIST

VERTICAL DEFORMATION, STRESS ACCUMULATION, AND SECONDARY FAULTING IN THE VICINITY OF THE TRANSVERSE RANGES OF SOUTHERN CALIFORNIA

by

DONALD A. RODGERS
Seismologist

1979

BULLETIN 203

CALIFORNIA DIVISION OF MINES AND GEOLOGY
1416 Ninth Street, Room 1341
Sacramento, California 95814

CONTENTS

ABSTRACT v

ACKNOWLEDGMENTS 1

INTRODUCTION 1

STRUCTURAL CHARACTERISTICS 3
San Andreas Fault 3
San Gabriel Fault 3
Garlock Fault 5
White Wolf Fault 5
Big Pine Fault 5
Santa Ynez Fault 5
Thrust Faults 5

SEISMICITY 6

GEODETIC CHARACTERISTICS 6
Triangulation Surveys 12
Taft–Mojave net 12
San Fernando–Bakersfield arc 12
San Luis Obispo–Avenal arc 12
Geodimeter Surveys 12
Fault–Crossing Survey Figures 12
Creepmeter Data 13
Level Surveys 13

MATHEMATICAL MODEL OF THE SAN ANDREAS FAULT 13
Previous Work 13
Review of Pertinent Features 13
Possible Mathematical Models 14
Details of the Selected Dislocation Model 15
Details of the half–space 15
Details of the boundary 16
Parameters of the Dislocation Model 16

CALCULATED VERTICAL DISPLACEMENT FIELDS 17

CALCULATED STRESS FIELDS 21
Results from Model 1 21
Results from Model 2 25
Discussion and Conclusions 25

SEISMICITY AND SECONDARY FAULTING DETERMINED FROM THE MODELS 39
Seismicity 39
Areas of potential failure 39
Historic seismicity compared to areas of potential failure 39
Secondary Faulting 40
Discussion and Conclusions 40

CONCLUSIONS AND SUGGESTIONS FOR FURTHER WORK 47

REFERENCES CITED 49

APPENDIX A. Strain Transition Zone on the San Andreas Fault Between Parkfield and Taft 53
APPENDIX B. Fault–Crossing Survey Figures 59

ILLUSTRATIONS

Figures

1. Location map 2
2. Selected faults with historic or Quaternary movement 4
3. Epicenters of earthquakes with magnitude 4 and greater 7
4. Historic fault breaks and associated earthquakes 8
5. Historic earthquakes with magnitude 5 and greater, 1850–1971 9
6. Triangulation nets for crustal movement studies 10
7. Geodimeter fault-monitoring program 11
8. Strain energy changes due to earthquakes, 1812–1967 14
9. Dislocation surface and its fit to faults 16
10. Coordinate system and schematic of dislocation surface 16
11. Vertical displacements of the ground surface calculated from model 1 19
12. Vertical displacements of the ground surface calculated from model 2 20
13. Isochromatics at the ground surface calculated from model 1 22
14. Contours of constant values of the sum of the principal stresses at the ground surface calculated from model 1 23
15. Principal stress trajectories at the ground surface calculated from model 1 24
16. Surface traces of the slip-planes calculated from model 1 26
17. Isochromatics at a depth of 10 km calculated from model 1 .. 27
18. Isopachs of the sum of the principal stresses at a depth of 10 km calculated from model 1 28
19. Isochromatics at a depth of 20 km calculated from model 1 .. 29
20. Isopachs of the sum of the principal stresses at a depth of 20 km calculated from model 1 30
21. Isochromatics at the ground surface calculated from model 2 31
22. Isopachs at the ground surface calculated from model 2 32
23. Principal stress trajectories at the ground surface calculated from model 2 33
24. Slip lines at the ground surface calculated from model 2 34
25. Isochromatics at a depth of 10 km calculated from model 2 .. 35
26. Isopachs of the sum of the principal stresses at a depth of 10 km calculated from model 2 36
27. Isochromatics at a depth of 20 km calculated from model 2 .. 37
28. Isopachs at a depth of 20 km calculated from model 2 38
29. Areas of potential failure at the ground surface calculated from model 1 41
30. Areas of potential failure at a depth of 20 km calculated from model 1 42
31. Areas of potential failure at the ground surface calculated from model 2 43
32. Areas of potential failure at a depth of 20 km calculated from model 2 44
33. Potential slip directions at the ground surface calculated from model 1 45
34. Orientation of potential fault planes at the ground surface calculated from model 2 46

A–1. Creepmeters, Geodimeter lines, and small survey figure, Parkfield 55
A–2. Geodimeter lines and data, 1959–1973, Hollister to Parkfield 56
A–3. Geodimeter lines and data, 1959–1973, Parkfield to Maricopa 56
A–4. Geodimeter lines normal to the San Andreas fault, 1971–1973, Parkfield to Maricopa 56
A–5. Fault model and predicted and observed line–length changes 57
A–6. Predicted and observed line–length changes, Parkfield Pentagon 58

B–1. Survey figures at aqueduct–fault crossing sites 60
B–2. Plan of the survey figure at the MAR site 65
B–3. Plan of the survey figure at the STADIUM site 65
B–4. Plan of the survey figure at the CAMP PARKS site 65
B–5. Plan of the survey figure at the UNION site 66
B–6. Plan of the survey figure at the VERAS site 66
B–7. Plan of the survey figure at the OSGOOD site 66
B–8. Plan of the survey figure at the TEM site 67
B–9. Plan of the survey figure at the SANTA site 67
B–10. Plan of the survey figure at the MEADE site 67
B–11. Plan of the survey figure at the RANCH site 68
B–12. Plan of the survey figure at the TEJON site 68
B–13. Plan of the survey figure at the RANCH–TEJON site 69
B–14. Plan of the survey figure at the QUAIL site 69
B–15. Plan of the survey figure at the HUGHES site 69
B–16. Plan of the survey figure at the BARREL site 70
B–17. Plan of the survey figure at the PEAR site 70
B–18. Plan of the survey figure and elevation changes at the DEVIL site 71
B–19. Plan of the survey figure and elevation changes at the RIALTO site 72
B–20. Plan of the survey figure and elevation changes at the COLT site 73
B–21. Geodimeter line–length changes, Palmdale to San Bernardino 74

Tables

1. Parameters of the models 18
A–1. Creepmeter data 53
B–1. Elevation differences relative to RANCH–D 62
B–2. Elevation differences relative to BARREL–B 63
B–2. Elevation differences relative to PEAR–G 63

ABSTRACT

The Transverse Ranges province consists of a set of east–trending mountains and geologic structures that are distinct from the general northwest–southeast grain of the other provinces of California. The Coast Ranges province to the north and the Peninsular Ranges province to the south are characterized by strike–slip movement on reasonably straight faults striking northwest. In the Transverse Ranges, thrust faulting is common. Most of the strike–slip faults are curved and strike approximately east. The persistent northwesterly trend of the San Andreas fault changes to an east trend in the Transverse Ranges forming a bend in the fault.

The proximity of the bend in the San Andreas fault to the Transverse Ranges suggests that there may be a direct relationship between the San Andreas fault and the structures in the Transverse Ranges. In this work, the bend in the San Andreas fault is approximated by a series of straight dislocation surfaces, and the displacement and stress fields produced at an observation point by each segment are summed. Two models with "locked" segments on the San Andreas fault 15 and 30 km deep are studied.

The calculated vertical displacement fields from the two models resemble the general topographic features of the Transverse Ranges, suggesting that the present topography may have been produced by the bend in the San Andreas fault. It is not possible to select between the two models of the San Andreas fault based on the topography alone.

Several conclusions result from the interpretation of the stress fields calculated from the two models.

First, it does appear to be possible to select between the two models based on the calculated stress fields. Model 2, the model with the locked zone 30 km deep, seems to explain the observed fault patterns and strain data better than model 1, the model with the locked zone 15 km deep. If this model is correct, the sliding part of the fault is deeper in the Transverse Ranges than in central California.

Second, the principal compressive stresses calculated from the model have a north–south orientation throughout most of the study area. This agrees with the conclusions drawn by other workers.

Third, the areas of potential failure determined from the model include many of the larger earthquakes in the Transverse Ranges; and the larger events that have not occurred in, or adjacent to, the area of potential failure can be related to movement on faults in the Peninsular Ranges.

Finally, the calculated stress system could explain the pattern of the faults in the Transverse Ranges having Holocene or Quaternary movement. This does not necessarily imply that the bend in the San Andreas fault is responsible for the origin of the Transverse Ranges. It does, however, mean that, given a complex set of faults of many different orientations, the stress system produced by the bend in the San Andreas fault will cause activity mainly on those faults that are favorably oriented to the stress system at the time of observation. For the same time interval, other less favorably oriented faults will show a much lower level of activity, even though these faults may have been much more active at some earlier time.

Vertical Deformation, Stress Accumulation, and Secondary Faulting in the Vicinity of the Transverse Ranges of Southern California[1]

by DONALD A. RODGERS

ACKNOWLEDGMENTS

Michael A. Chinnery helped to clarify many of my initial ideas and provided much encouragement when the work slowed down. William M. Chapple and John T. Alfors reviewed an earlier version of the thesis and provided many valuable criticisms. My wife Da'ad was very patient. I am very grateful to the California Division of Mines and Geology for support in the preparation of the thesis. In particular, Beryl Adrian was very understanding as she typed and retyped and retyped the thesis, and Gloria Tomei assisted with much typing and kept the wolves from Mrs. Adrian.

INTRODUCTION

It is generally accepted among earth scientists that the surface of the earth can be divided into several plates that are moving relative to one another (Morgan, 1968; Le Pichon, 1968; Atwater and Molnar, 1973). Each plate has a source (generally a mid–ocean rise) and a sink (either a trench or a mountain range). The plates can move past one another along transform faults.

Atwater (1970) and Anderson (1970) suggested that many of the geologic features of California could be explained in terms of the interaction between the Pacific and North American plates. They suggested that the San Andreas fault is behaving as a transform fault to accommodate most or all of the movement between the two plates. However, Hill (1971, 1974) has strongly challenged this interpretation.

The transform faults mapped in the ocean floors are generally very linear features (Morgan, 1968; Le Pichon, 1968) while the San Andreas fault trace contains several large bends. The bend in the San Andreas fault near Tejon Pass (figure 1) is of particular interest to California geologists because of its proximity to the Transverse Ranges geomorphic province.

The Transverse Ranges province consists of a distinct set of east–trending mountains and geologic structures that cut across the general northwest–trending grain of the other provinces of California (Bailey and Jahns, 1954, figure 1). The faulting of the Coast Ranges province to the north (Page, 1966) and the Peninsular Ranges province to the south (Jahns, 1954) is primarily characterized by strike–slip movement on reasonably straight faults striking northwest with only minor dip–slip activity. However, in the Transverse Ranges, there is a great deal of thrust–faulting (Bailey and Jahns, 1954; Dibblee, 1968; Crowell, 1968). Most of the strike–slip faults are curved and strike approximately east. The persistent northwesterly trend of the San Andreas fault in northern California changes to an east strike in the Transverse Ranges forming a bend in the fault.

The origin of the structures in the Transverse Ranges is still subject to much debate. There is some indication that the east–trending structures may have developed by late Cretaceous or early Tertiary time (Baird and others, 1974); but the Transverse Ranges trends were clearly developed by Miocene time and the present structures have developed since Miocene time (Jahns, 1973).

Benioff (1955), Jahns (1973), and many others have suggested that the bend in the San Andreas fault might be responsible for the post–Miocene compressive structures of the Transverse Ranges. Intuitively, this is reasonable, for one would expect compressive structures on the concave sides of the bends in the San Andreas fault. Additionally, there seems to be reasonably good evidence that part of the San Andreas fault between Tejon Pass and Cajon Pass is no older than Miocene (Jahns, 1973; Baird and others, 1974; Berry, 1974). Thus, the compressive structures of the Transverse Ranges and the severe bend in the San Andreas seem to be about the same age.

[1]This report represents a part of a dissertation accepted for the requirements of the degree of Doctor of Philosophy in Geological Sciences, Brown University, Providence, Rhode Island.

Figure 1. Location map of study area.

The current tectonic activity of the Transverse Ranges is not clear. There is a history of moderate seismicity (Hileman and others, 1974), and the 1971 San Fernando earthquake serves as a reminder that the province is still active. Most of the east–west trending faults seem to have been active in the last 1 to 2 million years, and some of these faults have clear evidence of Holocene movement (Jennings, 1973).

The proximity of the bend in the San Andreas fault to the Transverse Ranges suggests that there may be a direct relationship between them. In this paper, results from elastic dislocation theory (Chinnery, 1961, 1963) will be used to develop a mathematical model of the San Andreas fault in southern California. The deformation and stress fields calculated from the model will be compared to the topography and the mapped geology to determine any relationships between the San Andreas and the Transverse Ranges area. The boundaries of the study area are larger than those of the Transverse Ranges geomorphic province.

STRUCTURAL CHARACTERISTICS

San Andreas Fault

The San Andreas fault can be traced continuously for 520 miles from Point Arena in northern California to San Gorgonio Pass in southern California (Crowell, 1962, figures 3 and 5). Allen (1957) was unable to trace the fault through San Gorgonio Pass; rather, he shows it dying out before it reaches the Banning fault. He suggests that the San Jacinto fault is now the active trace of the San Andreas fault. However, Dibblee (1968) shows the San Andreas fault branching north of San Gorgonio Pass and continuing southward. If the continuity of the San Andreas fault through the San Gorgonio Pass area is accepted, the fault may be traced nearly 100 miles farther south to the eastern side of the Salton Sea. There, it is lost under alluvium. If present seismicity is accepted as a reasonably good indication of the location of the fault trace, then the broad line of earthquake epicenters running from the Salton Sea south to the Gulf of California (figure 3) suggests that the fault zone continues on into the Gulf (Richter, 1958, figure 28–1).

In northern California, the fault goes out to sea at Point Arena. However, ground breakage occurred at Shelter Cove after the 1906 earthquake, and Curry and Nason (1967) show the fault curving north parallel to the coast up to Shelter Cove rather than continuing northwest to Point Arena to explain both the ground breakage at Shelter Cove and the seismic profiles northwest of Point Arena that show no evidence of the northwest extension. On the basis of earthquake epicenters, magnetic anomalies, and topography, Oakeshott (1966) and Nason (1968) suggest that the fault zone bends at Cape Mendocino to strike nearly east–west along the Mendocino Escarpment. On the basis of very accurate epicenter determinations and first–motion studies, Bolt and others (1968) suggest that the fault divides into two branches near Cape Mendocino. One branch swings west to join the Mendocino Escarpment, and the other branch continues on a northwesterly strike from Cape Mendocino. If the extension of the fault northward as far as the Mendocino Escarpment is accepted, the San Andreas fault is well over 700 miles long, running from Cape Mendocino in the north to the head of the Gulf of California in the south.

North and south of the Transverse Ranges, the strike of the San Andreas fault is very nearly northwest–southeast, but in the Transverse Ranges the strike becomes west of northwest (figure 2). The dip of the fault in the study area is approximately vertical, and the sense of motion is right lateral. The amount of displacement on the fault in the study area appears to be 160–175 miles since the Oligocene (Crowell, 1962). Sag ponds and offset stream channels indicate that the San Andreas fault has been active in the Holocene in the study area. However, recent surveys of small geodetic figures crossing the fault from 1964–1972 show no movement on the San Andreas fault (Appendix B). Allen (1968) suggests that fault activity on this part of the San Andreas fault is evidenced by large infrequent earthquakes rather than by small earthquakes and fault creep.

The level of seismic activity is high along all of the San Andreas fault system from Hollister to the Mexican border, except on the fault segment from the Carrizo Plain to the vicinity of Cajon Pass ("Seismicity" in this report; Bolt and others, 1968; Bolt and Miller, 1971; Allen and others, 1965; Hileman and others, 1973). A microearthquake survey of the San Andreas fault system also supports this picture of the seismic activity (Brune and Allen, 1967). However, there is evidence of historic movement on this segment of the fault. The 1857 Fort Tejon earthquake apparently broke the ground surface from the vicinity of Cholame to somewhere between Cajon Pass and San Gorgonio Pass (Wood, 1955; Allen, 1968). These observations have led to the suggestion that this section of the fault is "locked" and is a likely spot for the next great earthquake in California (Allen, 1968).

San Gabriel Fault

The San Gabriel fault lies to the west of the San Andreas fault in the Transverse Ranges. The northern part of the fault trends approximately northwest, while the southern part of the fault has a more easterly trend. Crowell (1954) has presented evidence of about 20 miles of right–lateral strike–slip displacement since the early Miocene on the San Gabriel fault. There is some evidence (Crowell, 1968) that the southern part of the San Gabriel fault has been active in the Holocene, but there is no evidence of Holocene activity on the northern section. However, Jennings (1973) indicates Quaternary displacement on the northern part of the fault. Jahns (1973) suggests that, in the Miocene, the San Gabriel fault was the main trace of the San Andreas fault system. Jahns' reconstruction indicates that, by the middle Pliocene, the San Andreas bend had formed and the San Gabriel fault

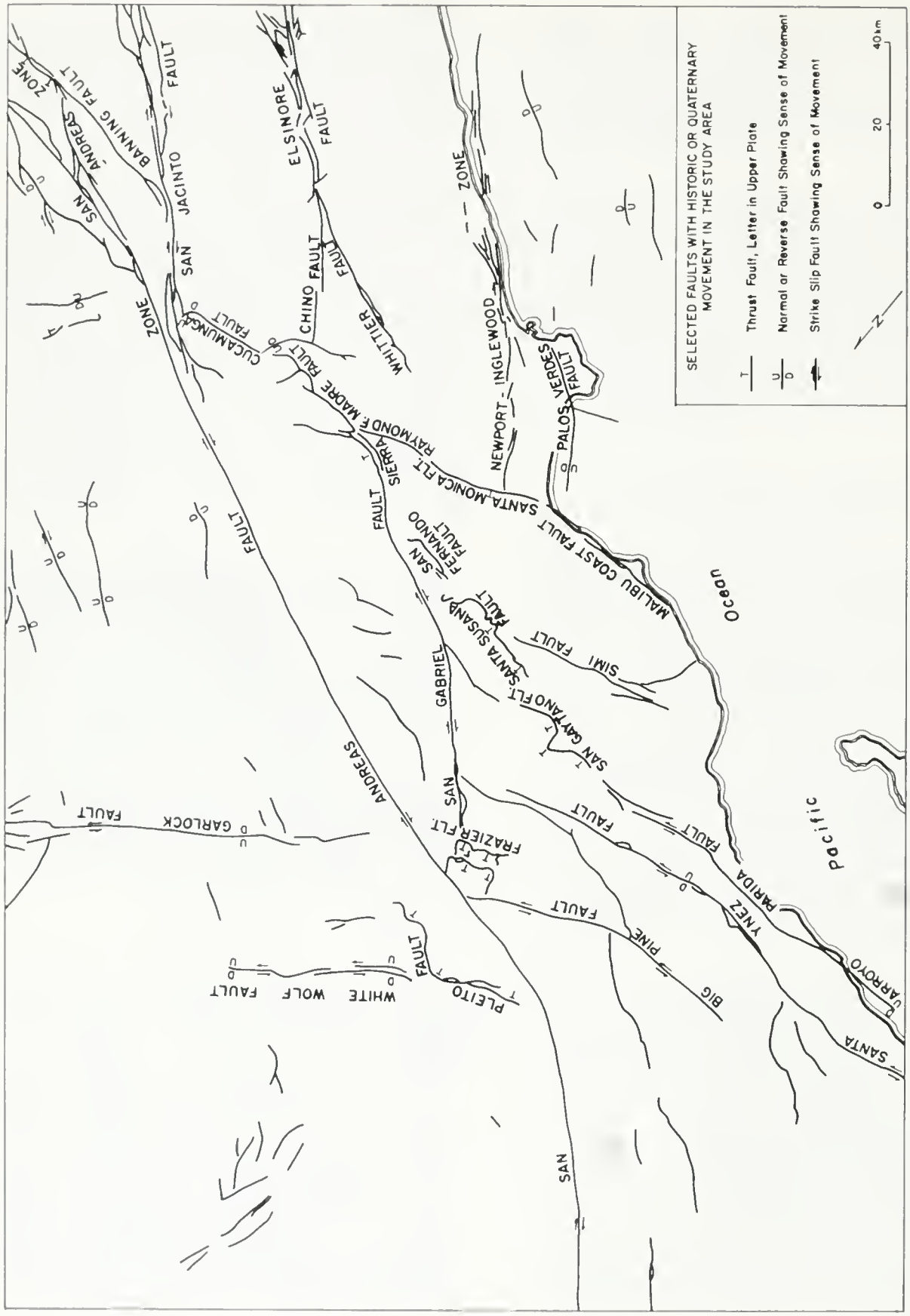

Figure 2. Selected faults with historic or Quaternary movement in the study area (faults modified from Jennings, 1973).

was no longer accounting for a major amount of the motion on the San Andreas system.

The San Andreas and the San Gabriel faults are the major right–lateral strike–slip faults in the Transverse Ranges. Since Jahns' reconstruction suggests that the bend of the San Andreas fault did not form until middle Pliocene time, in this paper I will concern myself only with the geologic history since middle Pliocene time.

Garlock Fault

The Garlock fault is a northeast–striking left–lateral strike–slip fault. The fault is approximately 260 km long, and evidence can be found for 38 to 64 km of left–lateral displacement (Davis and Burchfiel, 1973). There is also some evidence from geodetic data (Greensfelder and Bennett, 1973; Appendix B) and from offset stream channels and deposits that the Garlock fault is currently active. Davis and Burchfiel (1973) presented a summary of what is known about the Garlock fault together with an interesting hypothesis about its origin. They suggest that the Garlock fault may be an intracontinental transform fault rather than a major transcurrent fault, and their arguments are fairly convincing.

White Wolf Fault

The White Wolf fault is a left–lateral strike–slip fault parallel to, and northwest of, the Garlock fault. It is a high–angle reverse fault, dipping to the southeast with the southern block moving up relative to the northern block. The White Wolf fault is active and was the locus of the 1952 Arvin–Tehachapi earthquakes (Oakeshott, 1955).

On July 21, 1952, at 4:52 AM PDT, a 7.7 magnitude earthquake occurred on the White Wolf fault and was accompanied by 17 miles of surface faulting. Mapping of these movements indicated up to 2 feet of left–lateral strike–slip movement and 2 to 3 feet of vertical motion. The instrumental fault plane solution showed that the strike of the fault plane was about north 50° east and the dip was 60° to 66° to the southeast (Gutenberg, 1955). The fault plane solution also indicated that the south side of the fault moved up relative to the north side and that there was left–lateral strike–slip motion; thus, the fault plane solution agreed with observed surface faulting. Triangulation and leveling surveys after the earthquake by the U.S. Coast and Geodetic Survey showed that there was about 2 feet of left–lateral horizontal offset and 3 to 4 feet of vertical offset, with the south side of the fault moving up relative to the north side (Oakeshott, 1955).

Benioff (1955, p. 204) suggested that "...the distortion of that portion of the eastern block of the San Andreas fault moving southward along the curved restraint of the great bend must be principally in the form of a compression oriented approximately north–south. The White Wolf fault is thus a mechanism for relief of this localized stress."

Big Pine Fault

The Big Pine fault strikes approximately east–west and extends for about 50 miles to the west of the San Andreas fault. Its topographic expressions are similar to those of the San Andreas, the Garlock, and other large strike–slip faults. There may be as much as 14 miles of left–lateral offset (Hill, 1955; Carman, 1964); and in the Lockwood Valley area, there is some evidence of dip–slip motion, with the north side of the fault moving up relative to the south side on an approximately vertical fault (Carman, 1964). There is evidence that the Big Pine fault was active as recently as the Pleistocene; but there is no conclusive evidence that it has been active in the Holocene (Carman, 1964), although a large earthquake that occurred in 1852 may have had its epicenter on the Big Pine fault (Townley and Allen, 1939). Geodimeter surveys from about 1962 to the present do not indicate horizontal movement (Hofmann, 1968; California Division of Mines and Geology, unpublished data, 1973).

Santa Ynez Fault

The Santa Ynez fault is an east–west trending fault lying to the west of the San Andreas fault. It has been described in some detail by Dibblee (1950, 1966). The fault dip is vertical along the western section of the fault, approximately 50° to the south along the central section of the fault, and very steeply dipping to the north along the eastern section of the fault. Dibblee (1950, 1966) documented several miles of vertical offset on the Santa Ynez fault, the south side of the fault being elevated relative to the north side, and also found some evidence of horizontal offset, with the offset being in a left–lateral sense. The fault was certainly active in the Pleistocene and possibly in the Holocene (Dibblee, 1966, p. 76). A recent analysis of a first–order level survey suggests that there was no vertical movement on the fault from 1920 to 1971 (Buchanan and others, 1973). Schroeter (1972) presents some evidence that the central part of the Santa Ynez fault system has been active in the Holocene.

Thrust Faults

The study area contains many thrust faults (Hill, 1955, figure 1; Bailey and Jahns, 1954, plate 4; Bailey, 1954; Merrill, 1954; Crowell, 1968).

The Pleito fault, north of the San Andreas fault, seems to have been active in the Holocene (Crowell, 1968). It dips shallowly to the south, and the south side has moved up relative to the north side.

The Frazier Mountain and Pine Mountain thrust faults, south of the San Andreas fault, were active in the Pleistocene (Crowell, 1968); but there does not appear to be any reliable evidence of activity in the Holocene. As can be seen on figure 2, motion on the Frazier and the Pine Mountain faults is to the south.

The San Cayetano, the Oak Ridge, the Santa Susana, and the Sierra Madre faults may have been active in the

Holocene (Jennings, 1973). Again, figure 2 shows that motion on the San Cayetano, the Santa Susana, and the Sierra Madre faults is to the south, while motion on the Oak Ridge fault is to the north.

Finally, the zone of faulting defined by the Santa Monica, the Raymond Hill, and the Sierra Madre faults is characterized by a left-lateral displacement and seems to have been active in the Holocene (Yerkes and others, 1965).

SEISMICITY

The seismicity of southern California has been discussed in detail by Richter (1958) and Allen and others (1965), and Hileman and others (1973) published a catalog of instrumentally located earthquakes in southern California from 1932 to 1972. Figure 3 shows that the San Andreas fault north of the junction with the San Jacinto fault has been relatively inactive, while the San Andreas has been moderately active between the San Jacinto junction and the Salton Sea. The major seismic activity in southern California apparently was associated with the San Jacinto, the Newport–Inglewood, and the White Wolf faults. The small area near the San Gabriel fault is the aftershock zone of the 1971 San Fernando earthquake.

Comparing figures 4 and 5, it is clear that not all large historic events have documented surface faulting. However, there is some evidence of surface faulting associated with the 1852 earthquake on the Big Pine fault (Townley and Allen, 1939; Carman, 1964). There is also some indication of surface breakage associated with either the 1918 or the 1923 earthquakes on the San Jacinto fault (Donald L. Fife, California Division of Mines and Geology, personal communication, 1974).

The 1857 Fort Tejon earthquake on the San Andreas fault was one of the three largest earthquakes in California's recorded history (Wood, 1955), and the length of the fault break is well documented. There is reasonably good evidence that surface breakage extended to the vicinity of San Bernardino (Townley and Allen, 1939; Wood, 1955; California Division of Mines and Geology, unpublished data), and there is tenuous evidence that the faulting extended to the south of San Bernardino (Wood, 1955). The northern end of the fault break was probably in the vicinity of Cholame (Wood, 1955). The descriptions of the surface breaks clearly indicate large right-lateral offset, but the amount of offset was not measured anywhere. However, indirect evidence from offset stream channels in the Carrizo Plain suggests that the offset may have been as much as 10 meters (Wallace, 1968).

Relatively few of the earthquakes on figure 5 are located north of the trend defined by the Malibu–Santa Monica–Raymond–Sierra Madre–Cucamonga faults. This trend is the traditional southern boundary of the Transverse Ranges province, and the faults south of the trend have the same northwest orientation as the San Andreas system. In fact, an argument can be made that faults such as the Newport–Inglewood and the Elsinore are in some way ancestral to the San Andreas fault (Berry, 1973).

The magnitude 7.2 Arvin–Tehachapi earthquake in 1952 was the largest earthquake in the study area since 1857. Its effects are described in "Structural Characteristics". Earthquakes in 1952 and 1953 in the vicinity of the White Wolf and the Pleito faults may have been aftershocks of the 1952 earthquake, but the occurrence of two earthquakes in that area before 1952 suggests that these post–1952 earthquakes might not have been aftershocks.

The earthquake on April 4, 1893, between the San Gabriel and the San Andreas faults could have occurred on a western extension of the fault system that produced the 1971 San Fernando earthquake. Newspaper reports indicate that damage was greater to the west and northwest of San Fernando than in San Fernando (Townley and Allen, 1939). There is also evidence that indicates the weak possibility of surface faulting.

The series of earthquakes at the western end of the Malibu fault plus a magnitude 5.5 earthquake in 1973 (Ellsworth and others, 1973) in the same area suggest that the Malibu fault may be still active.

Historically, the Santa Barbara Channel has been the scene of minor to moderate seismic activity (Hamilton and others, 1969; Sylvester and others, 1970; Lee and Vedder, 1973); figure 3 shows the moderate earthquakes. Sylvester and others (1970) discussed an earthquake swarm that occurred in the Santa Barbara Channel in 1968. Movement on a northwest–striking structure is the preferred solution according to Sylvester and others (1970), although the major structural features of the Santa Barbara Channel strike approximately east–west. In contrast, Lee and Vedder (1973) produced a composite fault plane solution for earthquakes on or near one of the faults in the Channel, and they found left–lateral movement on an east–west plane.

Whitcomb and others (1973) discuss the relationship of the 1971 earthquake to the regional seismicity pattern. They suggest that the San Fernando earthquake may have occurred on a zone they call the Dume–Palmdale zone and that this zone shows up in seismicity trends from 1960 to 1970 (Whitcomb and others, 1973, figure 22). However, study of their epicenter plot (figure 22A) indicates that this zone is only vaguely developed in the data, if at all. Their epicenter plot suggests rather that the Transverse Ranges – Los Angeles Basin area, is an area of diffuse minor seismicity. Maps published by Hileman and others (1973) also support this interpretation.

GEODETIC CHARACTERISTICS

Since the 1906 earthquake in San Francisco, much effort has gone into the study of crustal movement using geodetic techniques. Greensfelder (1972) listed the loca-

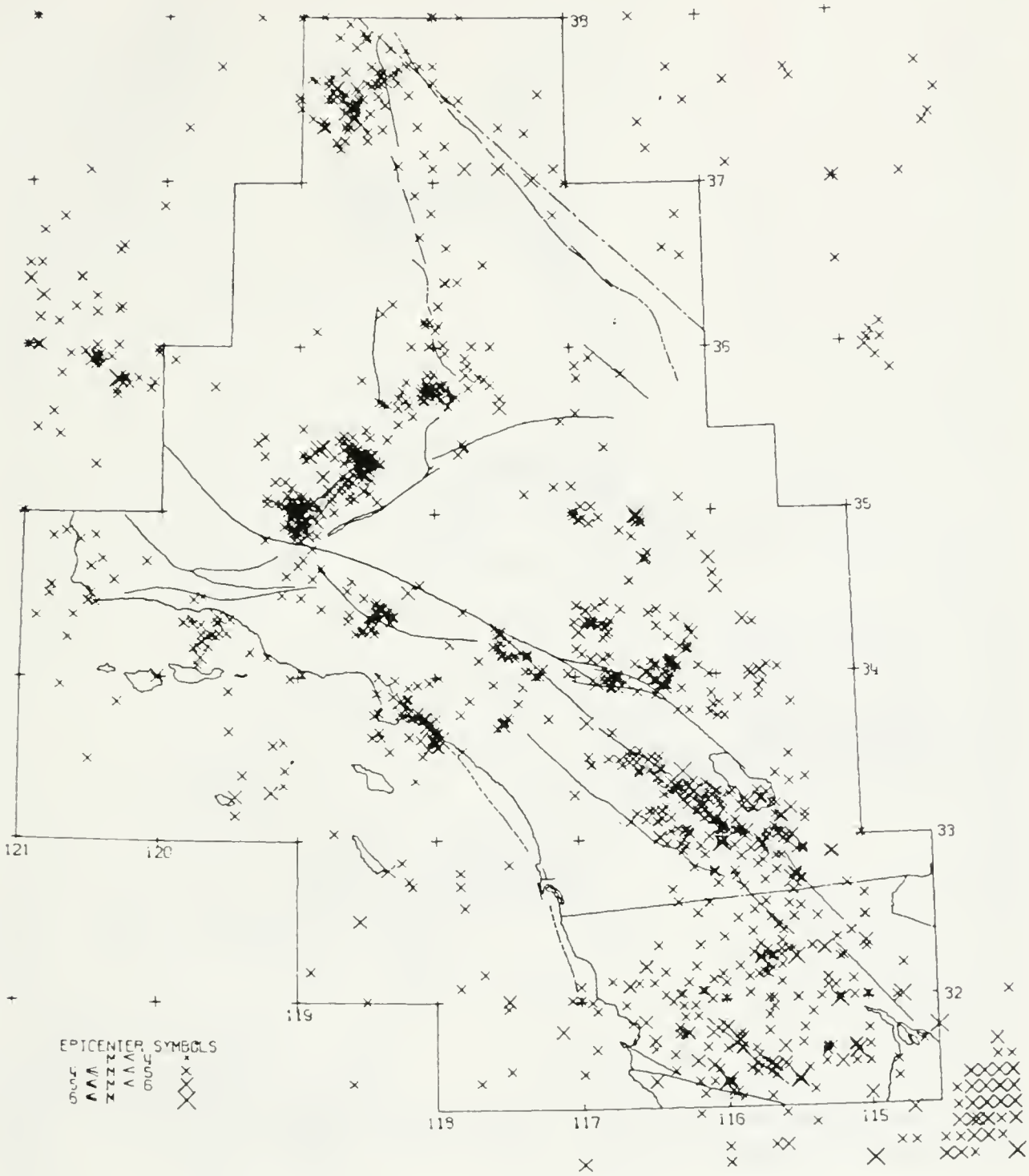

Figure 3. Epicenters of earthquakes in southern California with magnitude 4 and greater, 1932–72 (from Hileman and others, 1973, p. 64).

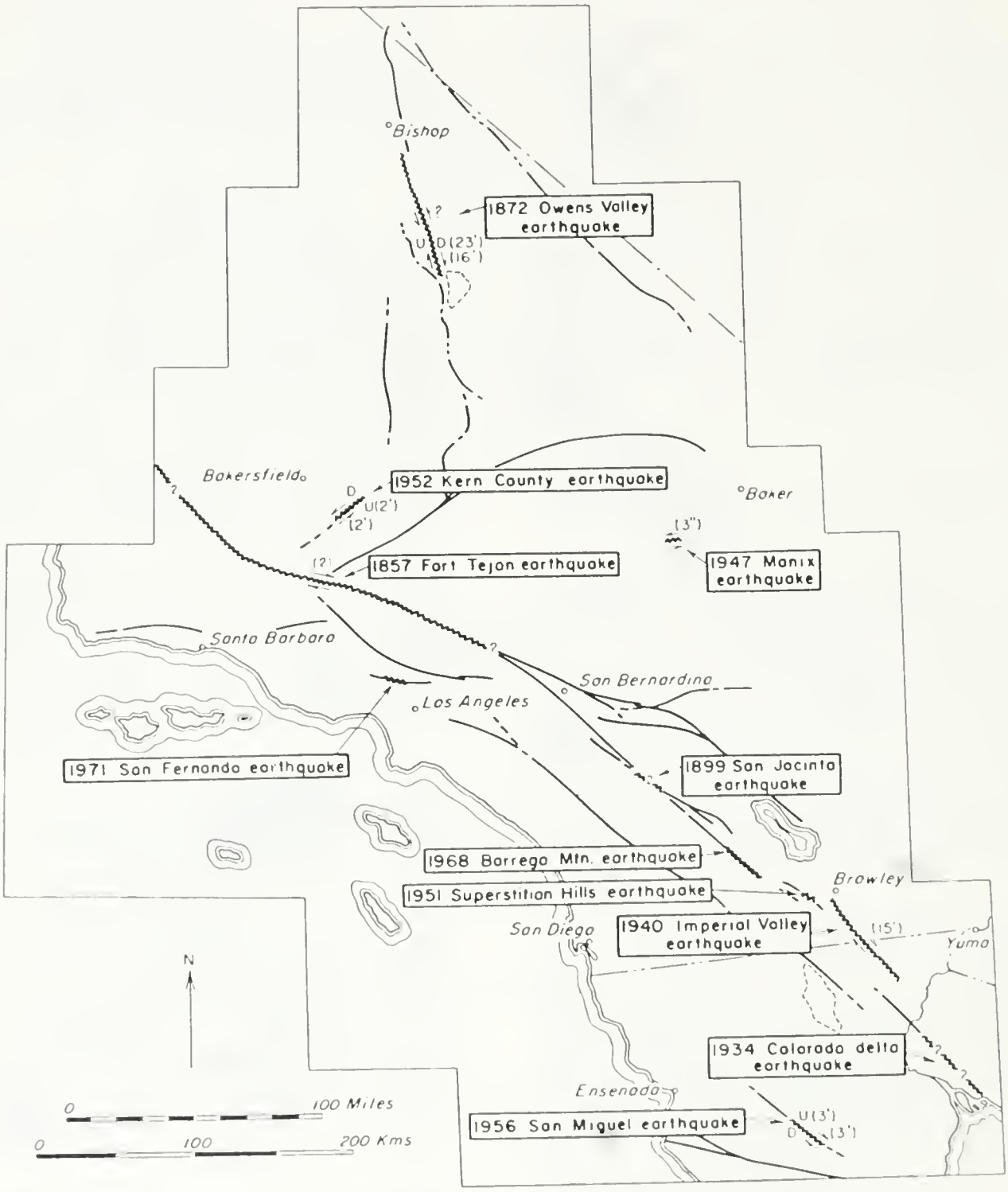

Figure 4. Historic fault breaks and associated earthquakes in the southern California region (from Hileman and others, 1973, p. 10, modified from Allen and others, 1965).

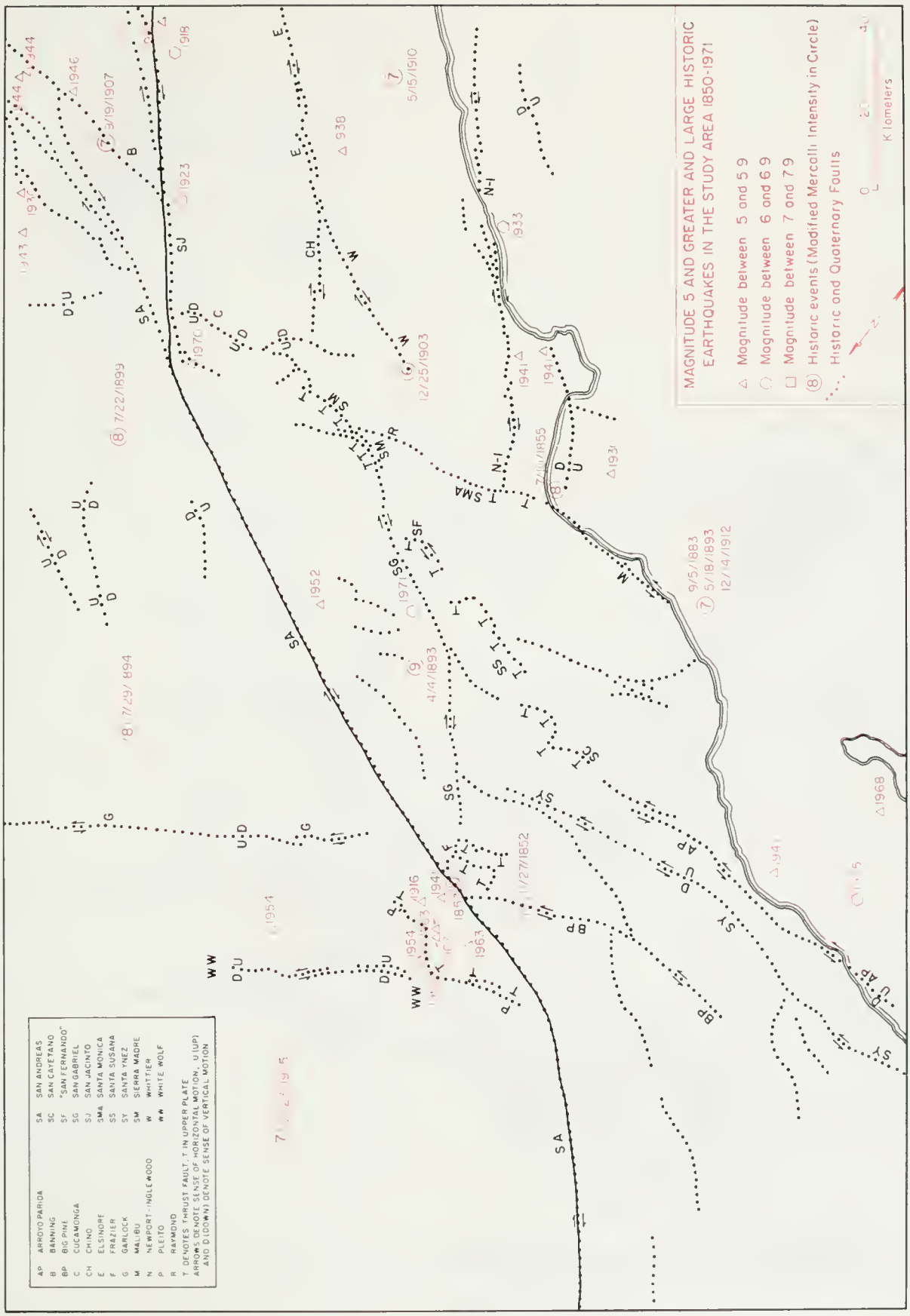

Figure 5. Historic earthquakes with magnitude 5 and greater in the study area, 1850–1971.

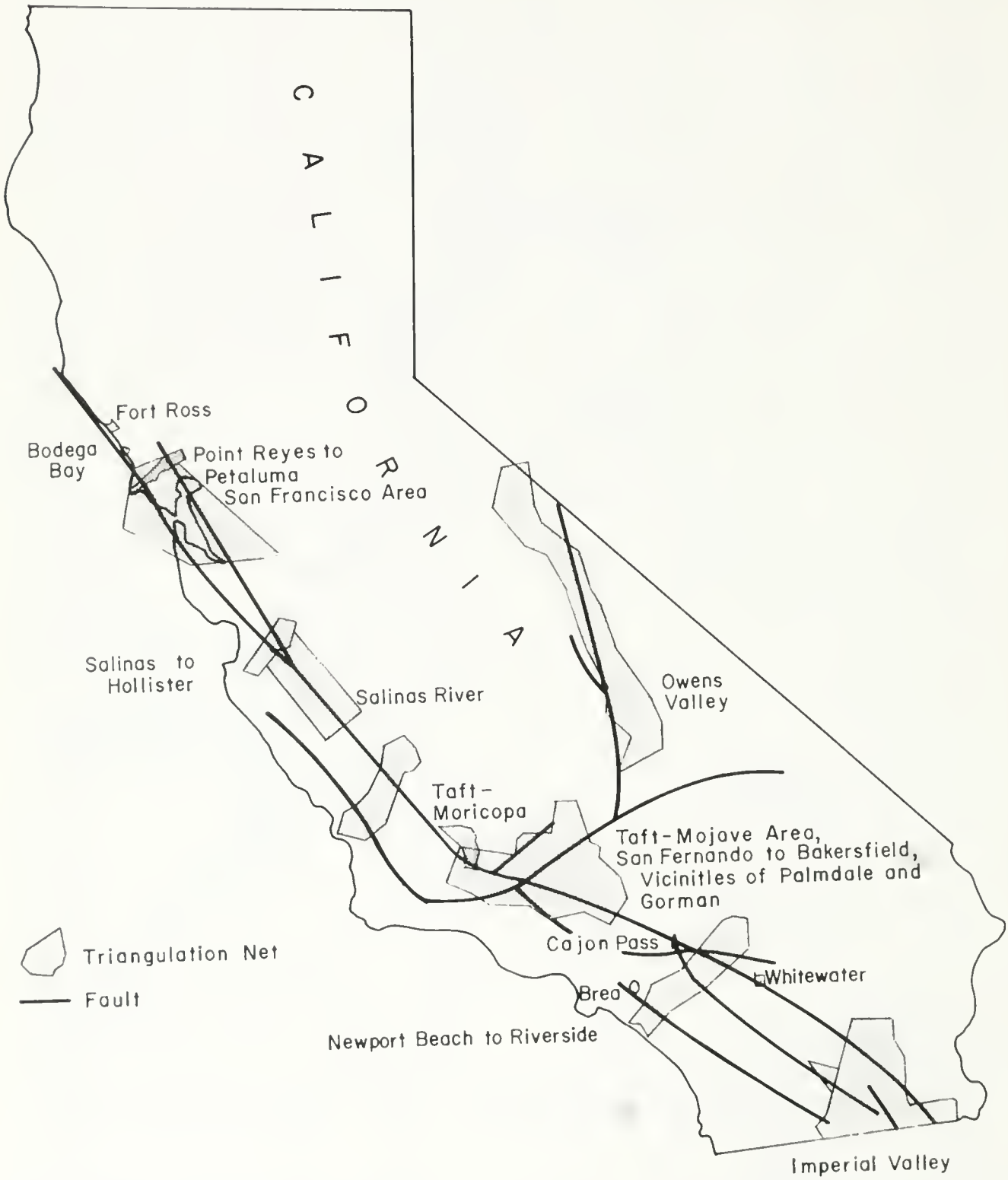

Figure 6. Triangulation nets for crustal movement studies (modified from Greensfelder, 1972, p. 5).

Figure 7. Geodimeter fault–monitoring program (from Greensfelder, 1972, p. 11).

tion and dates of these geodetic studies. Many analyses of the data have been made (see, e.g., Burford, 1966, and Savage and Burford, 1973, for partial lists of references).

Triangulation Surveys

Taft–Mojave Net

In 1959–1960, a large triangulation network was established in the study area (figure 6) by the U.S. Coast and Geodetic Survey and the California Department of Water Resources (Miller and others, 1969a). Many of the line lengths in the net were measured using a Model 2A Geodimeter. In 1967, the net was re–triangulated, and again selected lines were measured with the Geodimeter. The following results are quoted from the report (Miller and others, 1969a, page ii):

"The resultant position vectors and their corresponding 95% confidence error ellipses show that the changes in position are within the limits of observation. However, significant patterns exist. Strain is more evident than fault slippage. There is an area of expansion east of the Garlock fault and north of the San Gabriel fault. The remainder of the net generally contracts or compresses. Along the White Wolf fault, the Geodimeter results show there is left–lateral movement of about 9 cm for the interval 1959–1960 to 1967. On the San Andreas fault, west of the junction with the Garlock and San Gabriel faults, the Geodimeter results indicate right–lateral movement of about 9 cm for the 7–year period. Along the Garlock fault and the San Andreas fault east of the junction, the results indicate strain rather than slippage."

The establishment of this net represents a major step toward the study of crustal deformation in the study area. However, the results of the resurvey cannot be accepted without reservation. First, the overall accuracy of the survey was about 4 parts per million (Miller and others, 1969a, page ii). Thus, the results obtained are well within survey error, although the consistency of the results does give them greater credibility. Second, and perhaps more important, if the hypothesis of a time–varying strain field advanced by Greensfelder and Bennett (1973) is valid, it may be impossible to separate the effects of the time–varying strains and the tectonic strains. Certainly more resurveys of the net will be necessary to substantiate the results.

San Fernando–Bakersfield Arc

This triangulation arc (figure 6) was established in 1932 and resurveyed in 1952 and 1962 (Meade and Small, 1966). Some of the stations in the arc are common to the Taft–Mojave net (Miller and others, 1969b), and an extensive analysis of the 1962 survey is in essential agreement with the results from the Taft–Mojave net (Miller and others, 1969b). Once again, the results weakly suggest strain accumulation rather than fault slippage.

San Luis Obispo–Avenal Arc

This triangulation arc beyond the northern edge of the study area (figure 6) was established in 1932 and reobserved in 1951 and 1962 (Meade, 1968). Burford (1966) performed an extensive analysis of these data and found that they indicate right–lateral fault slippage along the San Andreas fault.

Geodimeter Surveys

In 1959, the California Department of Water Resources started measuring a network of 15–30 km length lines along the San Andreas fault system using a Model 2A Geodimeter (Hofmann, 1968). These data have been discussed in some detail by Hofmann (1968), Cherry and Savage (1972), Savage and Burford (1973), Savage and others (1973), Greensfelder and Bennett (1973), and in Appendix A of this report. Figure 7 shows most of the lines in the Geodimeter network.

The most pertinent information from these works is that strain is not accumulating along the San Andreas fault north of the vicinity of Parkfield and that strain is accumulating along the fault south of Parkfield (Hofmann, 1968; Savage and Burford, 1973). The relative motion between the two sides of the San Andreas fault is accommodated by fault creep at a rate of between 3 and 4 cm/year north of Parkfield. The Geodimeter work indicates that fault creep ends about 5 km south of Parkfield. Appendix A presents a dislocation model that explains the Geodimeter results in the Parkfield region.

Fault–Crossing Survey Figures

Beginning in 1964, thirty small survey figures were established across faults of the San Andreas system, many being located where facilities of the California Water Project cross these faults. Very little analysis of the results of these figures has been published. A compilation of the results and a brief analysis appears in Appendix B. In this section, I will summarize the results from Appendix B.

The survey figures indicate right–lateral movement on the San Andreas, the Hayward, and the Calaveras faults from near Berkeley to south of Parkfield with rates of from 5 to 15 mm/year. It is possible that movement in figure TEM, south of Parkfield, may represent strain accumulation rather than fault creep; but there is little doubt that the movement in the figures north of TEM represents fault creep.

From TEM south along the San Andreas fault to WRIGHT, the survey figures show no movement larger than the survey errors (a few millimeters). The figure at DEVIL, on the San Andreas fault, shows no movement until 1970; but between 1970 and 1972, there is evidence of right–lateral movement at a rate of several millimeters a year. At the same time, the two figures on the San Jacinto fault, COLT and RIALTO, indicate right–lateral movement at a rate of several millimeters a year until 1970 and no movement after 1970.

Finally, two figures on the Garlock fault (RANCH–TEJON) indicate left–lateral movement at a rate of 8 mm/year (Appendix B). Sites on other faults show no movement.

Creepmeter Data

Since the discovery of fault slippage near Hollister in 1956 (Steinbrugge and Zacher, 1960), much effort has been devoted to the study of this phenomenon (Nason, 1971, 1973; Yamashita and Burford, 1973). It is now known that fault slippage occurs on the Concord, the Calaveras, the Hayward, and the San Andreas faults (Nason, 1973). However, to my knowledge, there is no published evidence of slippage on any other faults.

The results of the creepmeter work that are pertinent to this study are contained in Yamashita and Burford (1973) and in Appendix A. At site XSC1, steady creep is occurring uniformly at a rate of about 24 mm/year; and at XDR1, steady creep occurs in steps at an average rate of 11 mm/year. At XGH1, the rate is about 2 mm/year; and, at the southernmost site, XWT1, there were two creep events between June 1969 and February 1973 that would give an average rate of about 2 mm/year.

Thus, the data suggest a rather dramatic drop in the creep rate between XDR1 and XGH1, a distance of about 5 km. However, it is possible that the sites at XGH1 and XWT1 do not cross the presently creeping trace of the fault. Two arguments suggest this may not be a valid explanation. First, continual examination of State Highway 46 (by Division of Mines and Geology personnel) where it crosses Cholame Valley has not yielded evidence of fault creep since the 1966 earthquakes. If creep is occurring at rates of 1 to 2 cm/year, it would certainly be observed in the highway. Second, the creepmeters are installed across the trace of surface faulting from the 1966 earthquakes, and it seems reasonable to expect that creep should occur on the 1966 break. The Division of Mines and Geology is conducting measurements on a survey figure crossing Cholame Valley to try to resolve this question.

Level Surveys

The U.S. Coast and Geodetic Survey (now National Ocean Survey) has been carrying out level surveys in California since 1906 (Meade and Small, 1966). However, very little has been published about the results of the leveling. Parkin (1948) discusses level changes around Los Angeles between 1906 and 1946, and he identifies significant subsidence near Long Beach and Santa Ana. Holdahl (1973) briefly considers the level results at the fault–crossing survey sites, but he does not present any of the data. Meade and Small (1966) discuss, again briefly, some leveling results along the San Andreas fault.

Buchanan and others (1973) discuss elevation changes in the western Transverse Ranges, and they report inflections in elevation changes that appear to be associated with faults. Castle and others (1974) present data from repeated level surveys between western Los Angeles and Sandberg and Palmdale. The results of these repeated levels show that Sandberg rose about 90 mm relative to Los Angeles between 1964 and 1968, giving a rate of about 18 mm/year. Palmdale rose about 180 mm relative to Los Angeles between 1964 and 1968, giving a rate of about 36 mm/year. They also point out elevation differences that they suggest might have been precursors to the 1971 San Fernando earthquake.

MATHEMATICAL MODEL OF THE SAN ANDREAS FAULT

I want to construct a mathematical model of the San Andreas fault in the Transverse Ranges that incorporates the data presented in "Structural Characteristics", "Seismicity", and "Geodetic Characteristics". The model will then be used to attempt to account for features of the Quaternary and present tectonic activity in the Transverse Ranges.

Previous Work

Two earlier studies have approached the problem of stress or strain accumulation in southern California. Smith and Van de Lindt (1969) calculated the changes in strain energy due to the introduction of stress–free surfaces (faults) in a pre–stressed plate in plane strain. They calculated the effects of movement on thirty–one faults from 1812 to 1966, and they found that the strain energy had increased in the eastern Transverse Ranges (figure 8). They also found an increase in strain energy north of the San Andreas fault near the White Wolf fault that was only partially relieved by the 1952 Arvin–Tehachapi earthquake.

This approach suffers from deficiencies, several of which are discussed by the authors. The model is two dimensional; hence, changes in strain cannot be calculated at depth, and the orientations of potential failure planes cannot be calculated. Their model considers only the strain changes due to movements on faults; it does not consider the strain or stress accumulation occurring between 1812 and 1966.

Rodgers and Chinnery (1973) attempted to deal with the problem of stress accumulation since the 1857 Fort Tejon earthquake. They used a dislocation model of the San Andreas fault that involved a locked fault segment extending from south of Parkfield to near San Bernardino. They found that the maximum shear stress increased in the Transverse Ranges and in the vicinity of the White Wolf fault. However, their work suffers from a major defect. The fault model they used had a total depth of 100 kilometers. A fault this shallow violates the assumption of two semi–infinite blocks moving past one another. The area where the largest errors are introduced is exactly the area of greatest interest, the area near the bend in the San Andreas fault.

Review of Pertinent Features

From the discussion in the previous chapters and in the Appendices, several important features of the San An-

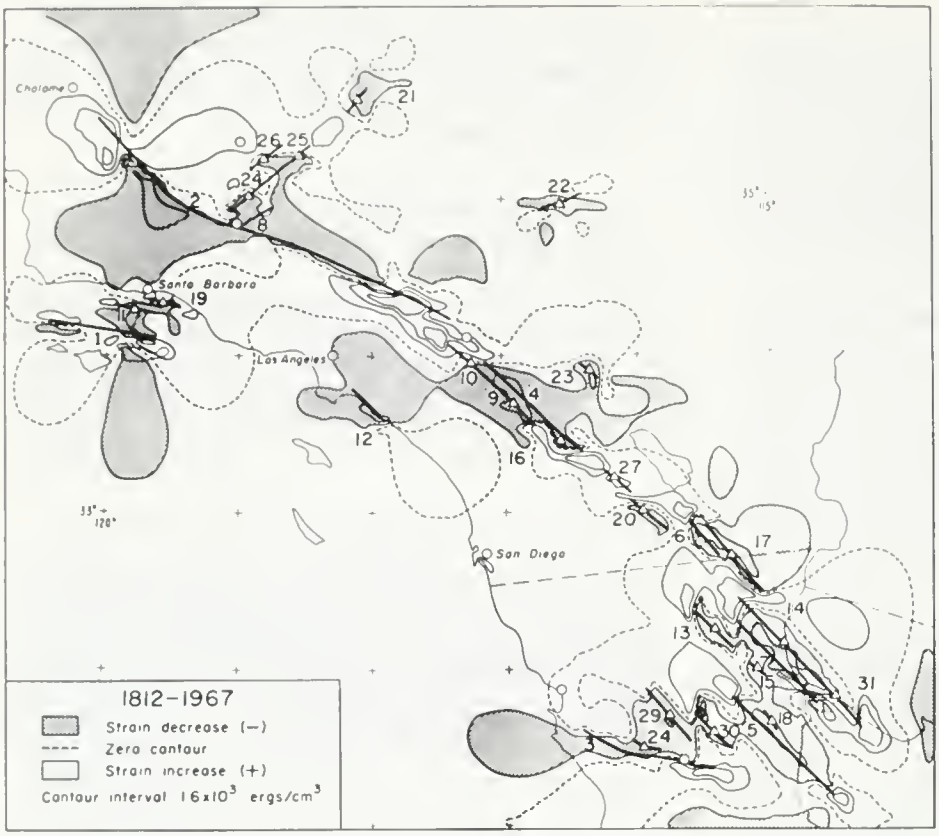

Figure 8. Strain energy changes due to earthquakes, 1812–1967 (from Smith and Van de Lindt, 1969, p. 1583).

dreas fault emerge that must be included in any model. The most obvious feature is the fact that the fault has a bend through the Transverse Ranges. The lack of creep on the fault south of the Parkfield–Cholame area, the lack of seismicity on the San Andreas fault between Parkfield and San Bernardino, and the lack of movement seen in the various geodetic networks must all be included in the model. The high seismicity of the San Jacinto fault and the relatively lower seismicity of the San Andreas fault south of San Bernardino must also be considered.

If the mathematical model is a good approximation of the real world, the stress fields calculated from the model should account for most of the features of the present activity in the Transverse Ranges. In particular, the east–west trending thrust faults and the mechanisms of the 1952 Arvin–Tehachapi and the 1971 San Fernando earthquakes should be reasonably well predicted.

Possible Mathematical Models

The situation to be modeled is that where two relatively thin plates (the lithosphere of Isacks and others, 1968) are moving past each other along a vertical boundary (transform fault), and both plates are riding over a much thicker and weaker layer (the asthenosphere of Isacks and others, 1968). The model should be three dimensional both to accommodate a curved boundary between the plates and to allow stresses, strains, and displacements to be calculated below the surfaces of the plates.

The plate could contain a crack that would approximate the boundary of interest. The only closed solutions to this problem of which I am aware involve single straight cracks where the plate is assumed to be in a state of plane strain. Thus, a curved boundary could not be modeled; there would be no variation of the calculated fields with depth, and inhomogeneities could not be included.

Another class of models is that involving cracks or dislocations in half-spaces. The equations for displacements, strains, and stresses due to a crack or dislocation in a homogeneous half-space have been developed in closed form and thus could be used fairly easily. Also, since dislocation models in particular are reasonably good representations of faults (Chinnery, 1961, 1963), models involving dislocations are desirable. The major drawback to a dislocation model is that the equations for a layered medium exist only in integral form, and the solutions require numerical integrations with their attendant problems of cost and accuracy. On the other hand, a dislocation model would allow a curved boundary between two blocks to be modeled; and it would allow the displacements, strains, and stresses to be calculated below the surface.

Some work has been done on the two–dimensional problem of a dislocation in a layered medium (McGinley, 1969; Chinnery and Jovanovich, 1972; Jovanovich and others, 1974a,b). This work could be used to estimate the effects of layering on the results from a three–dimensional homogeneous half–space model.

This is, then, the approach I will take. A model of the San Andreas fault in southern California will be constructed using a dislocation surface in a homogeneous half–space, and the effect of layering on the results will be estimated from the two–dimensional models.

Details of the Selected Dislocation Model

Dislocation theory has been used for straight finite faults (Chinnery, 1961, 1963), for finite faults with bends (Rodgers and Chinnery, 1973), and for infinitely long straight faults (Chinnery, 1961). In the case of a fault with a bend in it, the fault should be very long to remove the effects of the ends from the area of interest. I would like to use the expressions developed by Chinnery (1961, 1963) to model the present situation, because these expressions are closed and fairly simple. Unfortunately, to use these expressions, certain assumptions are immediately required. Chinnery's expressions were developed for a straight, finite, vertical strike–slip fault in an isotropic, homogeneous, linearly elastic half–space.

The expressions for a straight strike–slip fault can be used for the case of a curved fault if we approximate the fault with a series of straight fault segments. The displacements, strains, and stresses at an observation point can then be determined by summing the fields at the observation point that are produced by each of the straight segments. Care must be taken, of course, to ensure that all the fields are transformed into the same coordinate system. There will be some perturbations introduced into the calculated fields due to the use of finite segments; but, if enough segments are used and the grid of observation points is spaced properly, this effect can be greatly reduced.

Details of the Half–Space

The Transverse Ranges province is anything but an isotropic, homogeneous, linearly elastic half–space. The presence of mountains, faults, very different rock types, and deep subhorizontal discontinuities must change the calculated elastic fields. McGinley (1969) and Ben–Menahem and others (1970) have shown that, at distances of less than about 20°, the half–space adequately represents the curved earth. Since the area I am interested in is less than 3° across, at least the assumption of a flat earth should not be a problem.

The problem of inhomogeneities is not as easy to dismiss. Lateral changes in rock types will affect the calculated fields, but presumably the results would be fairly local in extent. These lateral inhomogeneities will almost certainly lead to local stress concentrations near the surface; but if their vertical extents are not great, their effects should be confined to areas near the inhomogeneities. In fact, the local stress concentrations from these inhomogeneities probably determine the local areas most susceptible to earthquakes.

Potentially more important is the problem presented by vertical inhomogeneities. The plate tectonics hypothesis as advanced by Isacks and others (1968) divides the outer part of the earth into three zones of very different physical properties. The upper zone, the lithosphere, is approximately 100 km thick, is fairly "strong", and exhibits more or less elastic behavior. The middle zone, the asthenosphere, is relatively much thicker and "weaker" and behaves more or less plastically. The third zone, the mesosphere, is relatively "stronger" than the asthenosphere and may or may not exhibit viscous properties.

On a finer scale, the upper 30 or so kilometers of the lithosphere in southern California is also divided into two or more layers or zones (Press, 1960; Healy, 1963). For example, the crustal model derived by Press (1960) has two layers in the crust above the crust–mantle boundary (the Moho). East of the San Andreas fault, the Moho is about 50 km deep (Press, 1960); while west of the fault, the Moho is only about 30 km deep (Healy, 1963).

Jovanovich and others (1974b) have considered the effects of layers on the far field strains and displacements from a dislocation. They used a two–dimensional model of a point source in a multi–layered medium and numerically evaluated the strain and displacement fields. Their results showed that a thick "weak" layer underlying a thick "strong" layer increases by a factor of 2 or less the strain and tilt fields one would get by using an identical source in a homogeneous half–space. They also showed that a relatively thin "weak" layer between two "stronger" layers drastically alters both the sign and magnitude of the strains calculated from an identical source in a homogeneous half–space.

Thus, based on the previous work, the effect of the lithosphere on the elastostatic fields calculated from my model would be to increase the calculated fields by perhaps as much as a factor of 2. The effect of a thinner, "weaker" layer on the calculated fields is somewhat unpredictable but could be drastic. There is some weak evidence for low–velocity zones in the crust (Landisman and others, 1971), but the presence of such zones is still far from certain (Healy, 1971; Warren and Healy, 1973). Therefore, all that can be said is that a thin low–velocity ("weak") layer might exist under the study area; and if it exists, its effect on the calculated fields is unpredictable. However, I do not feel that the present evidence for a crustal low–velocity zone is very good. For these reasons, the large–scale features of the elastostatic fields calculated from the homogeneous model are probably reasonable approximations of the fields that exist in the earth.

The basic model, then, is one of a curved dislocation surface in an isotropic, homogeneous, linearly elastic half-space. Recall, however, that I am trying to model the case of two plates moving past one another along a curved boundary. For the half-space model to fit this situation, it seems reasonable to require that the boundary extend vertically to infinity. Thus, we now have two quarter-spaces moving past one another on a curved boundary.

Details of the Boundary

Let us now consider the details of the boundary between the two blocks. First of all, I am really only interested in the small region in the vicinity of the curve in the boundary, so it seems reasonable to place the two ends of the boundary at a great distance from the bend. This will completely remove the end effects of the dislocation from the effects due to the bend.

The observed geological, seismological, and geodetic data suggest that, at the present time, the section of the San Andreas fault containing the bend is not moving but that the straight sections on either side of the bend are moving. These data led Allen (1968) to state that this part of the fault is "locked". What, then, is the mechanism of "locking"? Intuitively, one would expect the blocks to experience greater difficulty in moving around a bend than in moving along a straight boundary. Thus, when strain accumulation at either end of the bend has reached a high enough level, the "locked" section of the fault will fail and produce quite a large earthquake. Presumably, the amount of movement in the earthquake will relieve most or all of the accumulated strain.

The slip on the moving sections of the fault on either side of the bend is probably occurring as very slow viscoelastic creep with no release of seismic energy below about 20 km and as intermingled creep and small earthquakes above 20 km (Scholz and others, 1969; Brune, 1974). The slip behavior above 20 km is similar to the stick-slip behavior of rock specimens in the laboratory (Byerlee and Brace, 1968). Thus, it seems reasonable to assume that the "locking" mechanism around the bend is probably a large-scale example of stick-slip behavior.

The depth of the "locked" zone is also important. It seems reasonable to assume that the depth of the stick-slip behavior around the bend is about the same (20 km) as that of the straight sections. Additionally, it seems reasonable to say that the viscoelastic creep under the straight fault sections continues under the "locked" section.

The complete model is shown in figure 9, and figure 10 shows the coordinate system used. Note that most of the fault surface is a zone of stable sliding and that the locked zone is shallow compared to the total fault depth. In the next section, the parameters used for the model will be discussed together with the fit of the model to the real world.

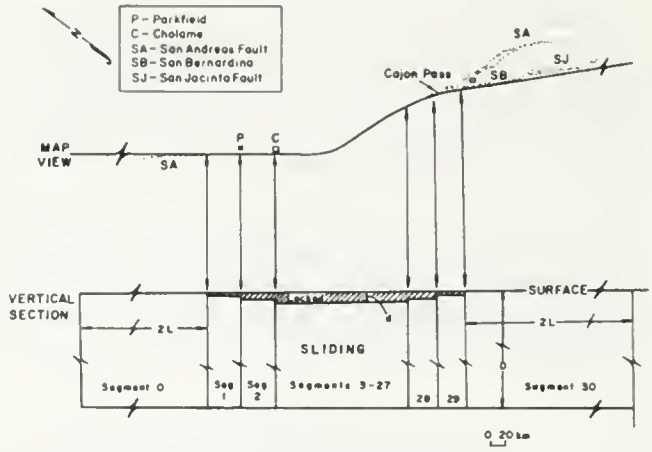

Figure 9. Dislocation surface and its fit to faults.

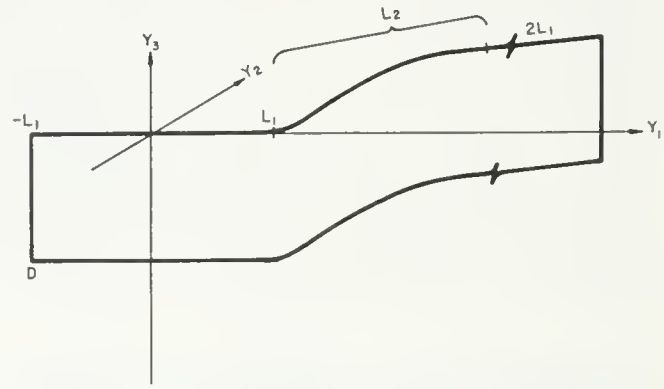

Figure 10. Coordinate system and schematic of dislocation surface.

Parameters of the Dislocation Model

To model the situation described previously, I need to determine as precisely as possible the extent of the active fault surface between the two blocks, the ends of the locked segment, the depth of the locked segment, and the amount of displacement on the fault. The lengths of the end segments and the depth of the bottom of the moving zone will be made very large as discussed in the last section. This will remove the effects of the ends and bottom of the fault. The other parameters can be determined from the geological, seismological, and geodetic data discussed earlier.

The boundary between the two blocks is distinct from the vicinity of San Juan Bautista to near Cajon Pass. All of the evidence indicates that the San Andreas fault is the only through-going, continuously or nearly continuously active fault; and it is reasonable to say that it represents the boundary between the blocks. However, south of Cajon Pass, the boundary is not so obvious. Allen (1957) was unable to trace the San Andreas fault through San Gorgonio Pass.

The San Andreas fault is not very active seismically between Parkfield and San Gorgonio Pass, and there is very little evidence of movement along the fault. However, the San Jacinto fault has had at least five earthquakes with magnitudes greater than 6.0 associated with it (figure 3), there has been surface breakage along most of its length (figure 4), and there is evidence of continuing movement along the fault (Appendix B). For these reasons, it seems reasonable to assume that the San Jacinto fault south of Cajon Pass is the boundary between the blocks and that there is some complex interaction between the San Andreas and the San Jacinto faults near Cajon Pass.

I have fitted straight fault segments to the traces of the San Andreas and San Jacinto faults as shown on the 1:250,000 sheets of the Division of Mines and Geology Geologic Map of California. Figure 9 shows the traces of the faults and the model fit to the faults. The agreement between the model and the mapped faults is very good from Parkfield to south of San Bernardino.

The northern end of the locked segment is probably determined to within 10 km by the seismicity, the abrupt cessation of fault creep, and geodetic evidence (Appendix A). The northern end of the locked segment was placed near Parkfield. The southern end is less well determined. There is no published evidence of surface creep along the San Jacinto fault, but there does appear to have been surface rupture associated with the large earthquakes along the fault trace south of San Bernardino. The south end of the locked zone was placed near San Bernardino, and it is probably accurate to within 30 km. It should be noted that the exact location of this end of the locked segment is less critical than the location of the north end, since I am mainly interested in the stress accumulation in the western Transverse Ranges province. The effects of changing the location of the southern end of the segment will not be large in the area of interest.

The depth of the bottom of the locked zone is more difficult to determine. It seems reasonable to assume that the depth of the locked segment corresponds roughly to the depth of the fault segment that exhibits stick–slip behavior in central California. The vertical extent of this segment is well defined by microearthquakes (Brune and Allen, 1967; Bolt and Miller, 1971), and the bottom of the zone seems to be between 12 and 15 km. The aftershocks of the 1966 Parkfield earthquake were no deeper than 15 km (Eaton and others, 1970), and a few microearthquakes located near the HUGHES fault–crossing survey site (figure B–1) were no deeper than 15 km (Brune and Allen, 1967). Thus, a depth of 15 km for the bottom of the locked segment of the fault seems to be indicated by the seismicity data. The bottom of the locked segment becomes progressively shallower to either end to smooth out end effects to some degree. Appendix A contains a discussion of the degree of control on the depth of the bottom of the locked segment near Parkfield. Figure 9 shows the shape of the locked segment used in this study. Due to the uncertainty of the depth of the locked segment, results from models with depths of 15 and 30 km will be used.

The amount of displacement on the moving segments is fairly well determined from the geodetic work. The estimated displacement rate on the San Andreas fault north of Parkfield is about 3 cm/year (Savage and Burford, 1973). The estimated displacement rate across the Imperial Valley may be as much as 8 cm/year (Whitten, 1960; Scholz and Fitch, 1969, 1971; Savage and Burford, 1971). Atwater and Molnar (1973) determined a post–4.5–million–year rate of slip of 5.5 cm/year from sea–floor spreading data. For the present study, a rate of 5 cm/year is used.

It should be instructive to look at the stress accumulation after the 1857 earthquake and before the 1952 Arvin–Tehachapi earthquakes; thus, the displacement on the moving segments for the 94 years 1858–1952 at a rate of 5 cm/yr is 4.7 meters. This is the value of the displacement used in this study. It should be noted that the value of the displacement does not affect the shape of the calculated displacement, strain, and stress fields. It affects only the value of these fields. Table 1 gives the parameters of the two dislocation models.

For the purposes of this calculation, Lame's constants are set equal (i.e., Poisson's Ratio = 0.25) and have a value of 3.10^{11} dynes/cm^2. This is a fairly common assumption that simplifies the calculations (Chinnery, 1961, 1963; Mansinha and Smylie, 1971).

The displacement on each fault segment was determined by $u_i = U/\cos \Theta_i$, where $U = 4.7$ meters, u_i = the displacement on the ith segment, and Θ_i is the angle the ith segment makes with the Y_i axis. This form of the displacement is required by the assumption of constant displacement in the blocks at some distance from the fault. If, say, the displacement were the same on each fault segment, this would mean the displacement parallel to the Y_i axis would have to vary.

The displacement on each segment was constant over the whole area of the segment. While this does produce discontinuities in the calculated fields at the edges of each segment, it is felt that this is not a problem so long as the observation points are greater than 10 km from the fault trace. This introduces some short–wavelength changes in the calculated fields, but proper grid spacing can eliminate these.

CALCULATED VERTICAL DISPLACEMENT FIELDS

Figures 11 and 12 show the vertical displacements of the ground surface produced by models 1 and 2. The vertical displacement fields from each model have the same overall shape, although there are some minor local variations. There is general uplift over much of the study

Table 1. Parameters of the models.

Segment number	Segment length 2L (km)	Displacement U (m)	Depth to top d1 (km)	Depth to top d2 (km)	Depth to bottom D (km)
0	100,000	4.70	0	0	100,000
1	50	4.70	5	10	100,000
2	50	4.70	10	20	100,000
3	3.62	4.75	15	30	100,000
4	9.50	4.70	15	30	100,000
5	4.74	4.71	15	30	100,000
6	6.12	4.72	15	30	100,000
7	5.74	4.70	15	30	100,000
8	6.38	4.70	15	30	100,000
9	3.12	4.72	15	30	100,000
10	8.00	4.70	15	30	100,000
11	1.05	4.76	15	30	100,000
12	8.38	4.71	15	30	100,000
13	7.38	4.75	15	30	100,000
14	8.00	4.80	15	30	100,000
15	3.88	4.75	15	30	100,000
16	4.24	4.89	15	30	100,000
17	4.24	5.00	15	30	100,000
18	13.38	5.27	15	30	100,000
19	9.74	6.43	15	30	100,000
20	11.74	5.60	15	30	100,000
21	4.24	7.24	15	30	100,000
22	3.50	6.01	15	30	100,000
23	9.00	5.32	15	30	100,000
24	32.74	5.51	15	30	100,000
25	15.24	5.30	15	30	100,000
26	9.00	5.22	15	30	100,000
27	7.74	5.27	15	30	100,000
28	42.24	5.14	10	20	100,000
29	42.86	4.82	5	10	100,000
30	100,000	4.76	0	0	100,000

area, with the largest uplift occurring in the vicinity of Mount Pinos and Frazier Mountain with a magnitude of between 40 and 45 cm. This suggests a maximum rate of uplift from 1858 to 1952 of about 4.3 to 4.8 mm/yr in the vicinity of Mount Pinos. The relative uplift is generally much lower near the Carrizo Plain, in the vicinity of San Bernardino, and in the vicinity of Lancaster and Palmdale.

Two points should be made about the vertical displacements. First, the area of greatest relative uplift is crudely reflected in the topography. Second, the displacement fields from each model resemble one another much more than one would expect.

The obvious question is whether the rather large values of the calculated vertical displacements are due to the use of a homogeneous half-space. Jovanovich and others (1974) have shown that, for a buried point source, the vertical displacements close to the source are smaller for the half-space model than for a model with a thin weak layer at the surface and that this half-space model has about the same value as a model with a buried thin weak layer. At greater distances from the source, the model with a buried thin weak layer produces larger vertical displacements than the half-space model or the model with a thin surface layer. Thus, in both layered cases, the homogeneous half-space produces a minimum estimate of the vertical displacement.

If the calculated vertical displacements are a reasonable representation of the "real" earth, it is necessary to ask whether some mechanism can operate to remove them in 100 years or less. Three such mechanisms come to mind: viscoelastic relaxation, isostatic adjustment, and erosion.

Singh and Rosenman (1974) have shown that, using viscoelastic models of the earth, displacements do not tend to die out with time. Therefore, I would not expect that the vertical deformation produced by either model 1 or model 2 would decrease in time due to a viscoelastic relaxation process. The only other ways to remove the vertical changes would be through either erosion or isostatic adjustment.

Hanks (1974) states that there is no evidence for a root under the San Gabriel Mountains (figures 11 and 12), and this suggests that isostatic adjustment is not occurring. His discussion does not rule out the possibility of some sort of broad regional compensation such as "...an elastic layer deformed by the vertical load exerted by the uplifted mass overlying a fluid substratum." (Hanks, 1974, p. 1226). However, the stresses produced from this model are not consistent with the observed north-south compression in the Transverse Ranges (Hanks, 1974), and Hanks suggests that the uplifted mass may be supported by the horizontal compression. He then proceeds to derive a value of about 1 kb for the mean horizontal stress neces-

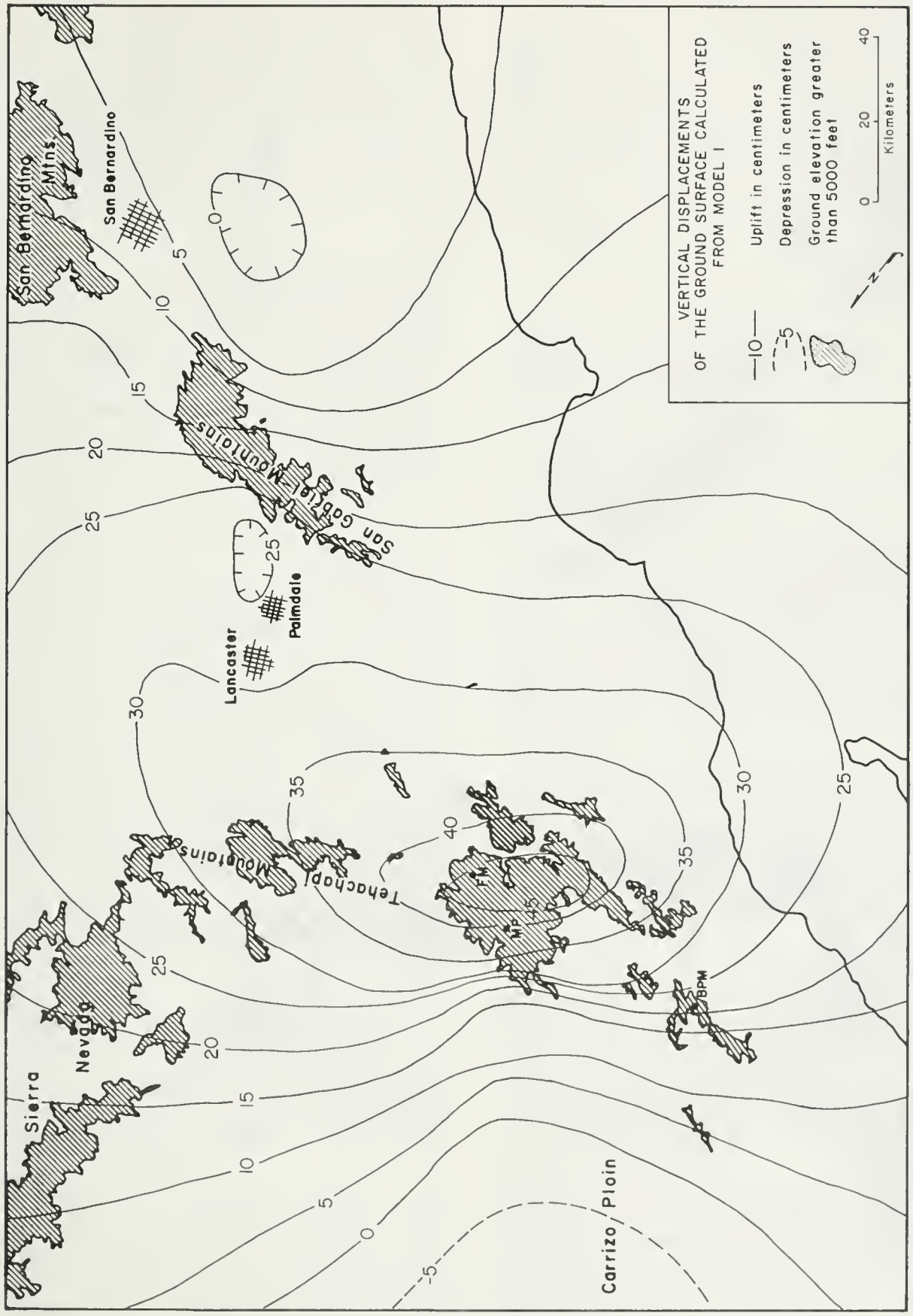

Figure 11. Vertical displacements of the ground surface calculated from model 1.

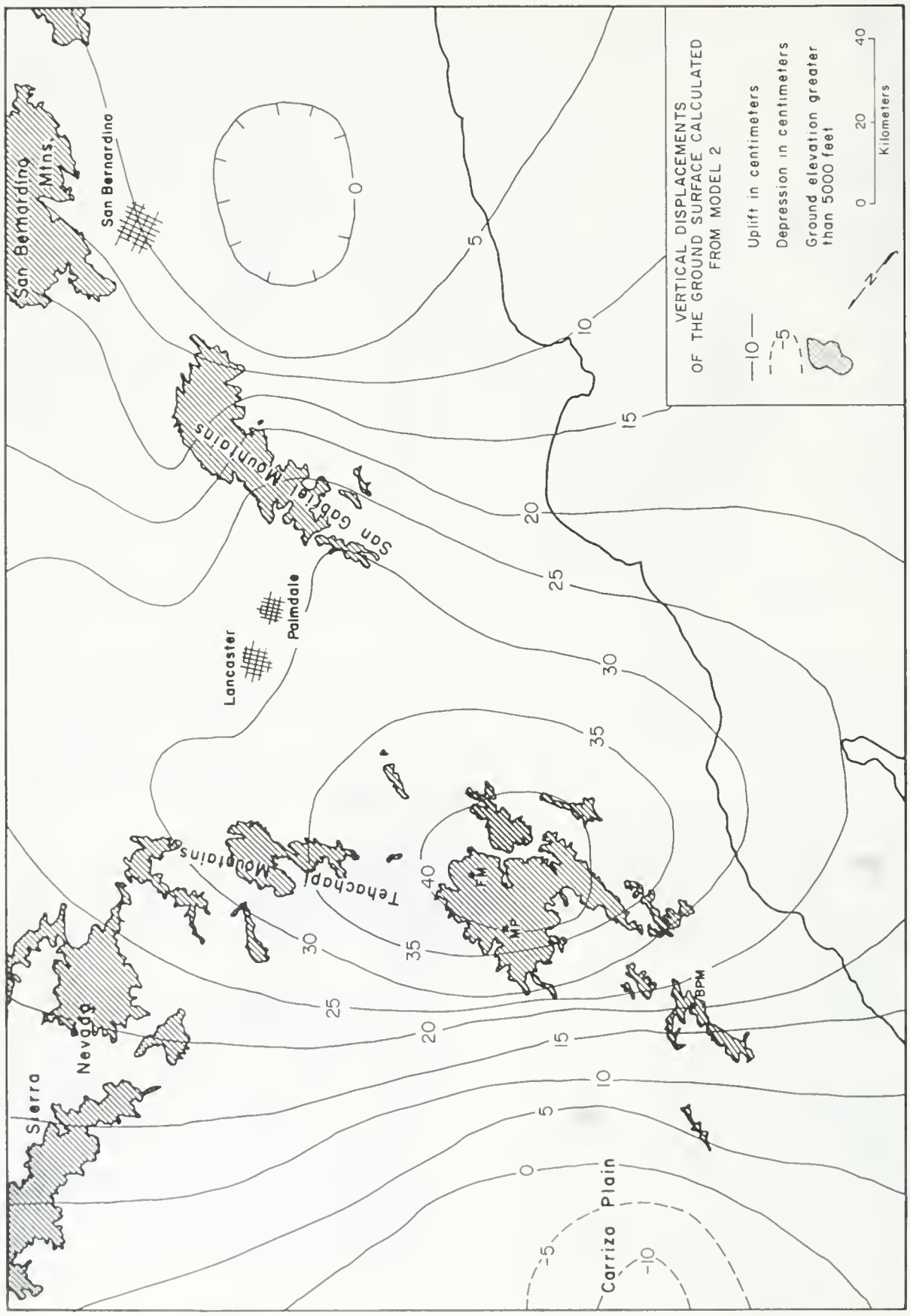

Figure 12. Vertical displacements of the ground surface calculated from model 2.

sary to hold up the elevated mass. But this estimate of the horizontal stress is about 100 times the horizontal stresses calculated from my model. The half-space model may underestimate the horizontal stresses, but it does not seem reasonable to say that the stresses are underestimated by 2 orders of magnitude. Thus, there may be some regional isostatic compensation operating to help to account for the difference between Hanks' (1974) estimate of the horizontal stress and the vertical horizontal stresses calculated from my model.

The elevation increases could also be removed by erosion if denudation is taking place at a rate of about 4 to 5 mm/yr. However, the highest observed denudation rate in the United States is only 0.8 mm/yr in the Eel River Basin in the northern Coast Ranges of California (Judson and Ritter, 1964). Since neither isostatic adjustment nor erosion seems to be occurring at a rate fast enough to remove the elevation increases indicated by the model, we are left with the possibility that the general form of the uplift of the Tehachapi Mountains and Transverse Ranges might be produced by the bend in the San Andreas fault.

CALCULATED STRESS FIELDS

All six stress components at each observation point were calculated for the two models. Due to the difficulty of attaching physical meaning to individual components of the stress tensor, the individual components will not be presented. Instead, other representations that, in a sense, summarize the stress tensor will be used. Isochromatics, or curves of constant maximum shear stress, will be presented. The isochromatics can be used to determine areas of potential failure. Isopachs, or curves of constant mean stress, will be presented because they can be used to help determine areas of potential failure (Chinnery, 1966a,b). To determine directions of potential failure, stress-trajectories (isostatics), or curves whose directions at any point are the directions of the principal stress axes, will be presented at the surface. Also, slip-lines, a set of orthogonal curves whose directions at any point represent the directions of the planes across which the maximum shear stresses act, will be presented for the models at the surface. This nomenclature follows that of Jaeger and Cook (1969, p. 17).

In general, it is not practical to present stress-trajectories and slip-planes at depth because the principal stress axes do not lie in one plane and the planes of maximum shear stress do not intersect one plane at 90°. Both of these conditions hold only at a free surface. I will not attempt to present here principal stress axes or potential failure planes below the surface.

Strictly speaking, the calculated stress fields presented here are changes in some (presumably non-zero) pre-existing stress field. However, I feel that the calculated stress fields may represent the present stress field reasonably well. Rosenman and Singh (1973) have shown that all the components of the stress tensor will fall off exponentially in time if faulting occurs in a viscoelastic half-space. For example, if the relaxation time is 50 years, in 100 years the stresses will have fallen to about 10% of the values at the time of failure; and if the relaxation time is 100 years, the values will have fallen to between 40% and 50% of the initial stress. This suggests that any stresses not relieved by the 1857 earthquake may have fallen to a relatively low value by 1952. Therefore, the stress field primarily responsible for the 1952 Arvin-Tehachapi earthquakes would have been the stress field due to the lack of movement on the locked segment of the San Andreas fault.

Results from Model 1

The stress data calculated from model 1 will be presented first. The stresses were calculated for depths of 0,10, and 20 km. A regional stress field of the form $\sigma_1 = \sigma_2 = \sigma_3 = \sigma = \rho g y_3$, where:

ρ is the density of the material,
g is the acceleration of gravity, and
σ_i are the principal stresses of the regional field,

should be added to the results.

This stress field is the lithostatic pressure at a depth y_3 and represents uniform compression. By leaving this stress field out, we can study the effects of the stress deviations produced by the bend that are related to failure criteria (Jaeger and Cook, 1969, p. 33). Note that such a regional lithostatic pressure will not affect the orientation of the principal stress axes. Of the quantities being presented, only the values of the average stress are affected by the lithostatic pressure.

Figure 13 shows the isochromatics (lines of constant maximum shear stress) calculated from model 1 at the ground surface. The maximum shear stress is quite large near the fault trace; and in some places, the values are very much larger than the 13 bars (13×10^6 dynes/cm^2) shown. Note particularly the lobe to the north of the White Wolf fault and the large, diffuse lobe including the Newport-Inglewood fault zone.

Figure 14 shows contours of constant values of the sum of the principal stresses. This quantity is three times the change in mean stress (Jaeger and Cook, 1969, p. 17). This change in mean stress shows areas where the lithostatic compression discussed earlier is either increased (positive values) or decreased (negative values). There is a broad zone of increased compression running north-south across figure 14 with areas of decreased compression near the Big Pine fault.

Figure 15 shows the calculated stress trajectories at the ground surface. The axis of greatest compression (dashed lines) trends generally north-south throughout most of the area, but this axis acquires a more southeast-to-east trend between the Newport-Inglewood fault zone and the San Jacinto fault zone.

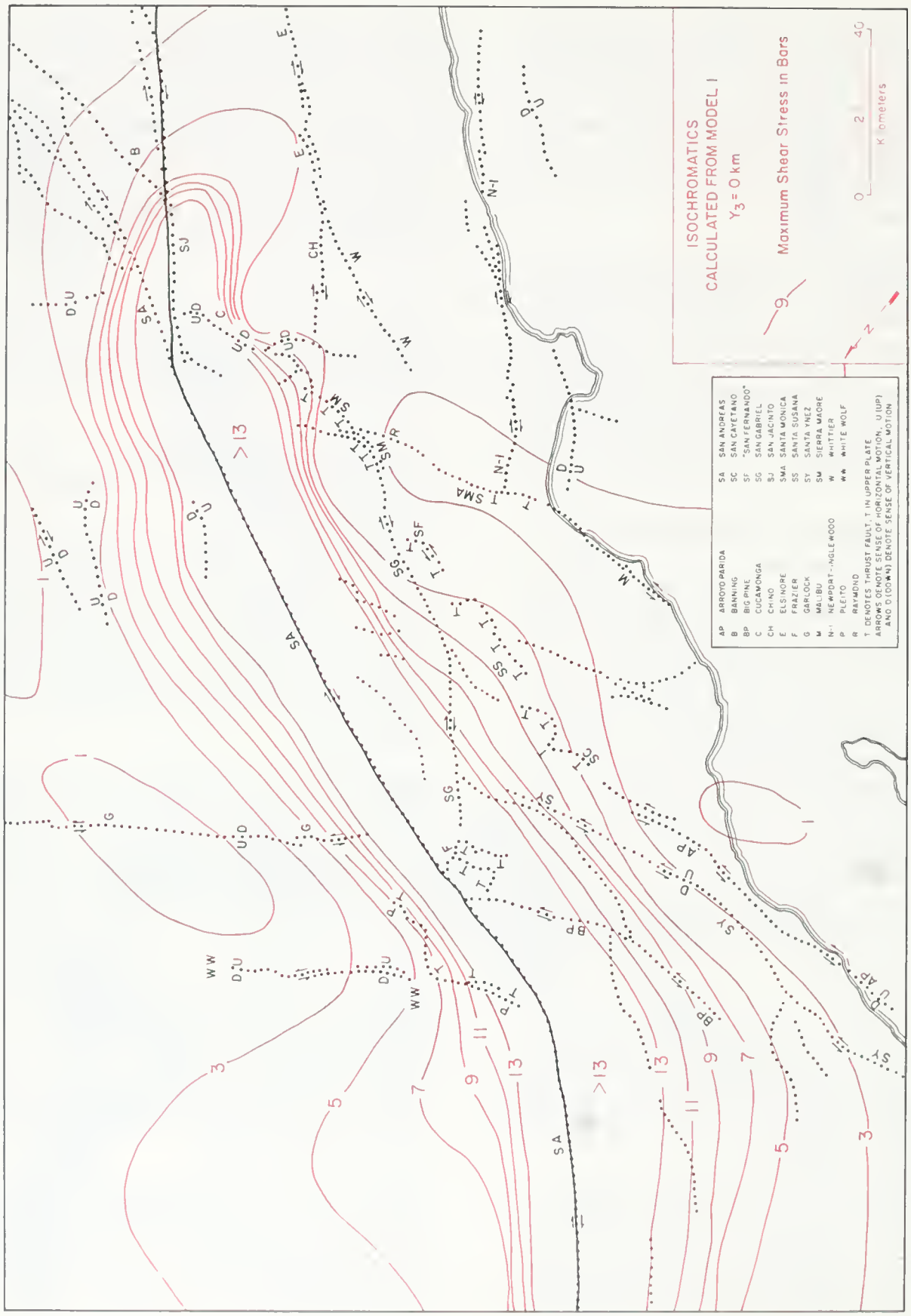

Figure 13. Isochromatics (lines of constant maximum shear stress) at the ground surface calculated from model 1.

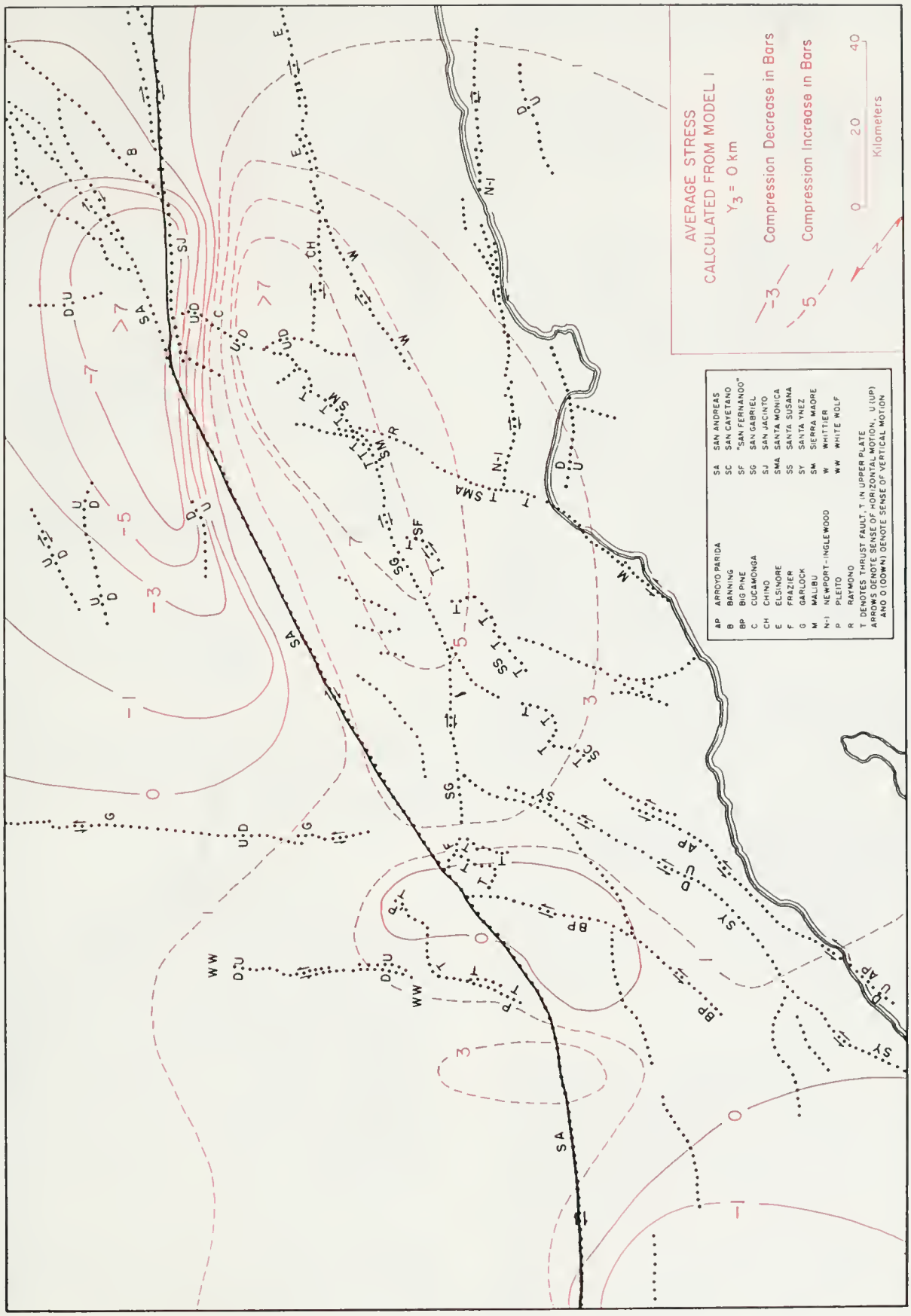

Figure 14. Contours of constant values of the sum of the principal stresses at the ground surface calculated from model 1.

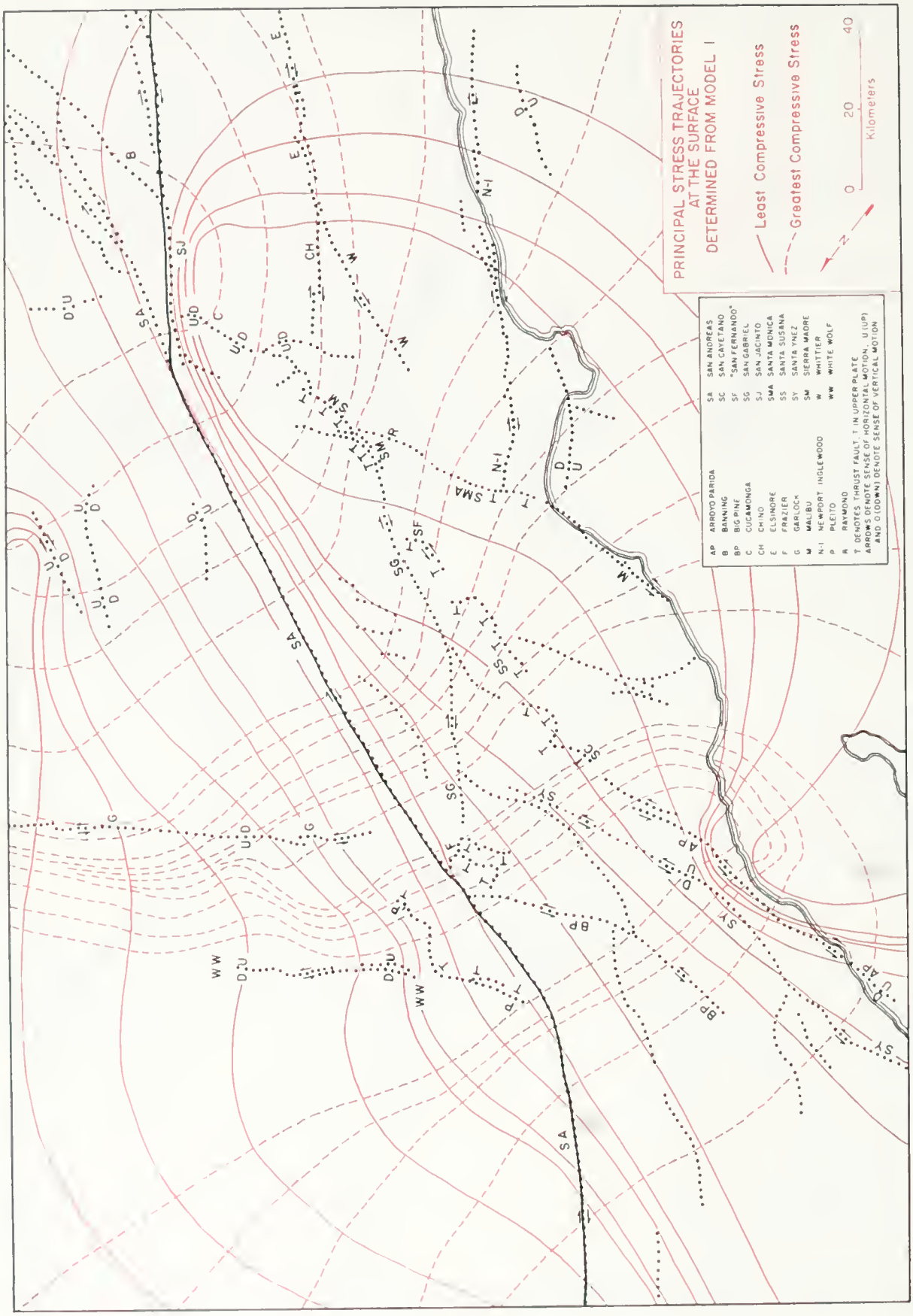

Figure 15. Principal stress trajectories at the ground surface calculated from model 1.

Figure 16 shows surface traces of the slip–planes (planes across which the maximum shear stress acts) at the surface. These planes make angles of 45° with the axis of greatest compression, and they are the planes on which failure should theoretically occur. However, laboratory experiments suggest that failure planes typically occur at angles of between 30° and 45° to the principal compression axis (Jaeger and Cook, 1969). Note that the right–lateral slip lines in figure 16 tend to be parallel or sub–parallel to most of the right–lateral faults in the area such as the Newport–Inglewood zone, the Whittier fault, and the San Gabriel fault. The left–lateral slip lines are sub–parallel to the Garlock, the Big Pine, the Pleito, and the Frazier faults.

Figure 17 shows the isochromatics calculated from model 1 at a depth of 10 km. The contours are similar to those of figure 13. Note the lobe near the western end of the White Wolf fault and the relatively steep stress gradient parallel to and on either side of the San Andreas fault.

Figure 18 shows contours of equal values of the sum of the principal stresses at a depth of 10 km. Figure 18 resembles figure 14 except that there is no area of decreased compression near the Big Pine fault.

Figure 19 shows the isochromatics at a depth of 20 km calculated from model 1. Note the similarity to figures 13 and 15. These figures indicate that the maximum shear stress is fairly constant with depth.

Figure 20 shows isopachs calculated from model 1 at a depth of 20 km. Once again, the features are generally similar to those of figures 14 and 18, but there are some local variations. Note, for example, the change in location of the zero contour near the Big Pine–San Andreas junction.

Results from Model 2

Model 2 has the depth of the bottom of the locked zone set at 30 km. The other parameters are the same as for model 1. Figure 21 shows the isochromatics calculated from model 2 at the ground surface. Comparing figure 21 with figure 13, we can see that the 3–bar contour is somewhat farther from the San Andreas fault for model 2, that the gradients in the stress field are less for model 2, and that the maximum shear stresses are lower near the fault for model 2. The general form of the isochromatics is about the same, with lobes of increased maximum shear stress developed north of the White Wolf and south of the Newport–Inglewood faults, and lows extending parallel to the Malibu–Santa Monica zone and the White Wolf fault.

Figure 22 shows the isopachs calculated from model 2 at the ground surface. There is an area of decreased pressure running across the figure parallel to the White Wolf and the Garlock faults. There are also areas of decreased pressure to the north of the San Andreas fault in the northeast part of the figure and a smaller area in the northwest corner of the figure.

Figure 23 shows the stress trajectories derived from model 2 at the ground surface. Note that, over most of the area covered by figure 23, the principal compressive stress is oriented north–south. The stress trajectories derived from model 2 are much smoother than those derived from model 1.

Figure 24 shows the slip lines calculated from model 2 at the ground surface. The right–lateral slip lines are generally sub–parallel to the San Gabriel, the Whittier, the Chino, and the Newport–Inglewood faults, while the left–lateral slip lines tend to make angles of 20 to 30° with the left–lateral faults, such as the White Wolf, the Garlock, the Santa Ynez, and the Malibu–Santa Monica faults. Part of the Big Pine fault is sub–parellel to a left–lateral slip line. The slip lines derived from model 2 are somewhat smoother than those derived from model 1.

Figure 25 shows the isochromatics calculated from model 2 at a depth of 10 km. The general features of figure 21 are present in figure 25.

Figure 26 shows the isopachs calculated from model 2 at a depth of 10 km. The area of decreased pressure at the surface (figure 22) parallel to the White Wolf and the Garlock faults is replaced by an area of slight pressure increase, but the other general features seen at the surface (figure 22) are present 10 km deep.

Figures 27 and 28 show the isochromatics and isopachs, respectively, calculated from model 2 at a depth of 20 km. Both figures show the same general features as figures 25 and 26.

Discussions and Conclusions

Several points have been demonstrated in this chapter. First, a north–south oriented compressive stress can be produced over most of the study area by the bend in the San Andreas fault. This is important because it removes the necessity of invoking such a regional stress system to account for the Transverse Ranges deformation. Instead, north–south compression exists as a natural consequence of the bend in the San Andreas fault.

Second, most of the faults in the Transverse Ranges that exhibit Holocene or Quaternary movement are parallel or sub–parallel to the calculated slip planes. Thus, the stress field produced by the bend in the San Andreas fault probably has been responsible for "selecting" which of the many faults in the Transverse Ranges have been active. For example, by reversing the movement on the San Andreas fault by 50 to 75 km (1 to 1.5 million years at a rate of 5 cm/yr), the western parts of the Santa Ynez and the Arroyo Parida faults would be moved to the south and east, and the observed movement on these faults would agree with that predicted by model 2. Recall that these faults were more active in the Pleistocene than in the

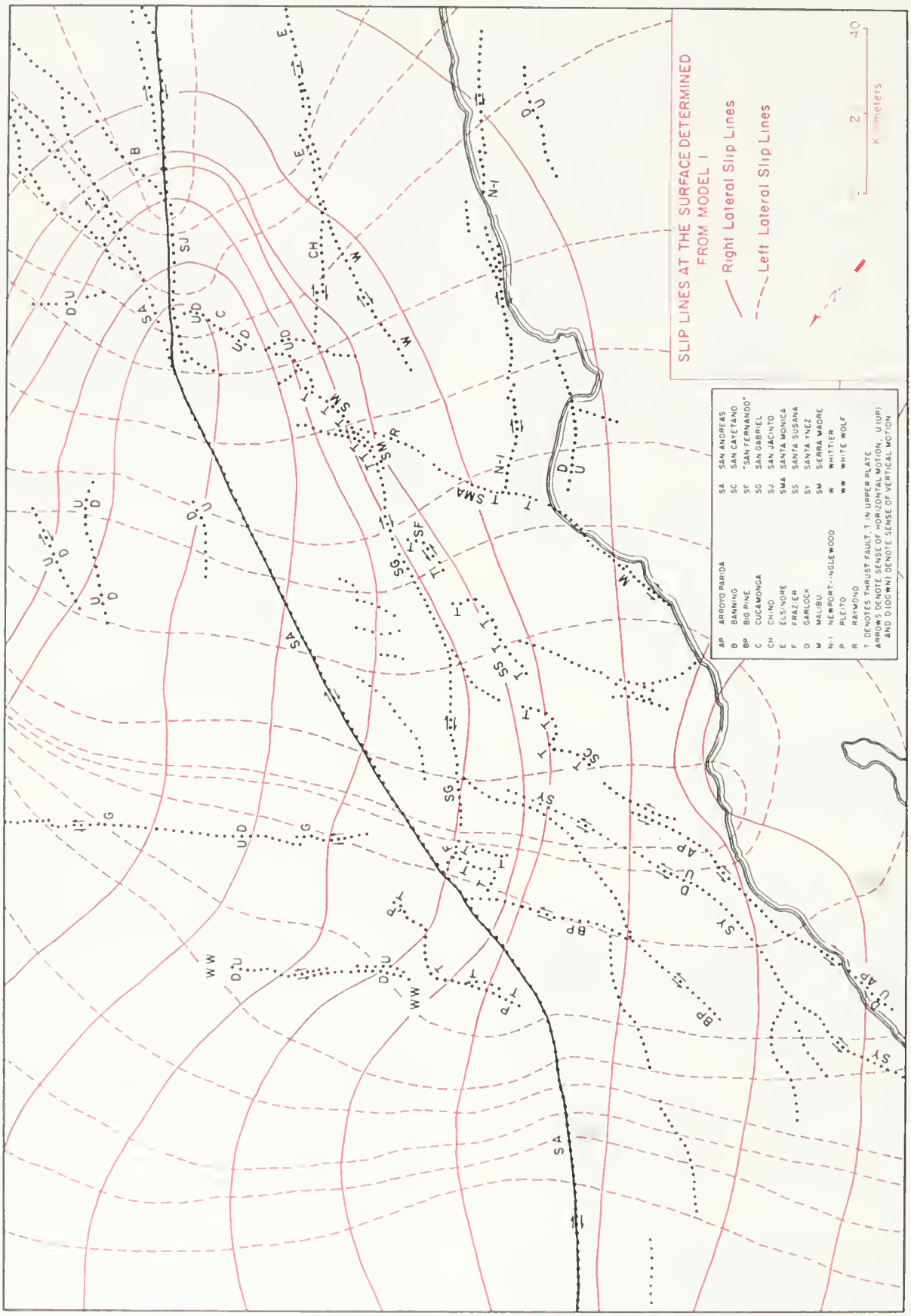

Figure 16. Surface traces of the slip-planes (planes across which the maximum shear stress acts) calculated from model 1.

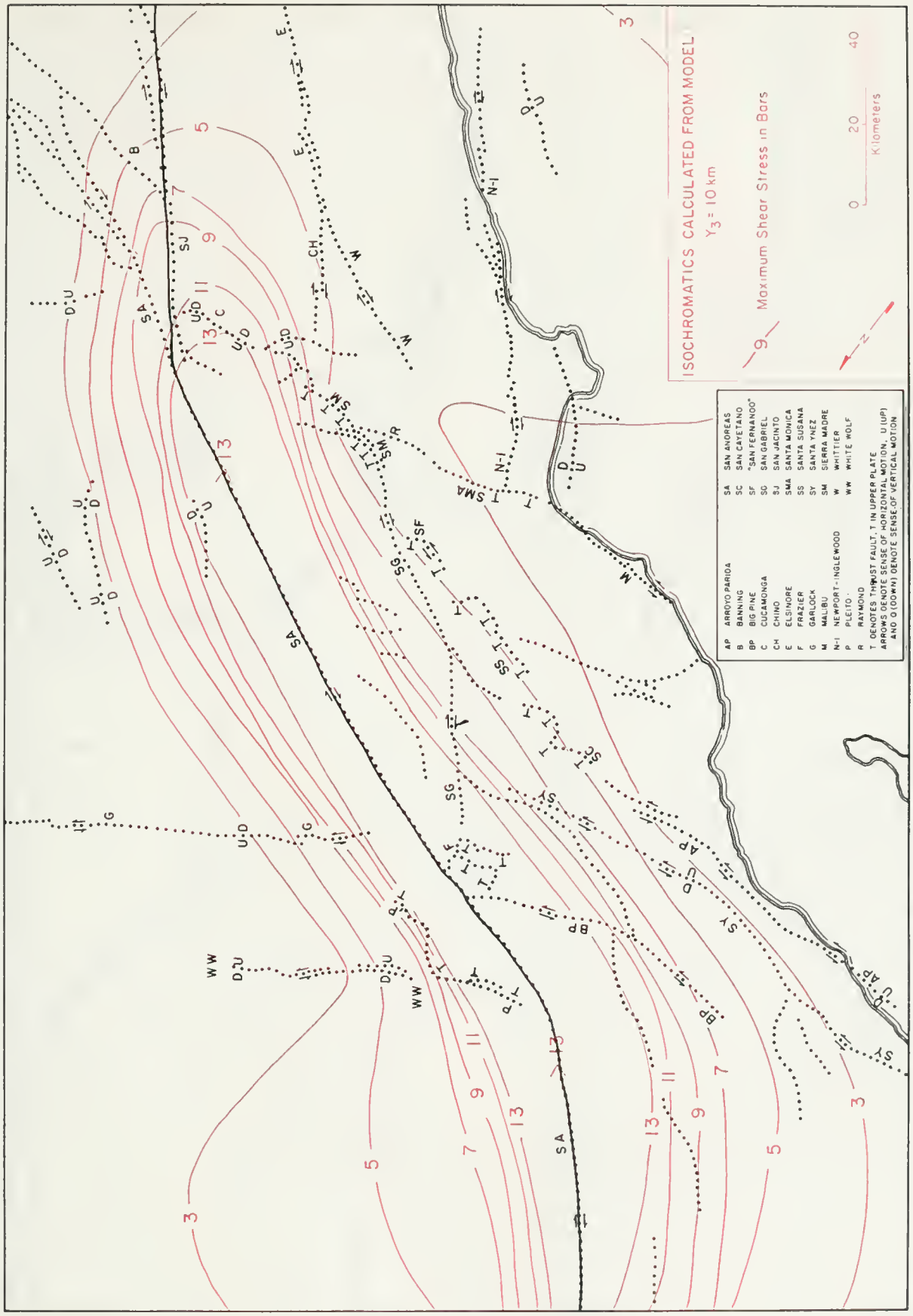

Figure 17. Isochromatics at a depth of 10 km calculated from model 1.

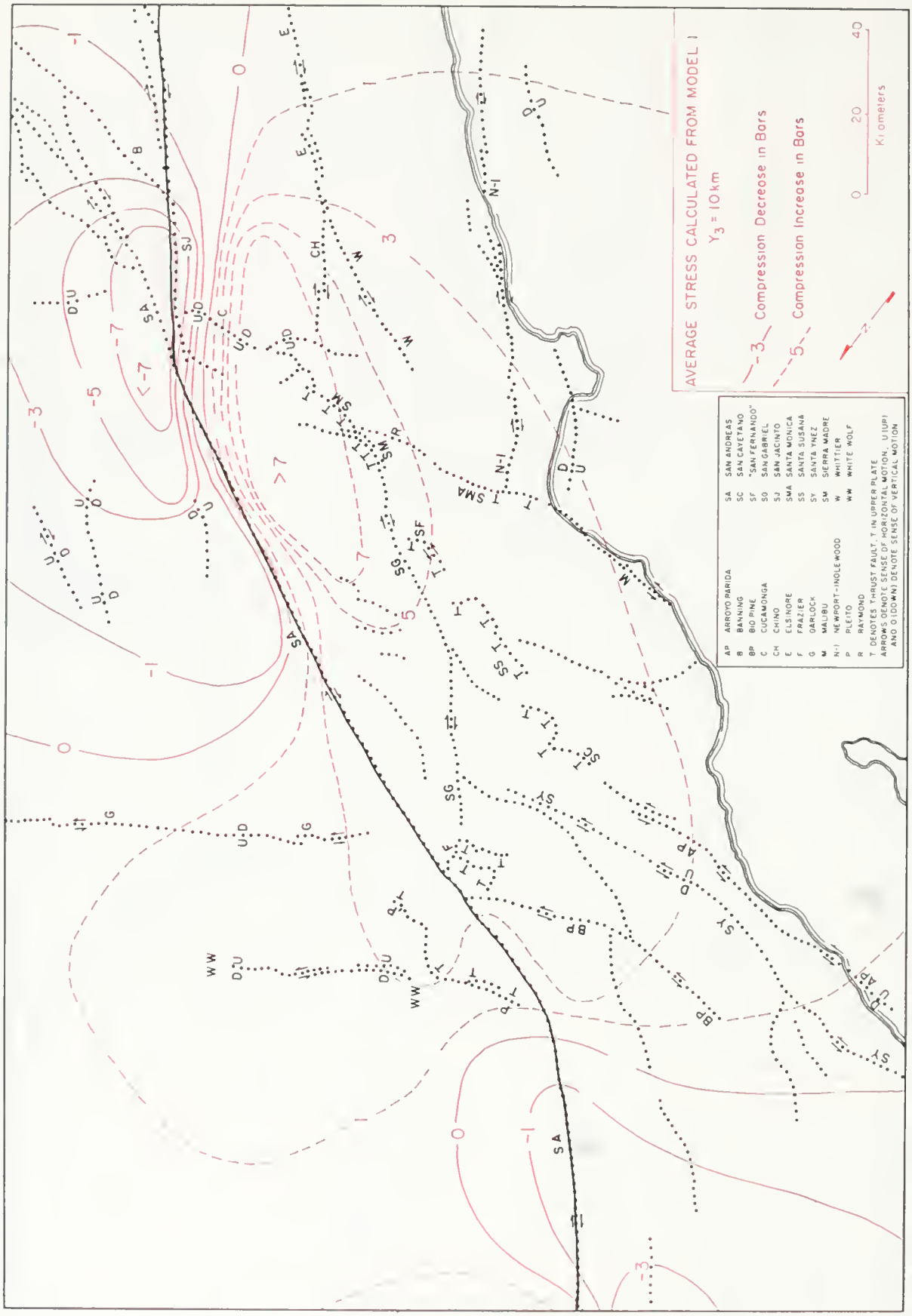

Figure 18. Contours of equal values of the sum of the principal stresses at a depth of 10 km calculated from model 1.

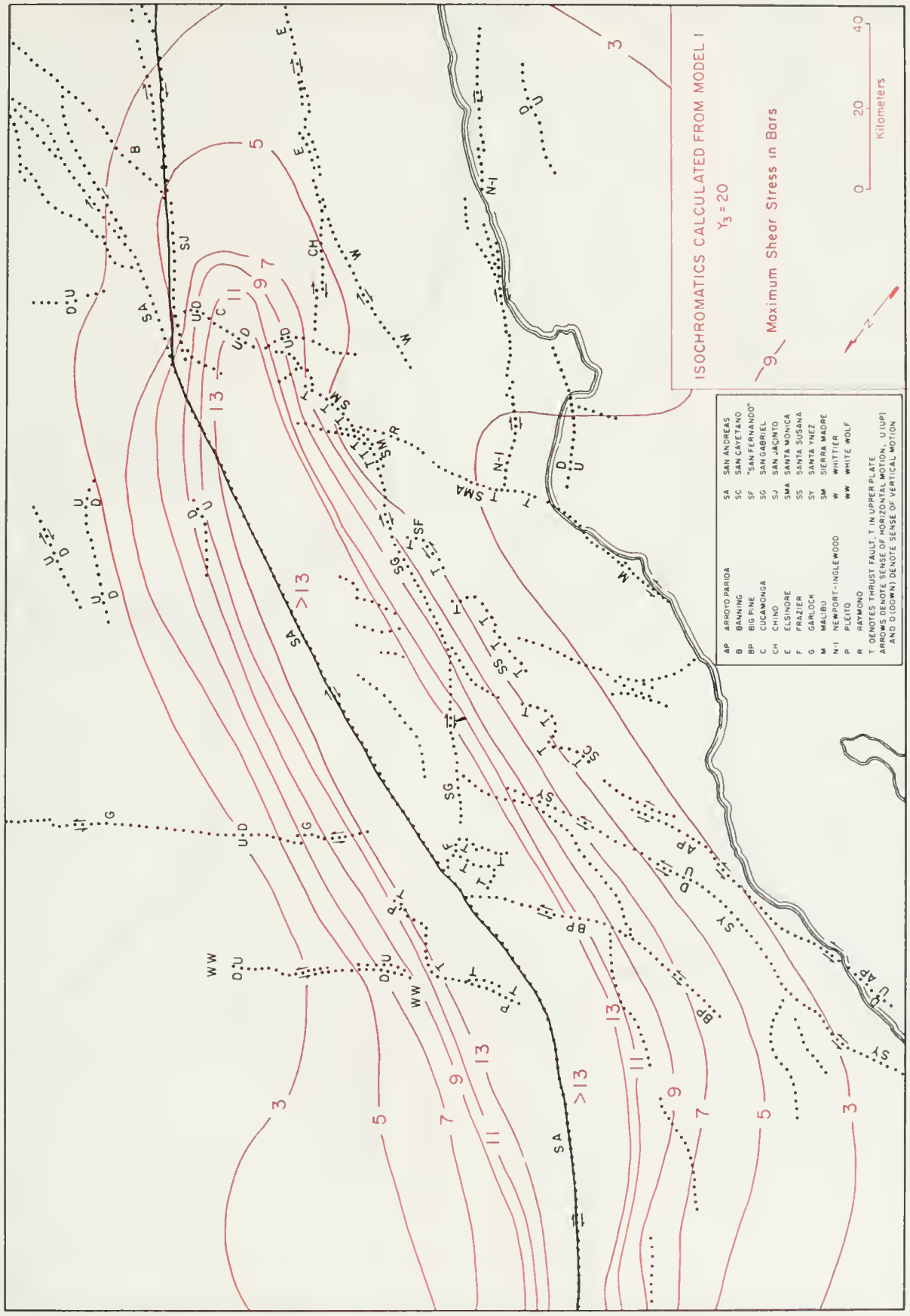

Figure 19. Isochromatics at a depth of 20 km calculated from model 1.

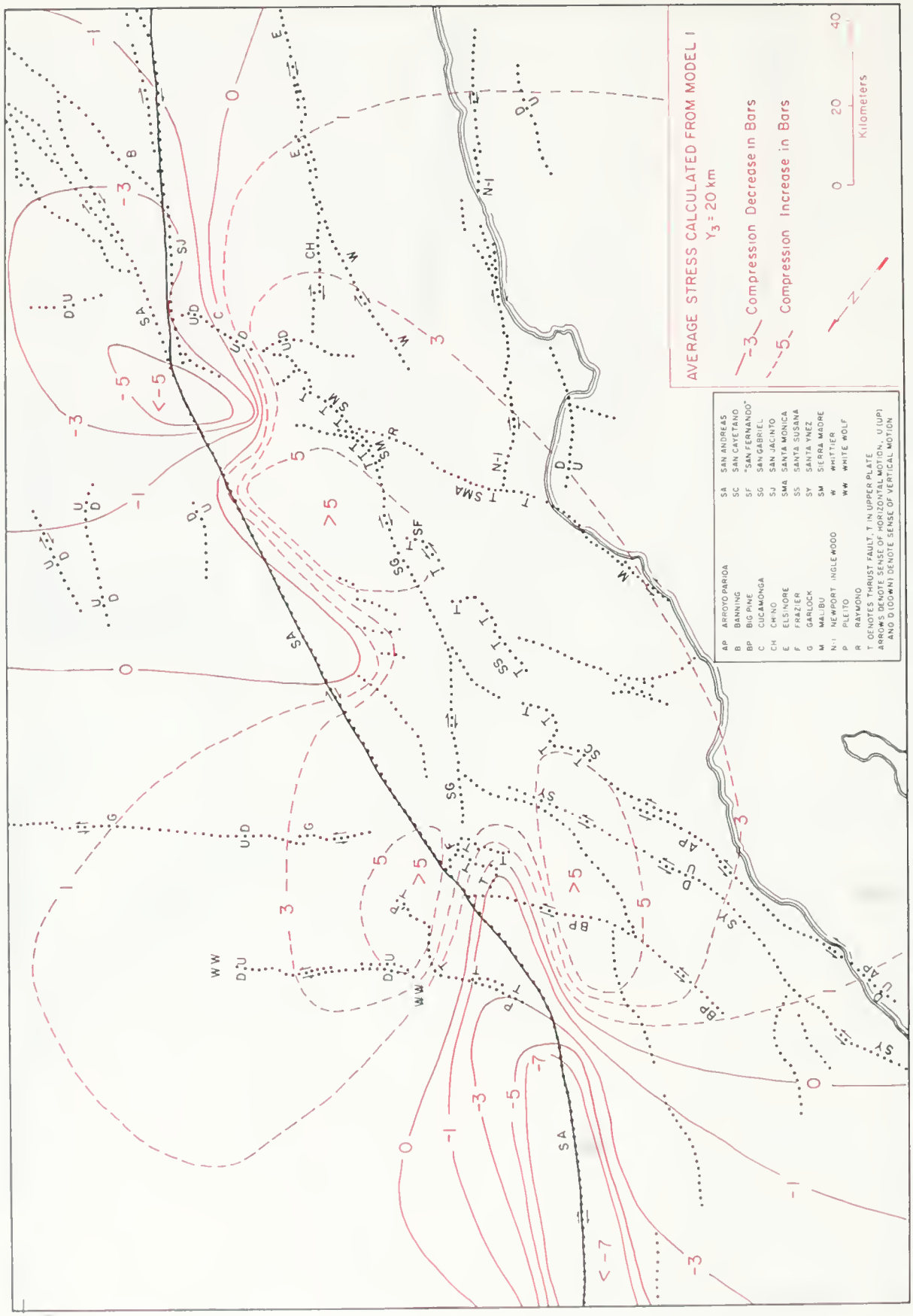

Figure 20. Isopachs (curves of a constant mean stress) at a depth of 20 km calculated from model 1.

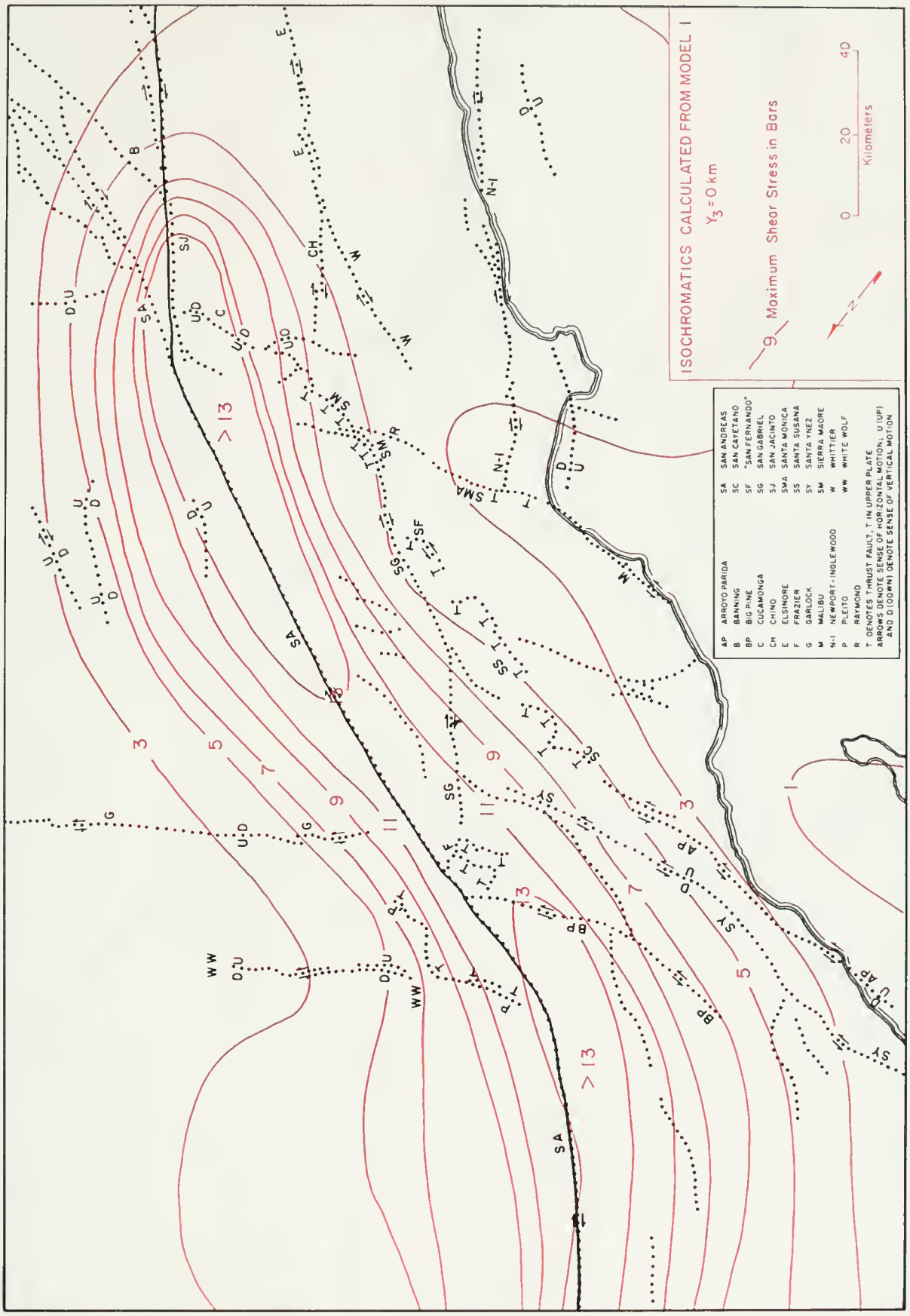

Figure 21. Isochromatics at the ground surface calculated from model 2.

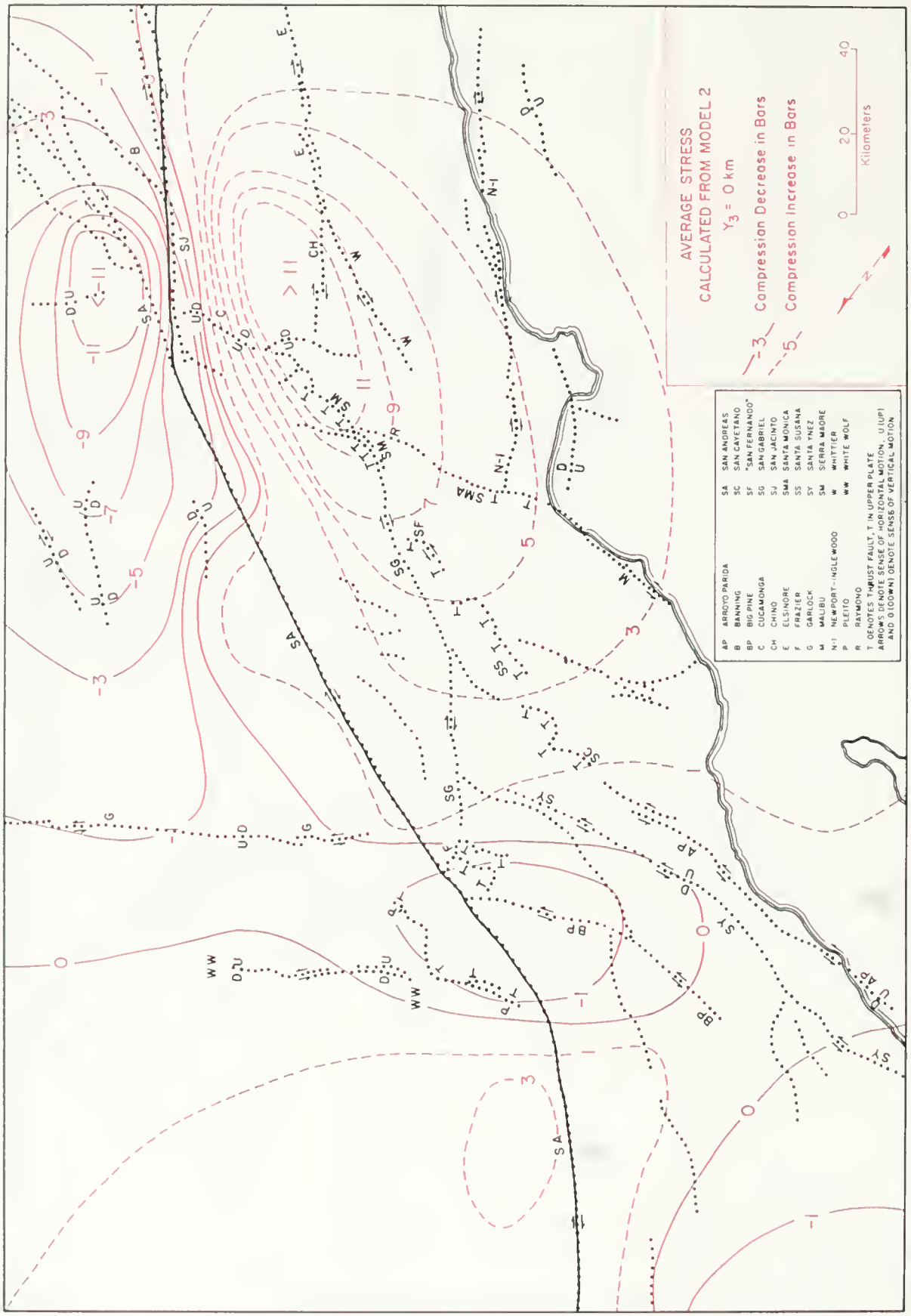

Figure 22. Isopachs at the ground surface calculated from model 2.

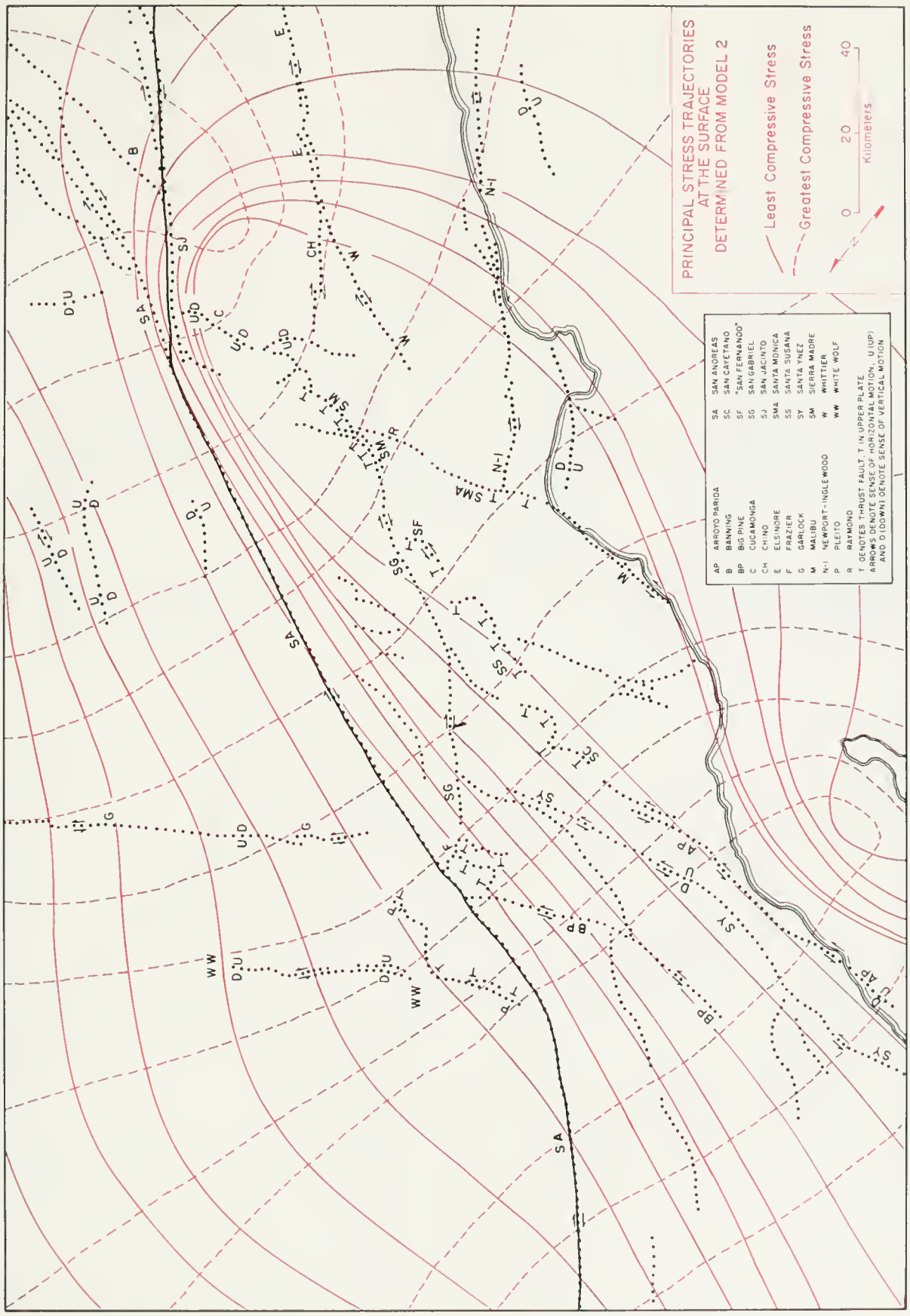

Figure 23. Principal stress trajectories at the ground surface calculated from model 2.

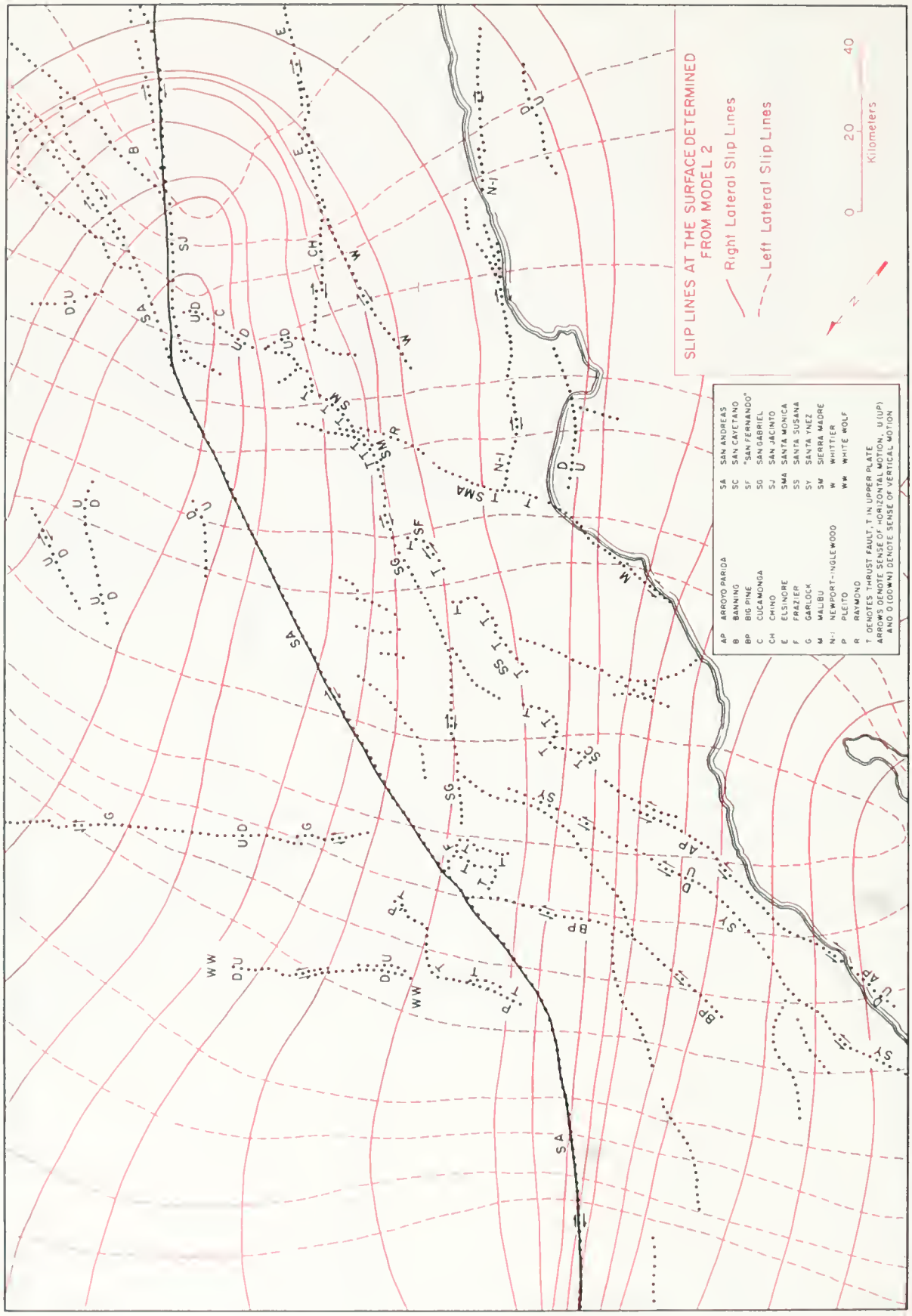

Figure 24. Slip lines at the ground surface calculated from model 2.

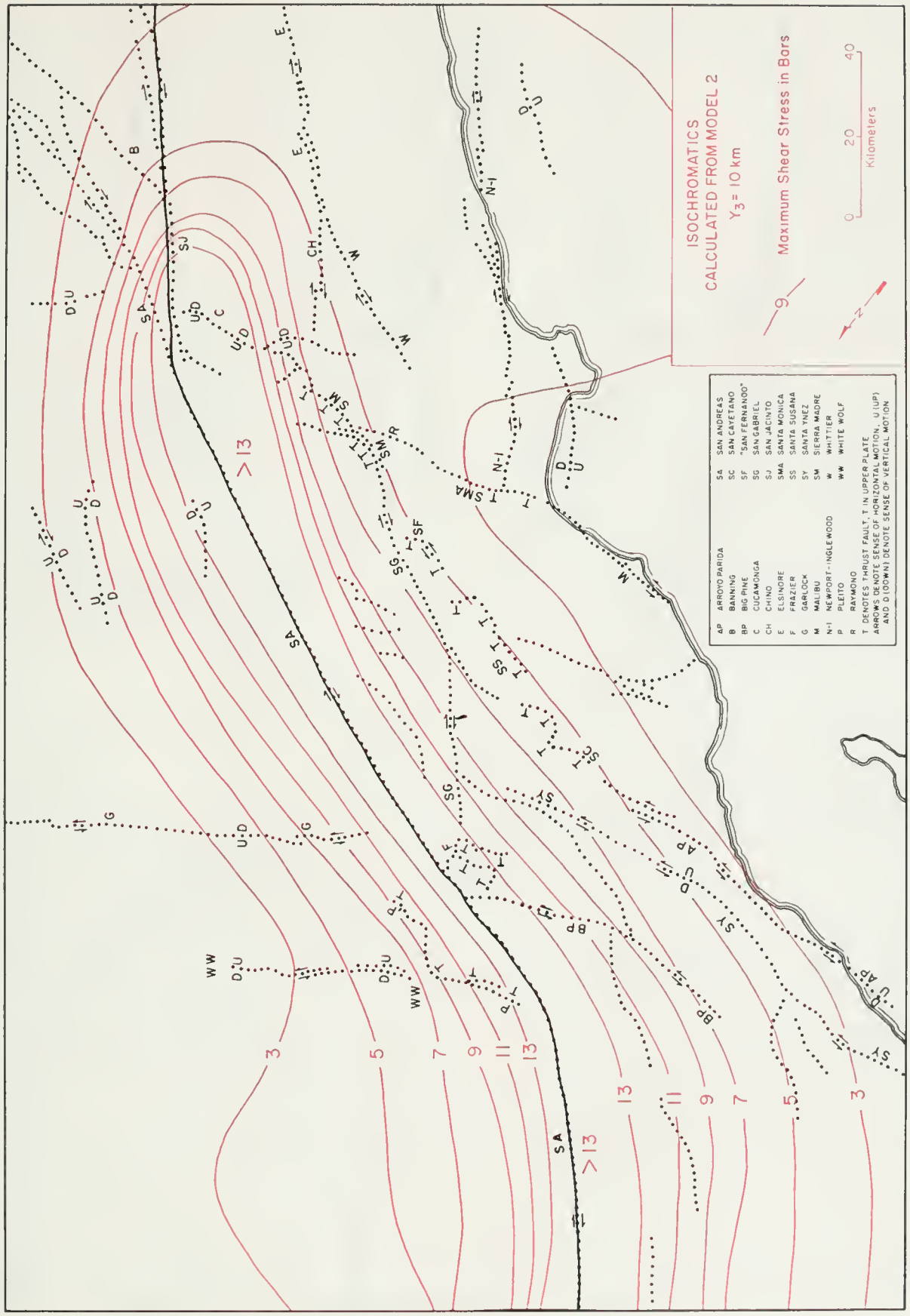

Figure 25. Isochromatics at a depth of 10 km calculated from model 2.

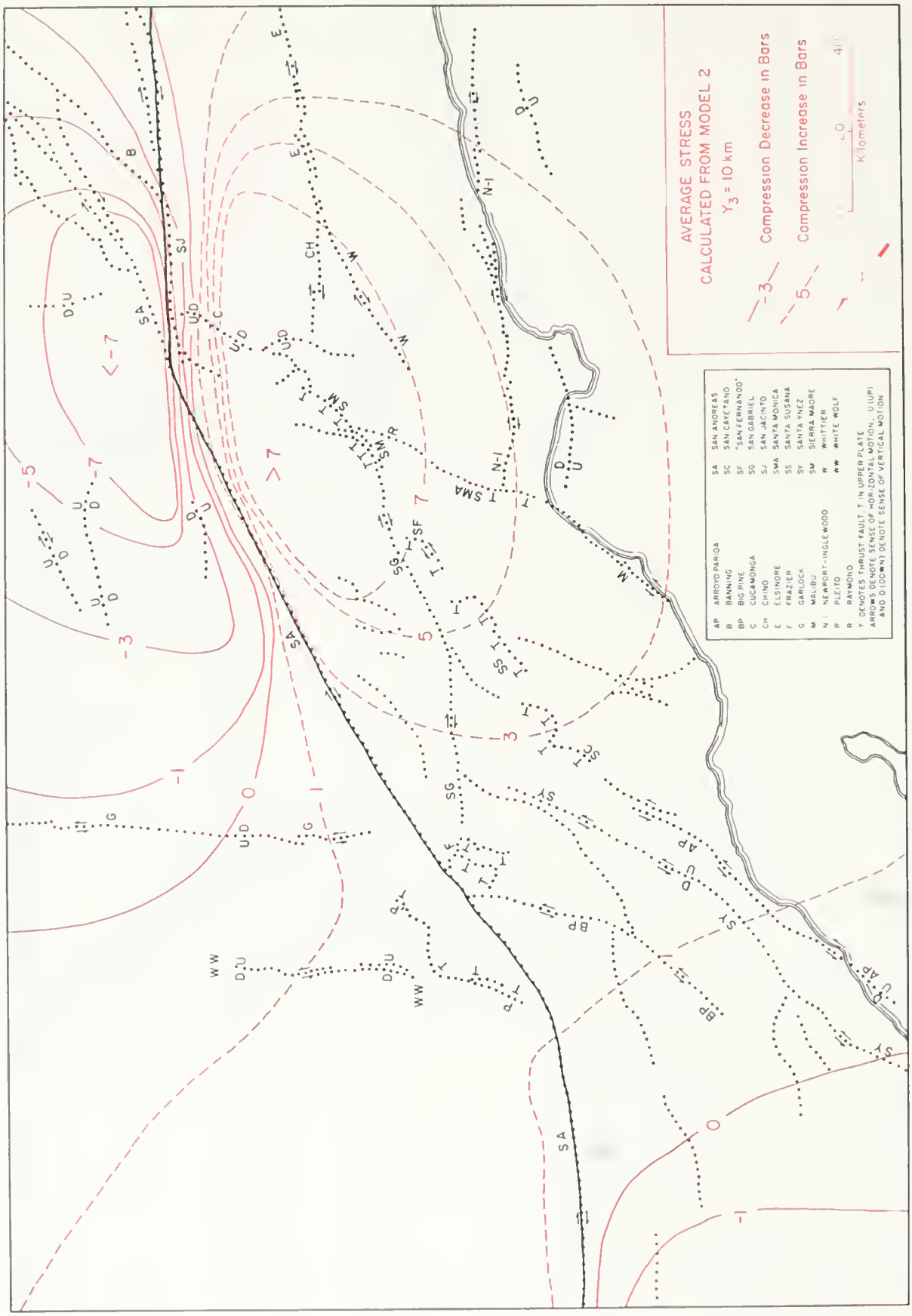

Figure 26. Isopachs at a depth of 10 km calculated from model 2.

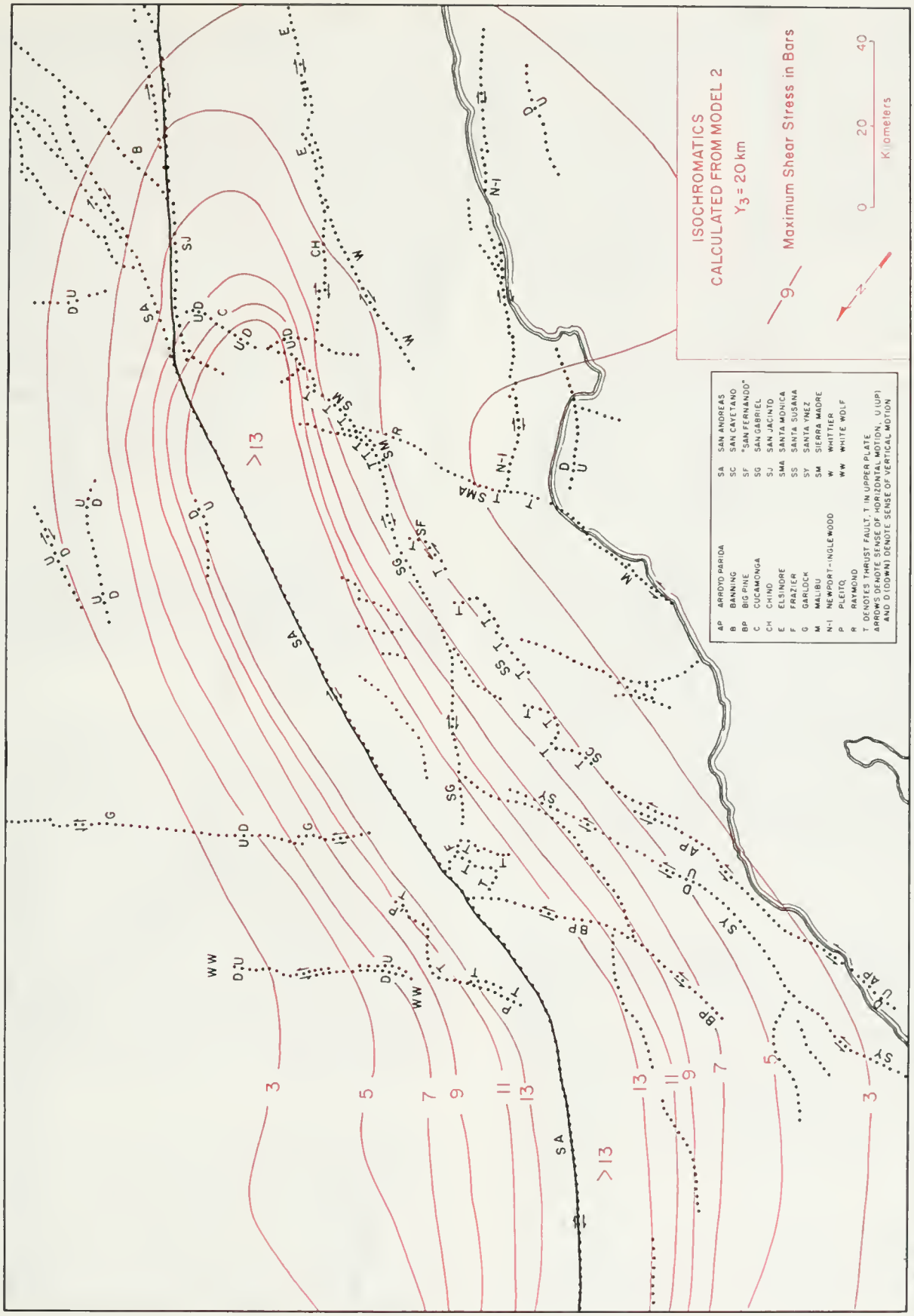

Figure 27. Isochromatics at a depth of 20 km calculated from model 2.

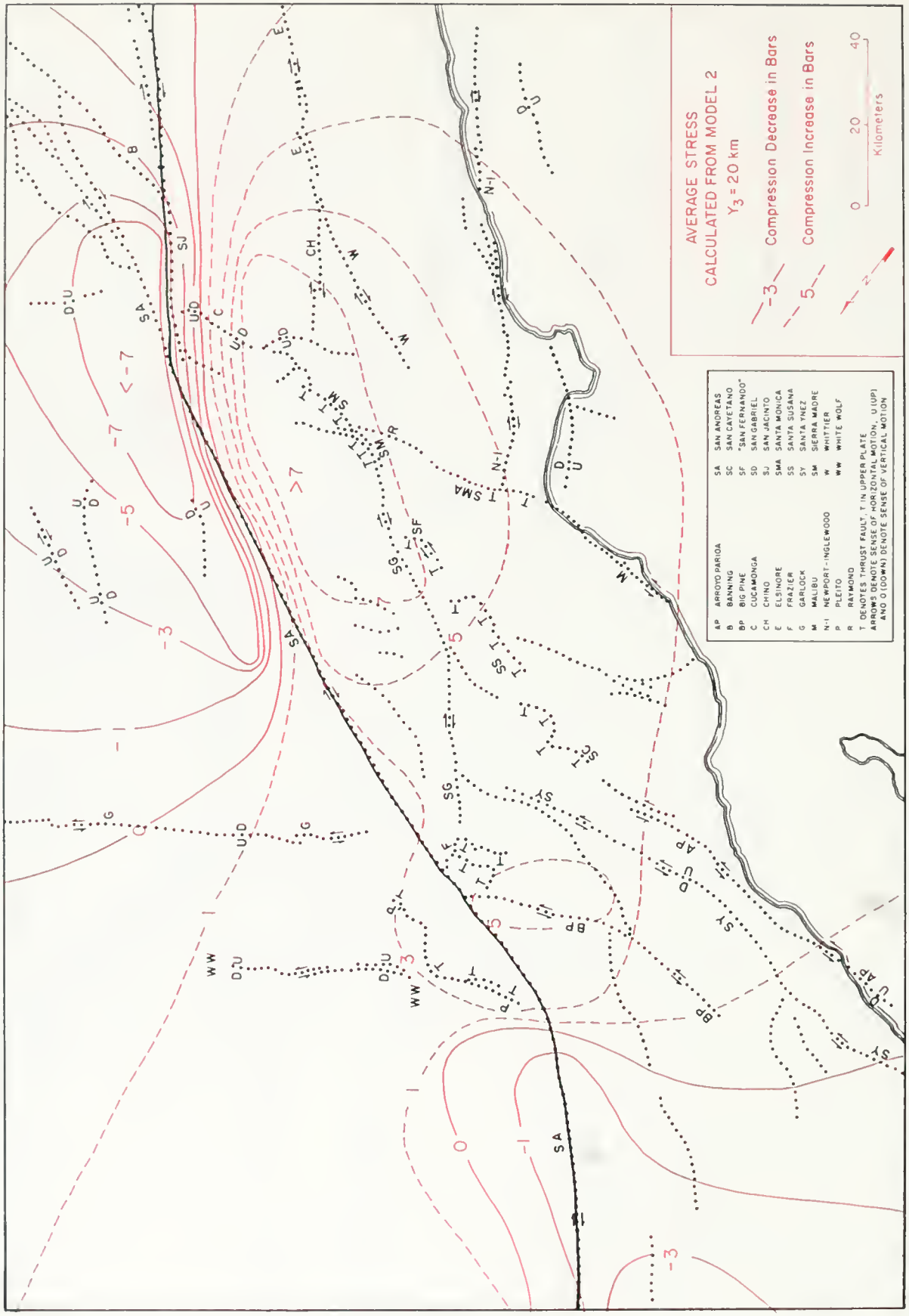

Figure 28. Isopachs at a depth of 20 km calculated from model 2.

Holocene ("Structural Characteristics"; Dibblee, 1966); this is to be expected from this model.

Third, when the predicted fault patterns of models 1 and 2 are compared to the observed faults, it is apparent that model 2 predicts the observed fault patterns better than model 1. This rather surprising result means that the depth of the locked zone is greater than would have been expected based on data from central California (see "Mathematical Model of the San Andreas Fault" and Appendix A). This in turn indicates that past geodetic measurements (particularly the Geodimeter measurements) may have been made too close to the San Andreas fault to observe strain accumulation. To test this, the California Division of Mines and Geology intends to establish one and perhaps two trilateration arcs between Tejon and Cajon Passes that will extend 75 to 100 kms approximately normal to the San Andreas fault.

SEISMICITY AND SECONDARY FAULTING DETERMINED FROM THE MODELS

I want to use the calculated stresses to try to draw conclusions about (a) the occurrence of larger earthquakes in the study area; (b) the observed faults in the study area which have evidence of Holocene or Quaternary movement; and (c) possible zones of future significant seismicity in the study area.

Seismicity

Areas of Potential Failure

Areas of potential activity can be determined from the isochromatic and isopach maps presented earlier if failure criteria are established. Chinnery (1966a, b) discusses a way to do this for a straight strike–slip fault. He first determines the shear stress drop τ°_{12} at the center of the fault; then, assuming the shear stress drop relieves all the accumulated shear stress, he adds two different regional stress fields, each of whose τ°_{12} component equals τ°_{12}, to the calculated stress change field. The resulting stress fields are thus the stress left in the ground after an earthquake. He then assumed that (1) secondary faulting is likely where the maximum shear stress equals or exceeds τ°_{12}; (2) secondary faulting is likely in regions where the average compressive stress is reduced; and (3) secondary faulting is less likely when the average compressive stress is increased.

The problem in the present work is somewhat different in that I have assumed there is no pre–existing regional stress field. Thus, I can go directly to the calculation of areas of potential failure. The level of maximum shear stress necessary to produce failure must first be determined. Chinnery (1966a) determined a value of τ°_{12} of about 5 bars from the long straight strike–slip fault model be used. In the Transverse Ranges, faulting is more often dip–slip than strike–slip, so this value of τ°_{12} might not apply. Thatcher and Hanks (1973) have shown that stress drops determined from S–wave spectra for earthquakes in the Transverse Ranges with magnitudes between 2.9 and 5.3 run from less than 1 bar to about 80 bars, with essentially no correlation between magnitude and stress drop. Savage and Wood (1971) quote a stress drop of about 10 bars for the magnitude 7.7 Arvin–Tehachapi earthquake; and estimates of the stress drop of the magnitude 6.5 San Fernando earthquake run from 21 to 34 bars (Hanks, 1974). If it is assumed that the stress drop in an earthquake completely relieves the maximum shear stress (τ_{max}), then all those areas where τ_{max} exceeds about 1 bar should be considered.

From the above discussion, areas of potential failure will be determined by the following rules:

(a) Failure is most likely in areas where the average compressive stress is reduced and where the maximum shear stress is greater than 3 bars.

(b) Failure is likely in areas where the average compressive stress has been slightly increased (by about 1 bar) and the maximum shear stress exceeds 5 bars.

(c) Failure is also likely in areas where the maximum shear stress exceeds 13 bars and the increase in average compressive stress does not exceed 7 bars.

For rule "a", the value of 3 bars is between the 1 bar or less found by Thatcher and Hanks (1974) and the 5 bars used by Chinnery (1966a). If the average compressive stress has been increased, it seems reasonable to require failure at a higher value of the maximum shear stress. Thus, while the values in rule "b" are somewhat arbitrary, they seem reasonable. Finally, it also seems reasonable to say that failure is also likely to occur even in those regions where the average compressive stress has increased if the maximum shear stress is very high. The values of 13 bars for the maximum shear stress and 7 bars for the average compressive stress are also arbitrary, but they do not appear to be unacceptable.

Historic Seismicity Compared to Areas of Potential Failure

Using these rules and the data from "Calculated Stress Fields", areas of potential failure were determined at the surface and at depths of 10 and 20 km for both models. Figures 29 to 32 show these areas at the surface and at a depth of 20 km for models 1 and 2, respectively. The potential failure areas at the 10 and 20 km depths were similar for each model, and hence, only the potential failure areas at 20 km are presented. Figures 29 to 32 also show the epicenters from figure 5. The accuracy of the pre–1932 epicenters is probably no better than ± 50 km, while the accuracy of the post–1932 epicenters is at worst about ± 15 km.

The only events that do not lie in, or near, the areas of potential failure are those to the south of the Malibu–Santa Monica–Raymond trend and three events offshore from the Arroyo Parida fault. The 1910 and 1938 (and possibly the 1903) events are probably associated with the

Elsinore fault, and three other events (1933 and two in 1941) are associated with the Newport–Inglewood fault. Recall that both the Newport–Inglewood and the Elsinore fault zones are characterized by predominantly right–lateral strike–slip motion, and they may be reacting to the same stress system that produces movement on the San Andreas fault. The occurrence of the other events in the Santa Barbara Channel, well away from the areas of potential failure, is more difficult to account for; but the events are probably far enough from the San Andreas fault that we should not expect the models to have much effect.

Note that the events in the eastern corner of the area are generally in an area of decreased average compressive stress, but the maximum shear stress is less than 3 bars. This suggests that rule "a" in "Areas of Potential Failure" may be somewhat conservative.

Figures 29 to 32 suggest that the areas of potential failure derived from models 1 and 2 do in fact delineate areas of high seismicity and that the seismicity in the Transverse Ranges is lower outside these areas of potential failure. Figures 31 and 32 further suggest that model 2 may be somewhat better than model 1, for the areas of potential failure determined from model 2 include somewhat more events north of the San Andreas fault.

Secondary Faulting

Theory suggests that, in unfractured material, failure should occur on the slip planes (Jaeger and Cook, 1969). The slip planes are at angles of ± 45° to the largest compressive stress axis, but laboratory evidence indicates that failure of initially unfractured rocks usually occurs on planes at angles of between 30° and 45° to the largest compressive stress axis (Jaeger and Cook, 1969). If the material contains fractures, then further slippage tends to occur on the previously existing fractures, even though these fractures may not make angles of 30° to 45° with the axis of greatest compression. Thus, the slip planes will be presented as the simplest way of visualizing the orientation of potential slippage.

By combining the areas of likely failure (figures 29 to 32) with the slip planes presented in "Calculated Stress Fields", the orientation of likely fault planes can be determined. Figure 33 shows the likely slip directions determined from model 1 at the surface. Of the left–lateral faults showing Holocene and Quaternary movement that lie within the region of potential failure, only the Big Pine fault is sub–parallel to a likely slip direction. A few right–lateral faults in the northwest corner of figure 33 are within the region of potential failure and have trends sub–parallel to likely slip directions. The extreme northern end of the San Gabriel fault also lies sub–parallel to a likely slip direction.

Figure 33 suggests that model 1 could produce the observed sense of movement on a few of the faults in the study area in the upper 1 to 2 km of the earth.

Figure 34 shows the orientation of likely fault planes at the surface determined from model 2. The left–lateral planes are sub–parallel to the White Wolf and the Garlock faults and parts of the Big Pine and the Santa Ynez faults. The right–lateral planes are sub–parallel to the northern part of the San Gabriel fault and to the faults in the northwestern corner of the figure.

When figures 33, 34, 15, and 23 are considered together, it is apparent that model 2 more accurately predicts the observed sense of motion on the White Wolf and the Garlock faults than does model 1. Model 2 also delineates areas of higher seismicity more clearly than does model 1. While neither model includes the 1971 San Fernando epicenter within an area of potential failure, the epicenter of this earthquake does lie closer to the area of potential failure determined from model 2 than that determined from model 1. Thus, the results of this study suggest that the depth of the locked section is greater than would have been estimated from epicenter data ("Mathematical Model of the San Andreas Fault").

Discussion and Conclusions

In this chapter, we have shown that both models 1 and 2 define reasonably well the areas in the Transverse Ranges where larger earthquakes have occurred, but model 2 tends to predict the observed motion on mapped faults better than model 1. Thus, I can use these results with a fair degree of confidence to discuss the future seismicity of the Transverse Ranges.

The following facts must be kept in mind, however. The occurrence of any earthquake in the Transverse Ranges does alter the stress fields presented in this Chapter; and the larger the earthquake, the greater will be its effect on the stress field. Thus, to arrive at the "real" stress field in the Transverse Ranges at the present time, I should include the effects of all the earthquakes which have occurred since 1857. I nonetheless feel that the results presented here can be used to draw general conclusions about the future seismicity of the Transverse Ranges.

Subject to these reservations, the following statements can be made. Any future large earthquakes can be expected to occur in, or very near, the areas of potential failure shown on figures 31 and 32. Only those faults that trend parallel or sub–parallel to those shown will be involved in the future large earthquakes. Of course, once the fault movement has been initiated, it could propagate well beyond the areas shown in figures 31 and 32.

Specifically, based on model 2, future large earthquakes in the Transverse Ranges are most likely on the Garlock fault, the Pleito fault, the Frazier fault, the Big Pine fault, and the northern end of the San Gabriel fault. If the thrust faults of the area—such as the San Cayetano, the Santa Susana, and the Sierra Madre—extend into the area of potential failure at depth, large earthquakes can be expected on them. Future movement on the Santa Ynez, the

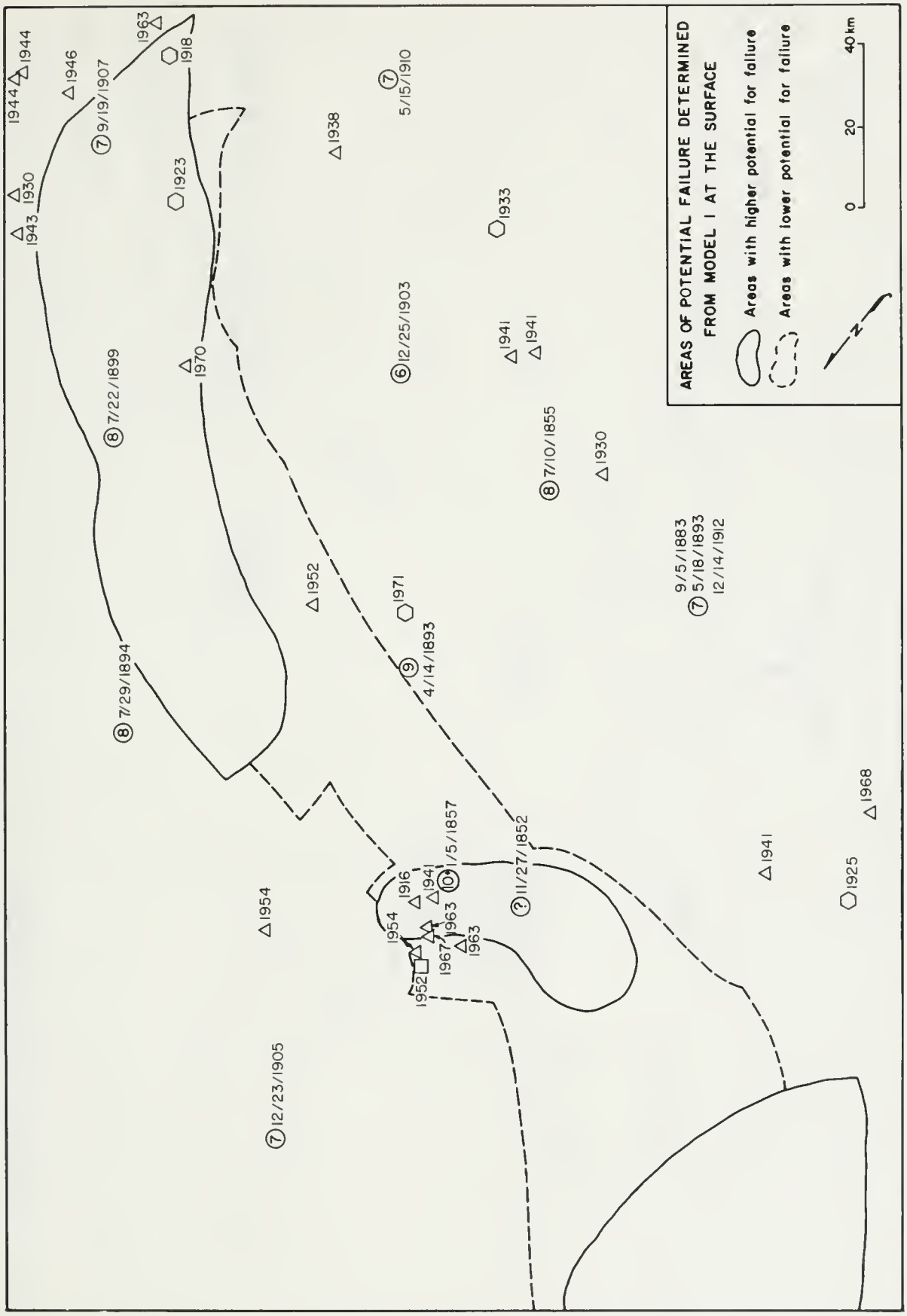

Figure 29. Areas of potential failure at the ground surface calculated from model 1.

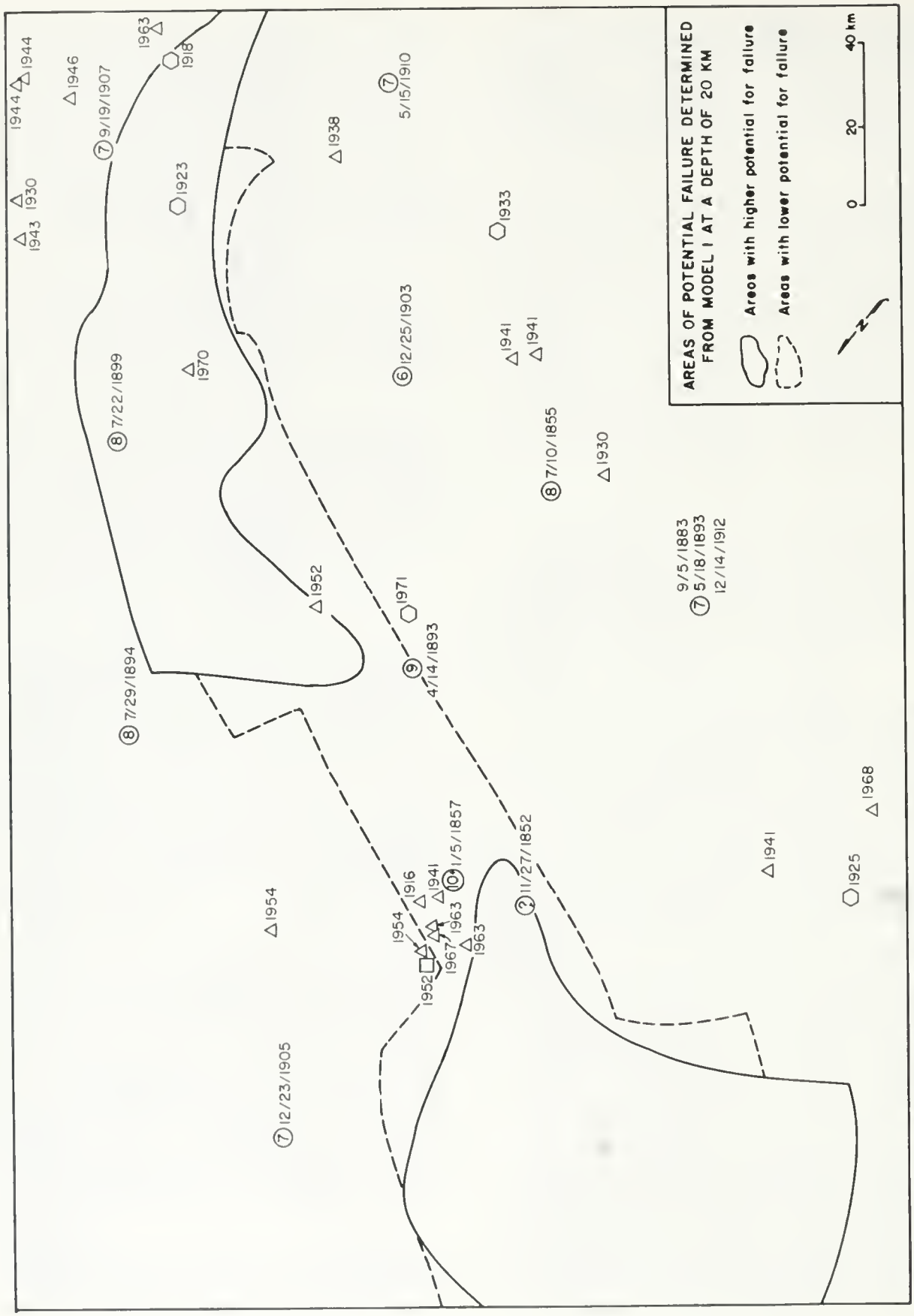

Figure 30. Areas of potential failure at a depth of 20 km calculated from model 1.

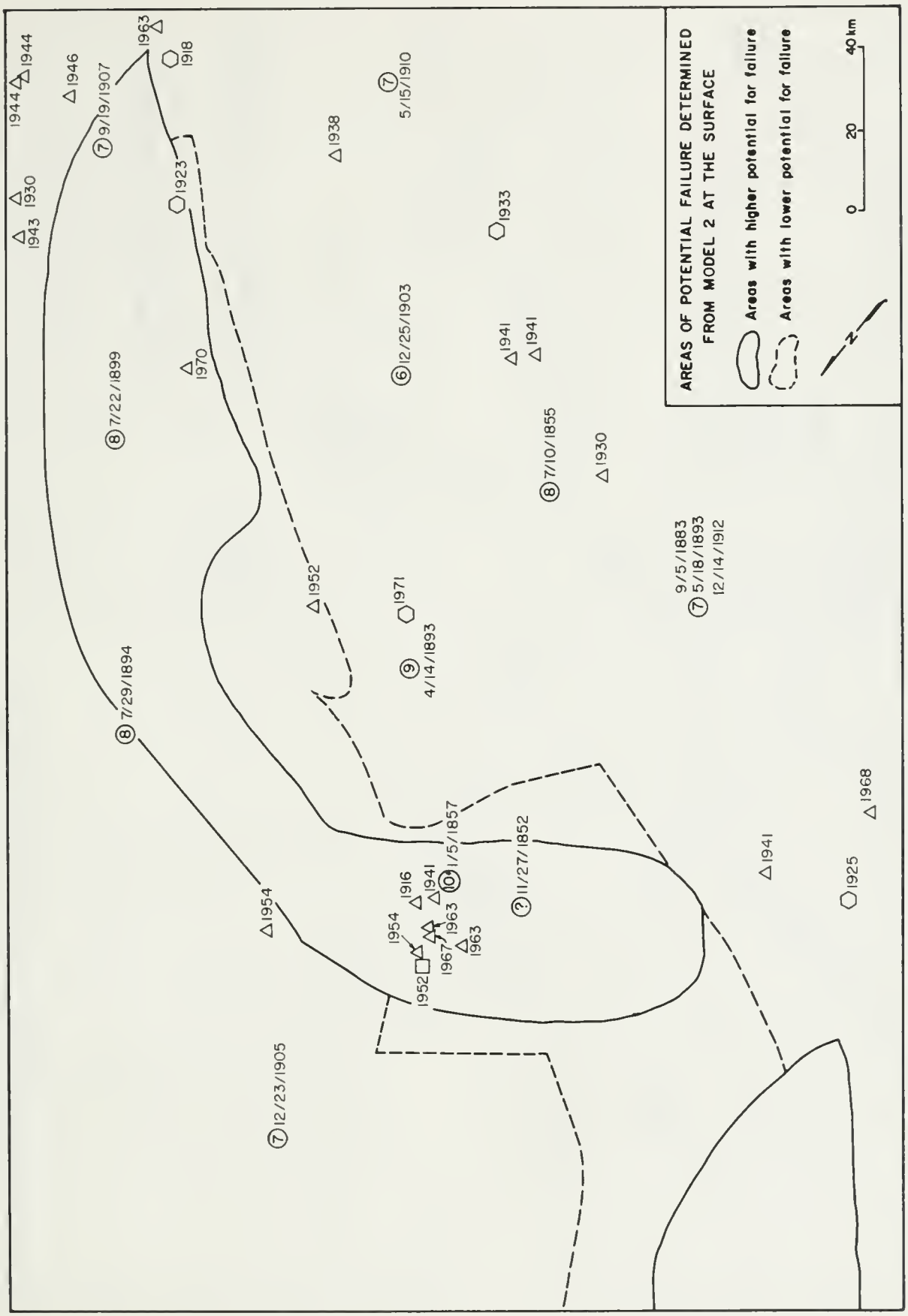

Figure 31. Areas of potential failure at the ground surface calculated from model 2.

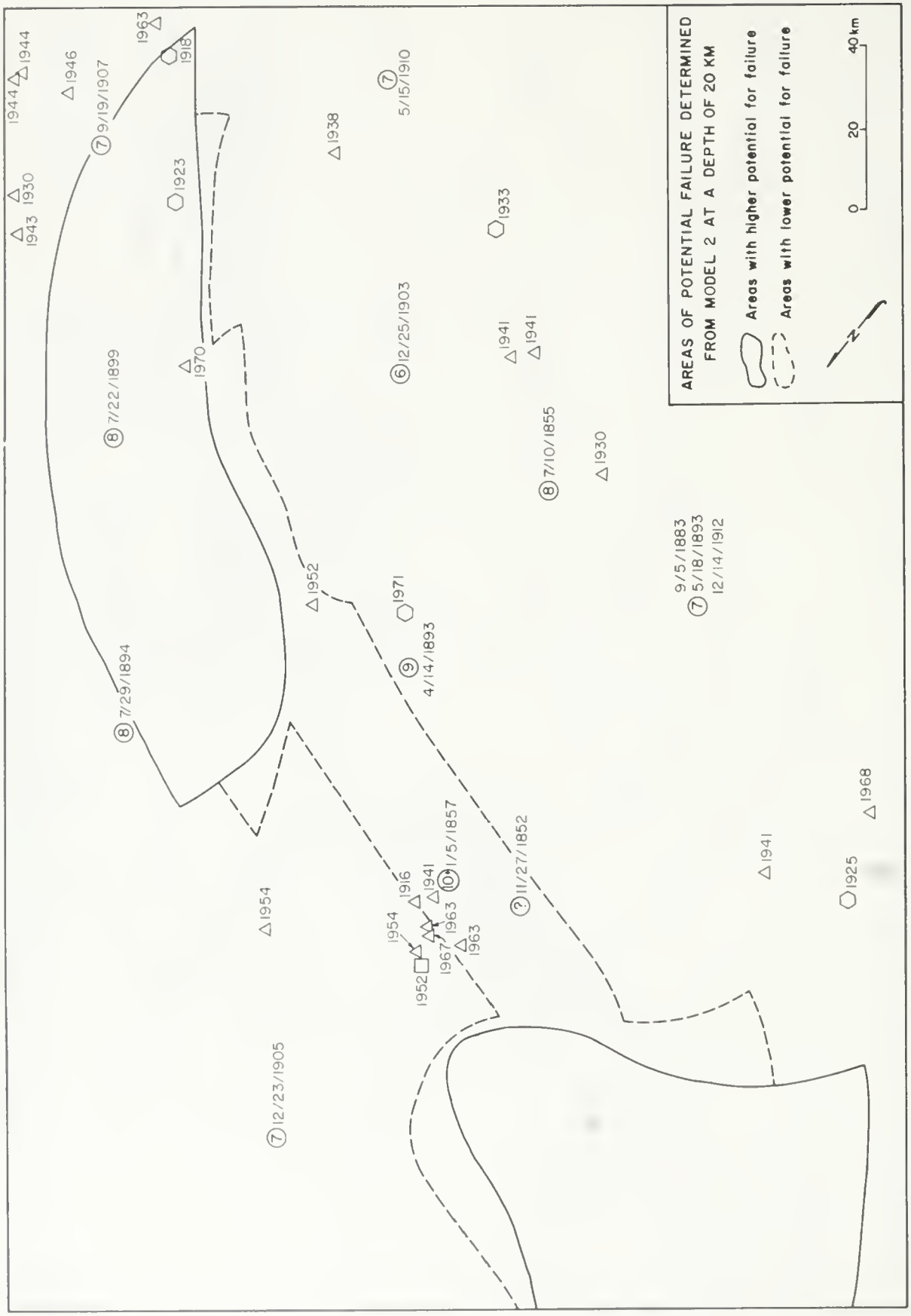

Figure 32. Areas of potential failure at a depth of 20 km calculated from model 2.

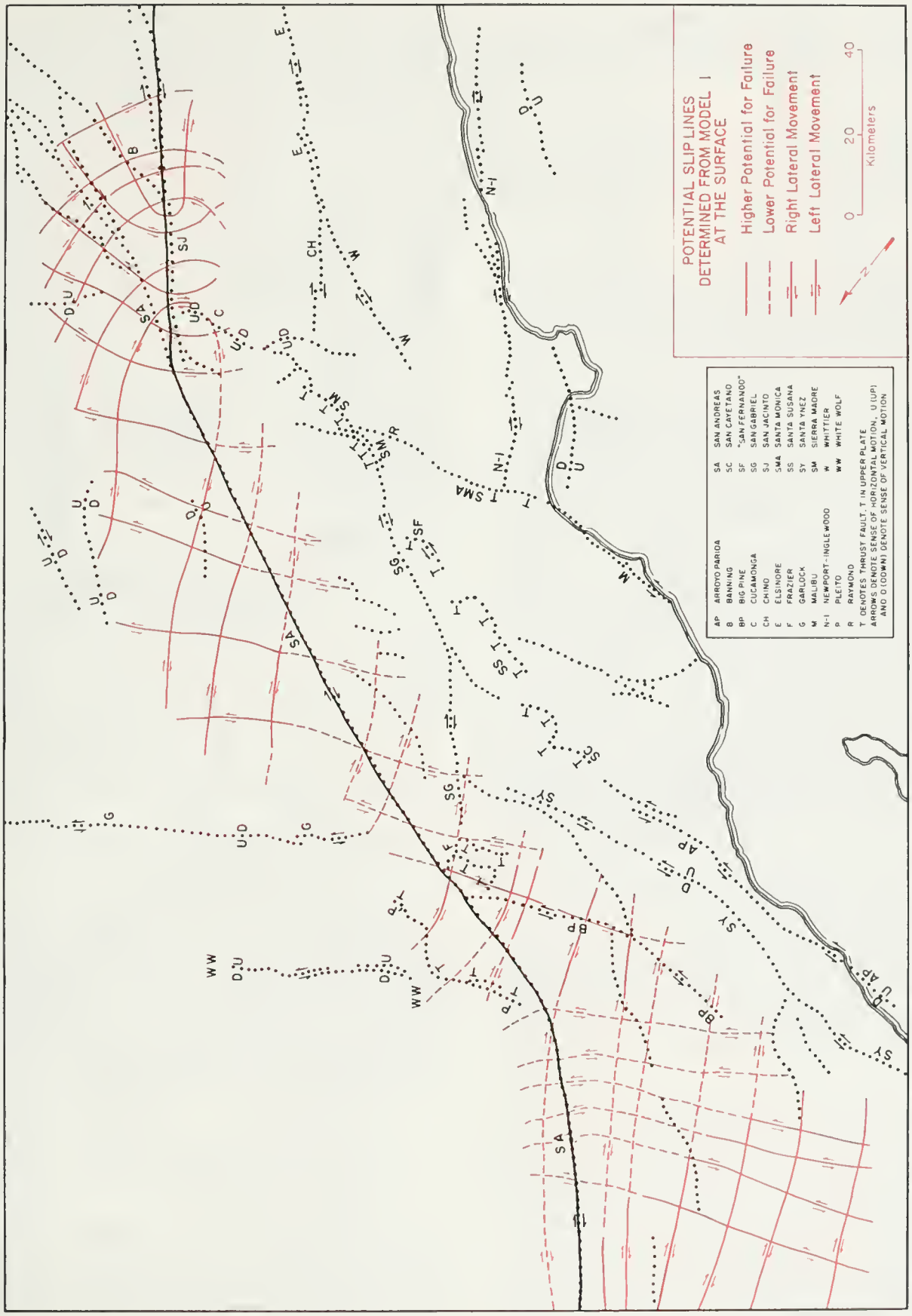

Figure 33. Potential slip directions at the ground surface calculated from model 1.

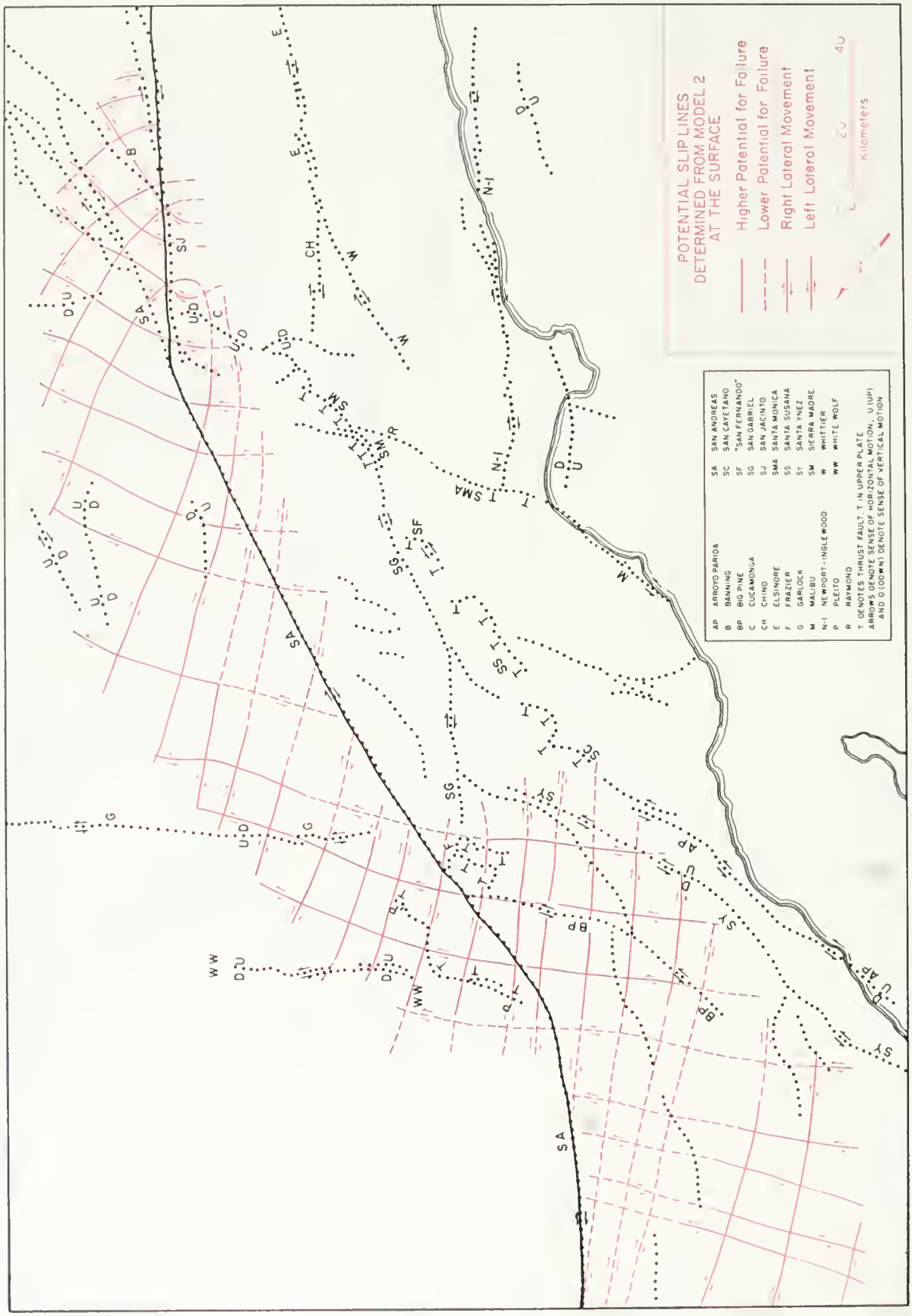

Figure 34. Orientation of potential fault planes at the ground surface calculated from model 2.

Arroyo Parida, the Malibu, the Santa Monica, and the Raymond faults is not indicated by the model. Thus, some stress system in addition to that produced by the San Andreas fault must be invoked to account for the observed Quaternary and Holocene movement on these faults.

A major question that arises is whether or not the calculated stress fields are large enough to produce the observed earthquakes. I am not requiring that the calculated stress be large enough to cause failure of virgin rock; but rather, I am asking that the stresses be large enough to initiate sliding on previously existing fractures. Intuitively, I would expect that the stress required to initiate sliding could be much less than that required to form new fractures (Jaeger and Cook, 1969). Recall also that the stress drops (1 to 80 bars) determined from S–wave spectra for earthquakes in the Transverse Ranges by Thatcher and Hanks (1973) and by Savage and Wood (1971) are within the range of calculated values of maximum shear stress. The deviatoric horizontal compressive stresses determined from the model are at least an order of magnitude less than the value of about 1 kilobar determined by Hanks (1974) for the 1971 San Fernando earthquake. However, as Hanks (1974) points out, this value seems to apply only to the first seconds of the fracture process, while the overall stress drop is on the order of 30 bars. It is entirely possible that this high stress is a stress concentration due to a local change in material properties.

It also should be pointed out that this model cannot be used to make specific earthquake predictions. The model is based on an isotropic, homogeneous half–space and the Transverse Ranges are anything but that. Local stress concentrations undoubtedly exist wherever the material properties change, and it is these local stress concentrations that must be responsible for individual earthquakes.

CONCLUSIONS AND SUGGESTIONS FOR FURTHER WORK

The vertical displacement and stress change fields have been calculated from a relatively simple dislocation model of the San Andreas fault in the Transverse Ranges. The calculated vertical displacement fields from two models resemble the general topographic features of the Transverse Ranges, and this suggests that the present topography may have been produced by the bend in the San Andreas fault. It does not appear to be possible to select between the two models of the San Andreas fault based on the topography above.

Several conclusions result from the interpretation of the stress change fields calculated from the two models.

First, it does appear to be possible to select between the two models based on the calculated stress fields. Model 2, the model with the locked zone 30 km deep, seems to explain the observed fault patterns and strain data better than model 1, the model with a 15–km–deep locked section. This, of course, means that the zone of stable sliding is deeper in the Transverse Ranges than in central California (see "Mathematical Model of the San Andreas Fault" and Appendix A).

Second, the principal compressive stresses calculated from the model have a north–south orientation throughout most of the study area. This agrees with the conclusions drawn by Hill (1955), Benioff (1955), and Hanks (1974).

Third, the areas of potential failure determined from the model include many of the larger earthquakes in the Transverse Ranges; and the larger events that have not occurred in, or adjacent to, the area of potential failure can be related to movement on faults in the Peninsular Ranges.

Fourth, the slip planes determined from the model for the 1952 Arvin–Tehachapi and the 1971 San Fernando earthquakes have azimuths similar to those of the observed fault planes, and the calculated principal stress system could certainly produce the sense of movement observed for these two earthquakes.

Finally, the calculated stress system could explain the pattern of faults having Holocene or Quaternary movement in the Transverse Ranges. This does not necessarily imply that the bend in the San Andreas fault is responsible for the origin of the Transverse Ranges. It does, however, mean that, given a complex set of faults of many different orientations, the stress system produced by the bend in the San Andreas fault will cause activity mainly on those faults that are favorably oriented to the stress system at the time of observation. For the same time interval, other less favorably oriented faults will show a much lower level of activity, even though these faults may have been much more active at some earlier time.

A complete discussion of the origin of the Transverse Ranges is beyond the scope of this paper. However, some brief comments must be made. The models discussed here do not produce stress fields that are large enough to initiate failure in fresh rock. Thus, the bend in the San Andreas fault probably did not produce the Transverse Ranges. But I do feel that the stresses produced by the bend are large enough to maintain at least some of the Transverse Ranges structures after these structures enter the stress fields.

There is reasonably good evidence for much greater displacements on the San Andreas fault system north of the Transverse Ranges than on the fault system south of the Transverse Ranges (Berry, 1973; Dickinson and others, 1972). The interpretation of this evidence is that the San Andreas fault system south of the Transverse Ranges is younger than the northern part of the system and that it probably took some time for the fault to propagate south from the present location of the Transverse Ranges. Thus, the fault probably "ended" in the vicinity of the Tehach-

api Mountains for a considerable length of time, and the analysis used by Chinnery (1966a, b) could be modified and applied to attempt to account for some or all of the structures of the Transverse Ranges. This seems to be a promising line of attack on the problem of the origin of the Transverse Ranges.

It is rather remarkable that the simple model of a dislocation in an isotropic, homogeneous, linearly elastic half–space can provide a fairly reasonable approximation of the observed faulting in such a heterogeneous environment as the Transverse Ranges. The model can be improved and made more realistic in several ways. First, the assumption of an elastic half–space can be relaxed and non–linear effects included by using the work of Rosenman and Singh (1973) and Singh and Rosenman (1974). This would not involve major changes to the computer programs used here, and it would allow a more realistic time history of the stress accumulation to be studied.

At the same time, the results of Mansinha and Smylie (1971) can be incorporated to study the effects that movement on some of the thrust faults in the area would have on the stress system due to the bend in the San Andreas fault. Thus, we would be able to follow the stress field through several cycles of accumulation and release on the San Andreas fault and perhaps study the development of the Transverse Ranges. These studies would still be an isotropic, homogeneous half–space model and would be fairly simple to carry out, for the equations all exist in a closed form and, hence, can be readily evaluated.

To construct an even more realistic model, a three–dimensional finite element model of the region would have to be used. This would mean, of course, that the basic equations would have to be integrated numerically for each model one is interested in. This would very likely be a time–consuming, expensive task, even on the present generation of high–speed computers.

Finally, any further work with these models will be hampered by the lack of geodetic observations in the region. Thus, it will be very difficult to select one model as "better" than another. As a result of the present study, the California Division of Mines and Geology is redirecting part of its Geodimeter measurement program to be able to obtain a greater amount of relevant data. In particular, trilateration arcs extending 50 to 75 km from the fault will be observed in an attempt to obtain more data on fault movements at depth.

REFERENCES CITED

Allen, C.R., 1957, San Andreas fault zone in San Gorgonio Pass, southern California: Geological Society of America Bulletin, v. 68, p. 315–350.

_____, 1968, The tectonic environments of seismically active and inactive areas along the San Andreas fault system, *in* Proceedings of conference on geologic problems of San Andreas fault system, Dickinson, W.R., and Grantz, Arthur, *editors:* Stanford University Publications, Geological Sciences, v. XI, p. 70–80.

Allen, C.R., St. Amand, P., Richter, C.F., and Nordquist, J.M., 1965, Relationship between seismicity and geologic structure in the southern California region: Seismological Society of America Bulletin, v. 55, p. 753–797.

Anderson, D.L., 1971, The San Andreas fault: Scientific American, v. 225, no. 5, p. 52–68.

Anonymous, 1967, Results of triangulation for earth movement study at California Aqueduct–fault crossing sites, Section 1, Supplement No. 2 – August 1967: U.S. Department of Commerce, National Ocean Survey.

Atwater, T., 1970, Implications of plate tectonics for the Cenozoic tectonic evolution of western North America: Geological Society of America Bulletin, v. 81, no. 12, p. 3513–3535.

Atwater, T., and Molnar, P., 1973, Relative motion of the Pacific and North American plates deduced from sea–floor spreading in the Atlantic, Indian, and South Pacific Oceans, *in* Proceedings of the conference on tectonic problems of the San Andreas fault system, Kovach, R.L., and Nur, Amos, *editors:* Stanford University Publications, Geological Sciences, v. XIII, p. 136–148.

Bailey, T.L., 1954, Geology of the western Ventura basin, Santa Barbara, Ventura, and Los Angeles Counties, *in* Geology of southern California, Johns, R.H., *editor:* California Division of Mines Bulletin 170, map sheet 4.

Bailey, T.L., and Johns, R.H., 1954, Geology of the Transverse Range province, southern California, *in* Geology of southern California, Johns, R.H., *editor,* California Division of Mines Bulletin 170, chapter II, p. 83–106.

Baird, A.K., Morton, D.M., Woodford, A.O., and Baird, K.W., 1974, Transverse Ranges province – A unique structural–petrochemical belt across the San Andreas fault system: Geological Society of America Bulletin, v. 85, no. 2, p. 163–174.

Benioff, H., 1955, Relation of the White Wolf fault to the regional tectonic pattern, *in* Earthquakes in Kern County, California, during 1952, Oakeshott, G.B., *editor:* California Division of Mines Bulletin 171, p. 203–204.

Ben–Menahem, A., Singh, S.J., and Solomon, F., 1970, Deformation of an homogeneous earth model by finite dislocations: Reviews of Geophysics and Space Physics, v. 8, p. 591–632.

Berry, Fred, 1973, Proposed solutions to certain tectonic problems of western North America with emphasis on California and the Basin and Range province: Unpublished manuscript.

Bolt, B.A., Lomnitz, C., and McEvilly, T.V., 1968, Seismological evidence on the tectonics of central and northern California and the Mendocino escarpment: Seismological Society of America Bulletin, v. 58, p. 1725–1767.

Bolt, B.A., and Marion, W.C., 1966, Instrumental measurement of slippage on the Hayward fault: Seismological Society of America Bulletin, v. 56, no. 2, p. 305–316.

Bolt, B.A., and Miller, R.D., 1971, Seismicity of northern and central California, 1965–1969: Seismological Society of America Bulletin, v. 61, no. 6, p. 1831–1847.

Brown, R.D. Jr., and Vedder, J.G., 1967, Surface tectonic fractures along the San Andreas fault, *in* The Parkfield–Cholame, California, earthquakes of June–August 1966: U.S. Geological Survey Professional Paper 579.

Brune, J.N., 1974, Current status of understanding quasi–permanent fields associated with earthquakes: EOS Transactions, v. 55, no. 9, p. 820–827.

Brune, J.N., and Allen, C.R., 1967, A micro–earthquake survey of the San Andreas fault system in southern California: Seismological Society of America Bulletin, v. 57, no. 2, p. 277–296.

Buchanan, J.N., Ziony, J.I., and Castle, R.O., 1973, Recent elevation changes across part of the Transverse Ranges near Ventura, California, *abstract:* Geological Society of America, Abstracts with Programs, v. 5, no. 1, Feb. 1973, p. 17.

Burford, R.O., 1966, Strain analysis across the San Andreas fault and Coast Ranges of California: Annales Academiae Scientiarum Fennicae, Series A, III, Geologica–Geographica, v. 90, p. 99–110.

Byerlee, J.D., and Brace, W.F., 1968, Stick slip, stable sliding, and earthquakes–effect of rock type, strain rate, and stiffness: Journal of Geophysical Research, v. 73, no. 18, p. 6031–6037.

Carman, M.F. Jr., 1964, Geology of the Lockwood Valley area, Kern and Ventura Counties, California: California Division of Mines and Geology, Special Report 81, 62 p.

Castle, R.O., Alt, J.N., Savage, J.C., and Balazs, E.I., 1974, Elevation changes preceding the San Fernando earthquake of February 9, 1971: Geology, v. 2, no. 2, p. 61–66.

Cherry, J.T., and Savage, J.C., 1972, Rock dilatancy and strain accumulation near Parkfield, California: Seismological Society of America Bulletin, v. 62, p. 1343–1347.

Chinnery, M.A., 1961, The deformation of the ground surface faults: Seismological Society of America Bulletin, v. 51, p. 355.

_____, 1963, The stress changes that accompany strike–slip faulting: Seismological Society of America Bulletin, v. 53, p. 921.

_____, 1966a, Secondary faulting – I. Theoretical aspects: Canadian Journal of Earth Sciences, v. 3, p. 163–174.

_____, 1966b, Secondary faulting – II. Geological aspects: Canadian Journal of Earth Sciences, v. 3, p. 175–190.

Chinnery, M.A., and Jovanovich, D.B., 1972, The effect of earth layering on earthquake displacement fields: Seismological Society of America Bulletin, v. 62, no. 6, p. 1629–1639.

Coffman, J.L., and von Hake, C.A., 1973, Earthquake history of the United States, Publication 41–1, Revised edition (through 1970): U.S. Department of Commerce, Environmental Data Service.

Crowell, J.C., 1954, Strike–slip displacement of the San Gabriel fault, southern California, *in* Geology of southern California, Johns, R.H., *editor:* California Division of Mines Bulletin 170, chapter IV, p. 49–52.

_____, 1962, Displacement along the San Andreas fault, California: Geological Society of America, Special Paper 71, 61 p.

———, 1968, Movement histories of faults in the Transverse Ranges and speculations on the tectonic history of California, *in* Proceedings of conference on geologic problems of San Andreas fault system, Dickinson, W.R., and Grantz, A., *editors:* Stanford University Publications, Geological Sciences, v. XI, p. 323–341.

Curray, J.R., and Nason, R.D., 1967, San Andreas fault north of Point Arena, California: Geological Society of America Bulletin, v. 78, p. 413–418.

Davis, G.A., and Burchfiel, B.C., 1973, Garlock fault – An intracontinental transform structure, southern California: Geological Society of America Bulletin, v. 84, p. 1407–1422.

Dibblee, T.W. Jr., 1950, Geology of southwestern Santa Barbara County, California: California Division of Mines Bulletin 150.

———, 1966, Geology of the central Santa Ynez Mountains, Santa Barbara County, California: California Division of Mines and Geology, Bulletin 186.

———, 1968, Displacements on the San Andreas fault system in the San Gabriel, San Bernardino, and San Jacinto Mountains, southern California, *in* Proceedings of conference on geologic problems of San Andreas fault system, Dickinson, W.R., and Grantz, A., *editors:* Stanford University Publications, Geological Sciences, v. XI, p. 260–278.

Dickinson, W.R., Cowan, D.S., and Schweickert, R.A., 1972, Test of new global tectonics–Discussion: American Association of Petroleum Geologists Bulletin, v. 56, no. 2, p. 375–384.

Eaton, J.P., O'Neill, M.E., and Murdock, J.N., 1970, Aftershocks of the 1966 Parkfield–Cholame, California, earthquake – A detailed study: Seismological Society of America Bulletin, v. 60, no. 4, p. 1151–1198.

Ellsworth, W.L., Campbell, R.H., Hill, D.P., Page, R.A., Alewine, R.W. III, Hanks, T.C., Heaton, T.H., Hilemon, J.A., Kanamori, K., Minster, B., and Whitcomb, J.H., 1973, Point Mugu, California, earthquake of 21 February 1973 and its aftershocks: Science, v. 182, p. 1127–1129.

Greensfelder, R.W., 1972, Crustal movement investigations: California Division of Mines and Geology, Special Publication 37.

Greensfelder, R.W., and Bennett, J.H., 1973, Characteristics of strain variation along the San Andreas fault from Geodimeter measurements, *in* Proceedings of the conference on tectonic problems of the San Andreas fault system, Kovach, R.L., and Nur, A., *editors:* Stanford University Publications, Geological Sciences, v. XIII, p. 54–63.

Gutenberg, B., 1955, The first motion in longitudinal and transverse waves of the main shock and the direction of slip, *in* Earthquakes in Kern County, California, during 1952, Oakeshott, G.B., *editor:* California Division of Mines Bulletin 171, p. 165–170.

Hamilton, R.M., Yerkes, R.F., Brown, R.D. Jr., Burford, R.O., and DeNoyer, J.M., 1969, Seismicity and associated effects, Santa Barbara region, *in* Geology, petroleum development, and seismicity of the Santa Barbara Channel region, California: U.S. Geological Survey, Professional Paper 679–D, p. 47–68.

Hanks, T.C., 1974, The faulting mechanism of the San Fernando earthquake: Journal of Geophysical Research, v. 79, no. 8, p. 1215–1229.

Healy, J.H., 1963, Crustal structure along the coast of California from seismic –refraction measurements: Journal of Geophysical Research, v. 68, no. 20, p. 5777–5787.

———, 1971, A comment on the evidence for a worldwide zone of low seismic velocity at shallow depths in the earth's crust, *in* The structure and physical properties of the Earth's crust, Heacock, J.G., *editor:* American Geophysical Union, Geophysical Monograph 14, p. 35–40.

Hileman, J.A., Allen, C.R., and Nordquist, J.M., 1973, Seismicity of the southern California region, 1 January 1932 to 31 December 1972: Seismological Laboratory, California Institute of Technology, Pasadena, California.

Hill, M.L., 1955, Nature of movements on active faults in southern California, *in* Earthquakes in Kern County, California, during 1952, Oakeshott, G.B., *editor:* California Division of Mines Bulletin 171, p. 37–40.

———, 1971, A test of new global tectonics; comparisons of northeast Pacific and California structures: American Association of Petroleum Geologists Bulletin, v. 55, no. 1, p. 3–9.

———, 1974, Is the San Andreas a transform fault? Geology, v. 2, no. 11, p. 535–536.

Hofmann, R.B., 1968, Geodimeter fault movement investigations in California: California Department of Water Resources, Bulletin 116–6, 183 p.

Holdahl, S.R., 1973, Studies of precise leveling at California fault sites, *in* Reports on geodetic measurements of crustal movement, 1906–71, Meade, B.K., *editor:* U.S. Department of Commerce, National Oceanic and Atmospheric Administration Paper 61.

Isacks, B., Oliver, J., and Sykes, L.R., 1968, Seismology and the new global tectonics: Journal of Geophysical Research, v. 73, no. 11, p. 5855–5900.

Jaeger, J.C., and Cook, N.G.W., 1969, Fundamentals of rock mechanics: Methuen and Company, Ltd., London.

Johns, R.H., 1954, Geology of the Peninsular Range province, southern California and Baja California, *in* Geology of southern California, Johns, R.H., *editor:* California Division of Mines Bulletin 170, chapter 2, p. 29–52.

———, 1973, Tectonic evolution of the Transverse Ranges province as related to the San Andreas fault system, *in* Proceedings of the conference on tectonic problems of the San Andreas fault system: Kovach, R.L., and Nur, A., *editors:* Stanford University Publications, Geological Sciences, v. XIII, p. 149–170.

Jennings, C.W., 1973, Preliminary fault map: California Division of Mines and Geology, Preliminary Report 13, scale 1:750,000.

Jovanovich, D.B., Husseini, M.I., and Chinnery, M.A., 1974a, Elastic dislocation in a layered half–space, I. Basic theory and numerical methods: Geophysical Journal of the Royal Astronomical Society, v. 39, p. 205–217.

———, 1974b, Elastic dislocation in a layered half–space, II. The point source: Geophysical Journal of the Royal Astronomical Society, v. 39, p. 219–239.

Judson, S., and Ritter, D.F., 1964, Rates of regional denudation in the United States: Journal of Geophysical Research, v. 69, no. 16, p. 3395–3401.

Kanamori, H., and Chung, W.Y., 1973, Temporal changes in P–wave velocity in southern California, *abstract:* EOS Transactions, v. 54, no. 11, p. 1135.

Landisman, M., Mueller, S., and Mitchell, B.J., 1971, Review of evidence for velocity inversions in the continental crust, *in* The structure and physical properties of the earth's crust, Heacock, J.G., *editor:* American Geophysical Union, Geophysical Monograph 14, p. 11–34.

Lee, W.H.K., and Vedder, J.G., 1973, Recent earthquake activity in the Santa Barbara Channel region: Seismological Society of America Bulletin, v. 63, no. 5, p. 1757–1774.

Le Pichon, X., 1968, Sea–floor spreading and continental drift: Journal of Geophysical Research, v. 73, no. 12, p. 3661–3697.

McGinley, J.R., 1969, A comparison of observed permanent tilts and strains due to earthquakes with those calculated from displacement dislocations in elastic earth models: Ph.D. thesis, California Institute of Technology.

Monsinha, L., and Smylie, D.E., 1971, The displacement fields of inclined faults: Seismological Society of America Bulletin, v. 61, no. 5, p. 1433–1440.

Meade, B.K., 1966, Horizontal crustal movements in the United States: Annales Academiae Scientiarum Fennicae, Series A, III., Geologica—Geographica, v. 90, p. 256–266.

_____, 1968, Report of the sub–commission for North America, Third symposium on recent crustal movements: International Association of Geodesy IUGG, Leningrad, USSR, May 1968.

_____, 1971a, Horizontal movement along the San Andreas fault system: Royal Society of New Zealand Bulletin, v. 9, p. 175–179.

_____, 1971b, Report of the sub–commission on recent crustal movements in North America: Paper presented at the XV General Assembly of IUGG, International Association of Geodesy, Moscow, USSR, August 2–14, 1971.

Meade, B.K., and Small, J.B., 1966, Current and recent movement on the San Andreas fault, *in* Geology of northern California, Bailey, E.H., *editor:* California Division of Mines and Geology, Bulletin 190, p. 385–391.

Merrill, W.R., 1954, Geology of the Sespe Creek–Pine Mountain area, Ventura County, *in* Geology of southern California, Jahns, R.H., *editor:* California Division of Mines Bulletin 170, map sheet 3.

Miller, R.W., 1966a, Results of triangulation for earth movement study at California Aqueduct–fault crossing sites, Section II, Supplemental No. 1 – September 1966: U.S. Department of Commerce, National Ocean Survey.

_____, 1966b, Results of triangulation for earth movement study at California Aqueduct–fault crossing sites, Section VI, North and South San Francisco Bay Aqueducts – November, 1966: U.S. Department of Commerce, National Ocean Survey.

_____, 1967a, Results of triangulation for earth movement study at California Aqueduct–fault crossing sites, Section VI, Supplement No. 3: U.S. Department of Commerce, National Ocean Survey.

_____, 1976b, Results of triangulation for earth movement study at California Aqueduct–fault crossing sites, Section I, Supplement No. 4 – November 1967: U.S. Department of Commerce, National Ocean Survey.

_____, 1968, Results of triangulation for earth movement study at California Aqueduct–fault crossing sites, Section V, Supplement No. 2 – October 1968: U.S. Department of Commerce, National Ocean Survey.

_____, 1969, Results of triangulation for earth movement study at California Aqueduct–fault crossing sites, Section II, Supplement No. 3 – August 1969: U.S. Department of Commerce, National Ocean Survey.

_____, 1970a, Results of triangulation for earth movement study at California Aqueduct–fault crossing sites, Section VI, Supplement No. 4 – March 1970: U.S. Department of Commerce, National Ocean Survey.

_____, 1970b, Results of triangulation for earth movement study at California Aqueduct–fault crossing sites, Section IV, Supplement No. 5 – March 1970: U.S. Department of Commerce, National Ocean Survey.

_____, 1970c, Results of triangulation for earth movement study, vicinity of Berkeley, El Cerrito, and Fremont, California, Supplement No. 1 – June 1970: U.S. Department of Commerce, National Ocean Survey.

_____, 1970d, Study of earth movement determined by triangulation, Camp Parks, vicinity of Pleasanton, California, Supplement No. 1 – June 1970: U.S. Department of Commerce, National Ocean Survey.

_____, 1970e, Results of triangulation for earth movement study at California Aqueduct–fault crossing sites, Section VI, Supplement No. 5 – June 1970: U.S. Department of Commerce, National Ocean Survey.

_____, 1971a, Results of triangulation for earth movement study at California Aqueduct–fault crossing sites, Section III, Supplement No. 2 – June 1971: U.S. Department of Commerce, National Ocean Survey.

_____, 1971b, Results of triangulation for earth movement study at California Aqueduct–fault crossing sites, Section IV, Supplement No. 6 – July 1971: U.S. Department of Commerce, National Ocean Survey.

_____, 1971c, Results of triangulation for earth movement study at California Aqueduct–fault crossing sites, Section II, Supplement No. 4 – July 1971: U.S. Department of Commerce, National Ocean Survey.

_____, 1972a, Results of triangulation for earth movement study at California Aqueduct–fault crossing sites, Section V, Supplement No. 3 – April 1972: U.S. Department of Commerce, National Ocean Survey.

_____, 1972b, Results of triangulation for earth movement study at California Aqueduct–fault crossing sites, Section I, Supplement 9 – September 1972: U.S. Department of Commerce, National Ocean Survey.

_____, 1972c, Results of triangulation for earth movement study at California Aqueduct–fault crossing sites, Section III, Supplement No. 3 – September 1972: U.S. Department of Commerce, National Ocean Survey.

_____, 1972d, Results of triangulation for earth movement study at California Aqueduct–fault crossing sites, Section IV, Supplement No. 7 – October 1972: U.S. Department of Commerce, National Ocean Survey.

Miller, R.W., Pope, A.J., Stettner, H.S., and David, J.L., 1969a, Crustal movement investigations–Triangulation, Taft–Mojave area, California, 1959–60, 1967, Operational Data Report C&GS DR–5: U.S. Department of Commerce, Coast and Geodetic Survey, June 1969, 106 p.

_____, 1969b, Crustal movement investigations–Triangulation, Taft–Mojave area, California supplement, Operational Data Report C&GS DR–6: U.S. Department of Commerce, Coast and Geodetic Survey, November 1969, 85 p.

Morgan, W.J., 1968, Rises, trenches, great faults, and crustal blocks: Journal of Geophysical Research, v. 73, no. 6, p. 1959–1982.

Nason, R.D., 1968, San Andreas fault at Cape Mendocino, *in* Proceedings of conference on geologic problems of San Andreas fault system, Dickinson, W.R., and Grantz, A., *editors:* Stanford University Publications, Geological Sciences, v. XI, p. 231–241.

_____, 1971, Investigation of fault creep slippage in northern and central California: Ph.D. thesis, University of California, San Diego, 232 p.

_____, 1973, Fault creep and earthquakes on the San Andreas fault, *in* Proceedings of the conference on tectonic problems of the San Andreas fault system, Kovach, R.L., and Nur, A., *editors:* Stanford University Publications, Geological Sciences, v. XIII, p. 275–285.

Nason, R.D., Philippsborn, F.R., and Yamashita, P.A., 1974, Catalog of creepmeter measurements in central California from 1968 to 1972: U.S. Geological Survey, Open–File Report 74–31.

Oakeshott, G.B., 1955, The Kern County earthquakes in California's geologic history, *in* Earthquakes in Kern County, California, during 1952, Oakeshott, G.B., *editor:* California Division of Mines Bulletin 171, p. 15–22.

_____, 1966, San Andreas fault in the California Coast Ranges province, *in* Geology of northern California, Bailey, E.H., *editor:* California Division of Mines and Geology, Bulletin 190, p. 357–373.

Page, B.M., 1966, Geology of the Coast Ranges of California, *in* Geology of northern California, Bailey, E.H., *editor:* California Division of Mines and Geology, Bulletin 190, p. 255–276.

Parkin, E.J., 1948, Vertical movement in the Los Angeles region, 1906–1946: American Geophysical Union Transactions, v. 29, p. 17.

———, 1965a, Results of triangulation for earth movement study at California Aqueduct–fault crossing sites, Section II, Wrightwood to Palmdale – November 1965: U.S. Department of Commerce, National Ocean Survey.

———, 1965b, Results of triangulation for earth movement study at California Aqueduct–fault crossing sites, Section III, Castaic to Lake Hughes – December 1965: U.S. Department of Commerce, National Ocean Survey.

———, 1966, Results of triangulation for earth movement study at California Aqueduct–fault crossing sites, Section IV, Sandberg to Wheeler Ridge – June 1966: U.S. Department of Commerce, National Ocean Survey.

Press, F., 1960, Crustal structure in the California–Nevada region: Journal of Geophysical Research, v. 65, no. 3, p. 1039–1051.

Rice, S.J., 1973, Geology and geologic hazards of the Novato area, Marin County, California: California Division of Mines and Geology, Preliminary Report 21, 47 p.

Richter, C.F., 1958, Elementary seismology: W.H. Freeman & Company, San Francisco, 768 p.

Rodgers, D.A., and Chinnery, M.A., 1973, Strain accumulation in the Transverse Ranges, southern California, *in* Proceedings of the conference on tectonic problems of the San Andreas fault system, Kovach, R.L., and Nur, A., *editors:* Stanford University Publications, Geological Sciences, v. XIII, p. 70–79.

Rosenman, M., and Singh, S.J., 1973, Stress relaxation in a semi–infinite viscoelastic earth model: Seismological Society of America Bulletin, v. 63, no. 6, p. 2145–2154.

Roubanis, A.S., 1963, Geology of the Santa Ynez fault, Gaviota Pass–Point Conception area, Santa Barbara County, California: M.A. thesis, University of California at Los Angeles.

Savage, J.C., and Burford, R.O., 1971, Discussion of paper by Scholz, C.H., and Fitch, T.J., Strain accumulation along the San Andreas fault: Journal of Geophysical Research, v. 76, no. 26, p. 6469–6479.

———, 1973, Geodetic determination of relative plate motion in central California: Journal of Geophysical Research, v. 78, no. 5, p. 832–845.

Savage, J.C., Prescott, W.H., and Kinoshita, W.T., 1973, Geodimeter measurements along the San Andreas fault, *in* Proceedings of the conference on tectonic problems of the San Andreas fault system, Kovach, R.L., and Nur, A., *editors:* Stanford University Publications, Geological Sciences, v. XIII.

Savage, J.C., and Wood, M.D., 1971, The relation between apparent stress and stress drop: Seismological Society of America Bulletin, v. 61, no. 5, p. 1381–1388.

Scholz, C.H., and Fitch, T.J., 1969, Strain accumulation along the San Andreas fault: Journal of Geophysical Research, v. 74, no. 27, p. 6649–6666.

———, 1971, Reply to comments by Savage, J.C., and Burford, R.O.: Journal of Geophysical Research, v. 76, no. 26, p. 6480–6484.

Scholz, C.H., Wyss, M., and Smith, S.W., 1969, Seismic and aseismic slip on the San Andreas fault: Journal of Geophysical Research, v. 74, no. 8, p. 2049–2069.

Schroeter, C.E., 1972, Stratigraphy and structure of the Juncal Camp–Santa Ynez fault slice, southeastern Santa Barbara County, California: M.A. thesis, University of California at Santa Barbara.

Singh, S.J., and Rosenman, M., 1974, Quasi–static deformation of a viscoelastic half–space by a displacement dislocation: Physics of the Earth and Planetary Interiors, v. 8, p. 87–101.

Smith, S.W., and Van de Lindt, W., 1969, Strain adjustments associated with earthquakes in southern California: Seismological Society of America Bulletin, v. 59, p. 1569.

Steinbrugge, K.V., and Zacher, E.G., 1960, Creep on the San Andreas fault—fault creep and property damage: Seismological Society of America Bulletin, v. 50, p. 389–396.

Sylvester, A.G., Smith, S.W., and Scholz, C.H., 1970, Earthquake swarm in the Santa Barbara Channel, California, 1968: Seismological Society of America Bulletin, v. 60, no. 4, p. 1047–1060.

Thatcher, W., and Hanks, T.C., 1973, Source parameters of southern California earthquakes: Journal of Geophysical Research, v. 78, no. 35, p. 8547–8576.

Townley, S.D., and Allen, M.W., 1939, Descriptive catalog of earthquakes of the Pacific Coast of the United States, 1769 to 1928, Chapter 1, Earthquakes in California, 1769 to 1928: Seismological Society of America Bulletin, v. 29, no. 1, p. 21–252.

Wallace, R.E., 1968, Notes on stream channels offset by the San Andreas fault, southern Coast Ranges, California, *in* Proceedings of conference on geologic problems of San Andreas fault system, Dickinson, W.R., and Grantz, A., *editors:* Stanford University Publications, Geological Sciences, v. XI, p. 6–21.

Warren, D.H., and Healy, J.H., 1973, Structure of the crust in the conterminous United States: Tectonophysics, v. 20, p. 203–213.

Whitcomb, J.H., Allen, C.R., Garmany, J.D., and Hileman, J.A., 1973, The 1971 San Fernando earthquake series—Focal mechanisms and tectonics: Reviews of Geophysics and Space Physics, v. 11, p. 693–730.

Whitten, C.A., 1960, Horizontal movement in the earth's crust: Journal of Geophysical Research, v. 65, p. 2839–2844.

Wood, H.O., 1955, The 1857 earthquake in California: Seismological Society of America Bulletin, v. 45, p. 47–67.

Wu, A.P., Kanamori, H., and Alewine, R.W. III, 1973, Temporal changes in Rayleigh–wave phase–velocity in southern California *abstract:* EOS Transactions, v. 54, no. 11, p. 1135.

Yamashita, P.A., and Burford, R.O., 1973, Catalog of preliminary results from an 18–station creepmeter network along the San Andreas fault system in central California for the time interval June 1969 to June 1973: U.S. Geological Survey, Open–File Report, 215 p.

Yerkes, R.F., McCulloh, T.H., Schoellhamer, J.E., and Vedder, J.G., 1965, Geology of the Los Angeles basin, California—an introduction: U.S. Geological Survey, Professional Paper 420–A.

Submitted for publication December 1974.

Appendix A

STRAIN TRANSITION ZONE ON THE SAN ANDREAS FAULT BETWEEN PARKFIELD AND TAFT, CALIFORNIA

Several authors have pointed out that fault creep on the San Andreas fault dies out in the vicinity of Parkfield (Allen, 1968; Nason, 1971; Yamashita and Burford, 1973), and the rapid decrease in seismicity south of Parkfield has also been noted (Brune and Allen, 1967; Allen, 1968; "Seismicity", this work). Allen (1968) suggested that the segment of the San Andreas fault south of Parkfield is locked, and Rodgers and Chinnery (1973) presented a model of the San Andreas fault incorporating the locked section.

There were exhaustive studies of the continuing deformation along the fault for several months following the 1966 Parkfield earthquakes; but to my knowledge, no work has been published that considers the details of strain variation along the San Andreas fault since then. In this work, I will examine in some detail the geodetic evidence south of Parkfield that delineates the strain transition zone, and I will present a dislocation model that adequately explains the major findings of the geodetic work.

PREVIOUS WORK

Cherry and Savage (1972) analyzed the results of repeated trilaterations of the pentagonal survey figure near Parkfield (figure A–1). They fitted straight lines to the line–length changes, plotted the rate of length change against the azimuth of the line, and fitted a strain field to the results. They found a strain field with an essentially east–west–oriented principal extension and very little or no compression. Greensfelder and Bennett (1973) suggested that a straight line fit to the data does not reflect what is actually occurring and that a sinusoidal curve is a better fit to the data.

GEODETIC EVIDENCE OF THE TRANSITION ZONE

Figure A–1 shows selected lines from the California Geodimeter Network and all operating creepmeters south of Stone Canyon (XSC1). It also shows the location of fault–crossing survey site TEM (see Appendix B). The area I shall be most concerned with is between Stone Canyon and Simmler.

Let me first consider the creepmeter data (table A–1). The creepmeter at Carr Ranch may not be across the presently active fault trace, which would explain the zero creep rate between XDR1 and XGH1. It is clear that the creep changes dramatically between XDR1 and Twisselman Ranch, going to essentially zero over a distance of about 30 km. Again, it is possible that the instruments south of XDR1 do not cross the presently active fault trace; but, since the U.S. Geological Survey instruments were installed across the surface break of the 1966 Parkfield earthquakes (Yamashita and Burford, 1973), this does not seem very likely. Also, creep is observed at XGH1 and XWT1; and, even though the rate is very low, this indicates that the fault trace on which the instruments are located is at least intermittently active.

Table A–1. Creepmeter data. All instruments installed in 1969 and still operating in 1974.

Site	*Creep rate (mm/yr)*	*Source*
XSC1	24	Yamashita and Burford (1973)
XDR1	11	Yamashita and Burford (1973)
Carr Ranch	0	James Hileman, California Institute of Technology, personal communication, 1974
XGH1	2	Yamashita and Burford (1973)
XWT1	3	Yamashita and Burford (1973)
Twisselman Ranch	0	James Hileman, California Institute of Technology, personal communication, 1974

The survey figure TEM (figure A–1) is discussed in some detail in Appendix B. There is a suggestion of right–lateral displacement across the fault with a rate of several millimeters per year; but, as discussed in Appendix B, this may be an effect due to the rapid change in the creep rate in this area.

Observations of the California Goedimeter Network also give some indication of the extent of the transition zone (figures A–2, A–3, and A–4). The dashed lines on the plots are included only to suggest trends in the data. They are fitted to the data by eye.

Lines 25 through 31 in figure A–2 show a reasonably smooth change in length from 1959 through 1973. The average rate for these lines is about 27 mm/year (Savage and others, 1973). Note the abrupt change in rate in line 32 before and after the 1966 Parkfield earthquakes. The reason for this change is not clear, for line 31, with nearly the same azimuth, does not show such a change in rate. However, the important point here is the essentially linear trends shown by all the lines north of Parkfield.

Figure A–3 shows Geodimeter lines between Parkfield and Maricopa which cross the fault at acute angles. Note that line 33 has a linear trend from 1959 to 1963 and from 1966 to 1969. It has been suggested (Hofmann, 1968; Greensfelder and Bennett, 1973) that the anomalous change in the line length between 1964 and 1966 was a precursor to the 1966 earthquakes. If this is true, then the line behavior after 1969 suggests that an earthquake may be imminent in the Parkfield area.

Prior to 1966, lines 35 and 39 show very little net change in line length. After the 1966 Parkfield earthquakes, both lines show a net change in length of several centimeters; and, from about 1969 on, the two lines show very little net change. Lines 40 and 46 (figure A–3) show essentially no change from 1959 to 1973.

Thus, the Geodimeter lines that cross the fault at an angle suggest that there is a change in the strain pattern on the segment of the fault spanned by lines 33 and 35.

Similarly, Geodimeter lines approximately perpendicular to the fault (figure A–4) indicate a change in the strain pattern between lines 291 and 297. Measurements were initiated on line 297 to fill in between lines 291 and 263. Unfortunately, soon after line 297 was established, the large changes in line 263 started dying out. Note that the behavior of line 297 does agree with that of line 263.

To summarize, the geodetic data indicate a major change in the strain release pattern along the San Andreas fault between Parkfield and Simmler (figure A–1). The data from measurements very near, or on, the fault trace suggest that this change occurs between TEM and the creepmeter at Twisselman Ranch.

DISLOCATION MODEL OF THE TRANSITION ZONE

The dislocation model we will construct must satisfy the geodetic observations of the previous section. In addition, the model will try to account for the periodic changes in Geodimeter line length discussed by Greensfelder and Bennett (1973).

The displacement fields calculated from several possible models were compared to the Geodimeter observations. The model which best fit the data is fairly simple and will be presented here. The model starts with an infinitely long straight fault slipping from 20 km to infinity at a rate of 3 cm/year (figure A–5). The displacement field is calculated using the expressions given by Savage and Burford (1973).

To this is added the displacement field of the fault surface shown in figure A–5 which has a 0.5–km–deep locked segment from Parkfield to near line 291, and a 20–km–deep locked segment from line 291 south. A model was tried that had a 4–km–long, 0.5–km–deep slipping segment centered on TEM, but it did not significantly improve the fit of the model to the data.

Using the model shown in figure A–5, the changes in Geodimeter line lengths, dl/dt, were calculated for the lines shown in figures A–5 and A–6. The straight lines on the graphs show the calculated length change rates.

In addition, a displacement perpendicular to the fault of the form

$$U = U_0 \sin (t/\tau)$$

with $U_0 = 3$ cm, $\tau = 7$ years, and t in years was added to the displacement field calculated from the model. This is shown by the sinusoidal curves in figures A–5 and A–6. The phase was determined such that the best fit was obtained for line F in figure A–6. Thus, all the changes are in phase. The period of seven years is the average for the whole network as determined by Greensfelder and Bennett (1973). The amplitude of 3 cm is somewhat arbitrarily chosen.

DISCUSSION AND CONCLUSIONS

The calculated length change rates in figure A–6 agree well with the observed data except for the strain steps due to the 1966 Parkfield earthquakes. The sinusoidal curves do not significantly improve the fit of the calculated length change rates to the data for the long Geodimeter lines.

The linear rates calculated for the Parkfield pentagon do not fit the data very well; but except for line A, the sinusoidal rates give a remarkably good fit to the data (figure A–6). And even for line A, the calculated length changes agree in phase but not in slope.

Thus, we have derived a simple dislocation model that accounts for the trends in the Geodimeter data. In addition, we have indicated that the periodic fluctuations in line length pointed out by Greensfelder and Bennett (1973) can be accounted for by a simple assumption. The origin of a periodic displacement perpendicular to the San Andreas fault is not clear at this time.

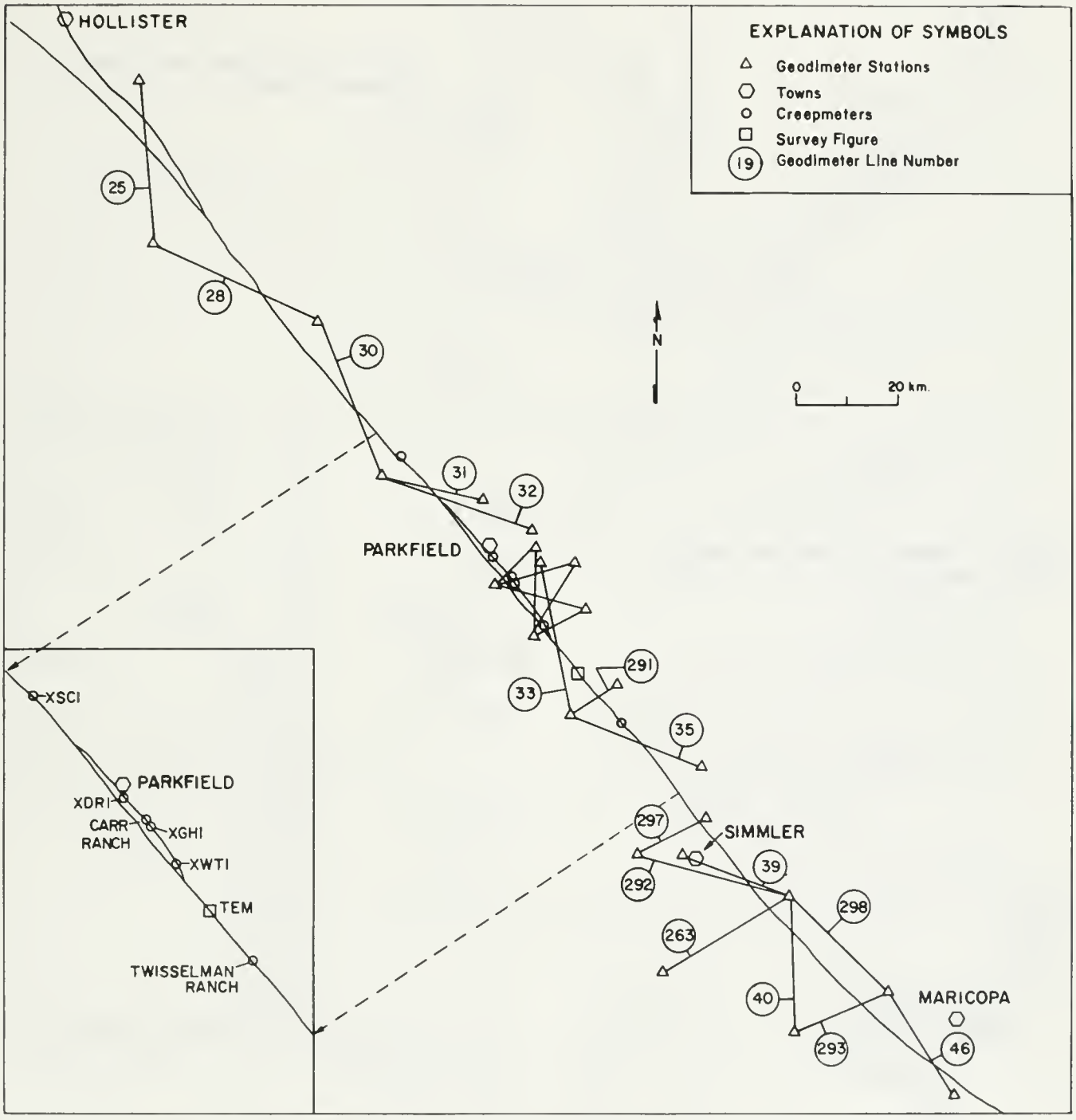

Figure A–1. Creepmeters, Geodimeter lines, and small survey figure in the vicinity of Parkfield.

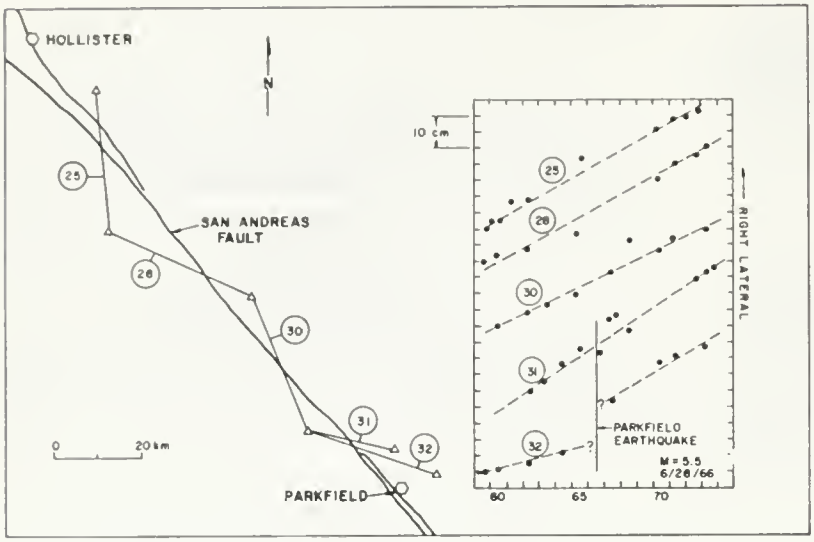

Figure A–2. Geodimeter lines and data, 1959–73, Hollister to Parkfield.

Figure A–3. Geodimeter lines and data, 1959–73, Parkfield to Maricopa.

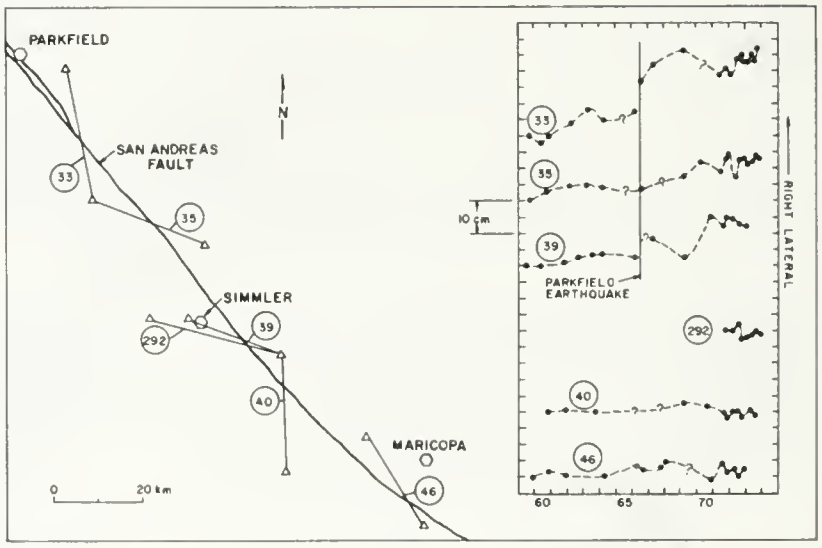

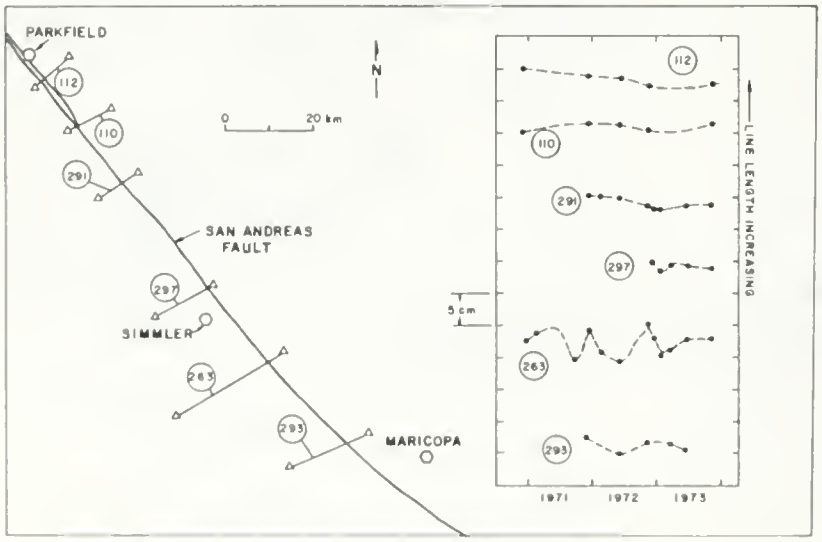

Figure A–4. Geodimeter lines normal to the San Andreas fault, 1971–73, Parkfield to Maricopa.

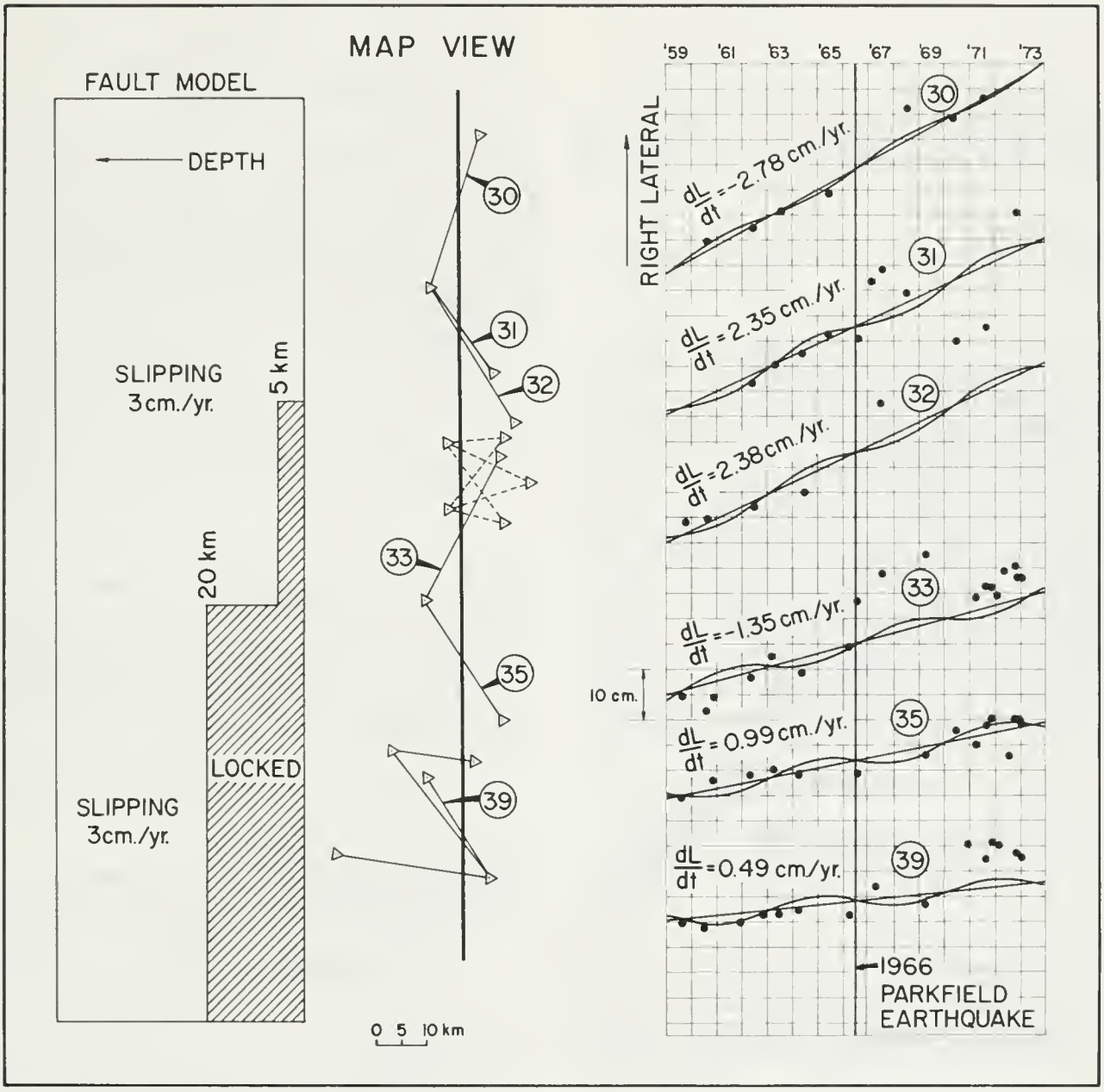

Figure A–5. Fault model and predicted and observed line length changes.

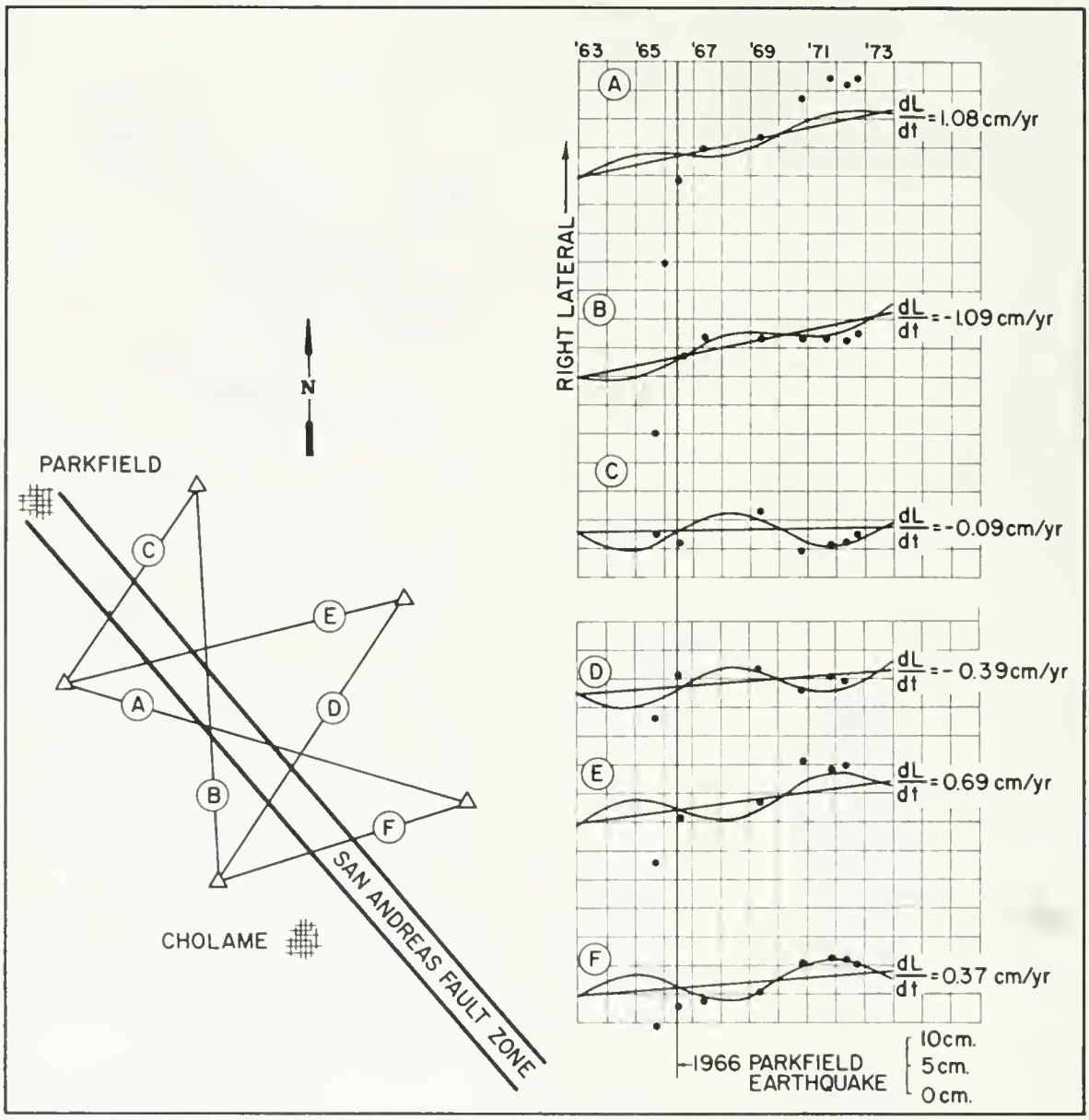

Figure A–6. Predicted and observed line length changes, Parkfield pentagon.

Appendix B

FAULT–CROSSING SURVEY FIGURES

INTRODUCTION

In 1964–1966, thirty small survey figures were established across several faults of the San Andreas fault system by the U.S. Coast and Geodetic Survey in cooperation with the California Department of Water Resources (Meade, 1966, 1968, 1971a, 1971b). The data and preliminary analyses of results from reobservation of these figures have been released in an informal manner in a series of reports titled "Results of Triangulation for Earth Movement Study at California Aqueduct–Fault Crossing Sites". Meade (1966, 1968, 1971a, 1971b) briefly reported on the results from these survey figures. However, to my knowledge, a systematic comparison and interpretation of these results has not been published. Hence, in this Appendix, I will present the results from the surveys of these figures and attempt a partial analysis of the results.

Figure B–1 shows the locations of the survey sites. I will discuss each site, moving from north to south.

TOLAY

This figure was established on the north shore of San Pablo Bay in 1965 and resurveyed once, in 1967 (Greensfelder, 1972). The figure was supposed to span the possible northern extension of the Hayward fault, but the exact location of any fault in this area is difficult to ascertain (Rice, 1974). In addition, there were large, inexplicable triangle closures in the 1965 survey (Miller, 1967a). First–order levels were also run at the site in 1965.

All the angle changes were within survey error and, hence, any fault movement is unresolvable.

MAR (MIRA VISTA)

This site was established on the Hayward fault (figure B–2) in 1966 and resurveyed in 1968 and 1970. Miller (1970c) notes that the 1968 and 1970 results are probably more reliable since the astronomic azimuths in those years are in good agreement, while the 1966 azimuth is some 5 seconds smaller.

There is some indication of right–lateral movement shown in the position vectors, but Miller (1970c) suggests this may be due to changes in the astronomic azimuths. It is interesting to note that the astronomic azimuths of both B–A and B–C increased. This suggests there could be another unrecognized fault trace between stations B and C.

STADIUM

This site was established on the rim of Memorial Stadium on the University of California's Berkeley campus in 1966. Earlier observations had indicated that the stadium was built across the Hayward fault (figure B–3) and that creep on the fault was pulling it apart (Bolt and Marion, 1966). The taped base line and the observed astronomic azimuth of the original survey in 1966 agree with those observations in the resurveys of 1967 and 1968 (Miller, 1970c). Thus, this figure can be considered to be quite stable.

Changes in azimuth of lines A–D and B–C suggest an average creep rate over the three years of 5 mm/year (Miller, 1970c).

CAMP PARKS

This site consists of four figures established in 1964. Three of the figures cross the Pleasanton fault zone (figure B–4), and the fourth is a line across the Calaveras fault. I will not discuss the alignment. The figures were resurveyed in 1965 and 1969 (Miller, 1970d). The 1969 survey tied the three figures on the Pleasanton fault together. The maximum triangle closures are within first–order survey specifications. However, in the figure PFS, the base line 2–5 increased 4 mm and underwent an astronomic azimuth change of 4 seconds between 1964 and 1965. The length increase of the base line would account for the overall expansion of the figure in 1965. The base line and its azimuth remained relatively constant in 1969, thus suggesting that the observed length changes may be more reliable. The length and azimuth of the base line 3–4 of PFE suggest that the observed line–length changes are fairly reliable. The base line 1–2 of PFW underwent a shortening of 1 cm between 1965 and 1969, which would account for the large amount of shortening of the figure between 1965 and 1969.

Miller (1970d, p. 4) interprets these results as follows:

> "At Site PFS, there was systematic right–lateral movement of about 18 mm for the 5–year interval 1964–1969. Changes at Site PFE do not indicate significant movement, but at Site PFW from 1965 to 1969, there is an indication of about 1 cm relative movement."

However, the changes in the astronomic azimuths of the base lines may indicate regional strain accumulation rather than fault slippage. The three figures each have two stations in the fault zone, and this may introduce unpredictable changes into the results. It is probably necessary in a situation like this to have several longer lines that would span the whole fault zone to resolve the problem.

In 1974, personnel from the California Division of Mines and Geology observed these figures, using an MA–100 Tellurometer. The observed line lengths agreed with the adjusted length of the 1969 triangulation survey to within the errors of the Tellurometer ($\pm$ 1.5 mm). The more recent work suggests that, if fault slippage occurred, it occurred as an event between 1965 and 1969. This would be in agreement with creepmeter data which shows that fault creep on the Hayward–Calaveras fault is more "eventful" than steady–state (Nason and others, 1974).

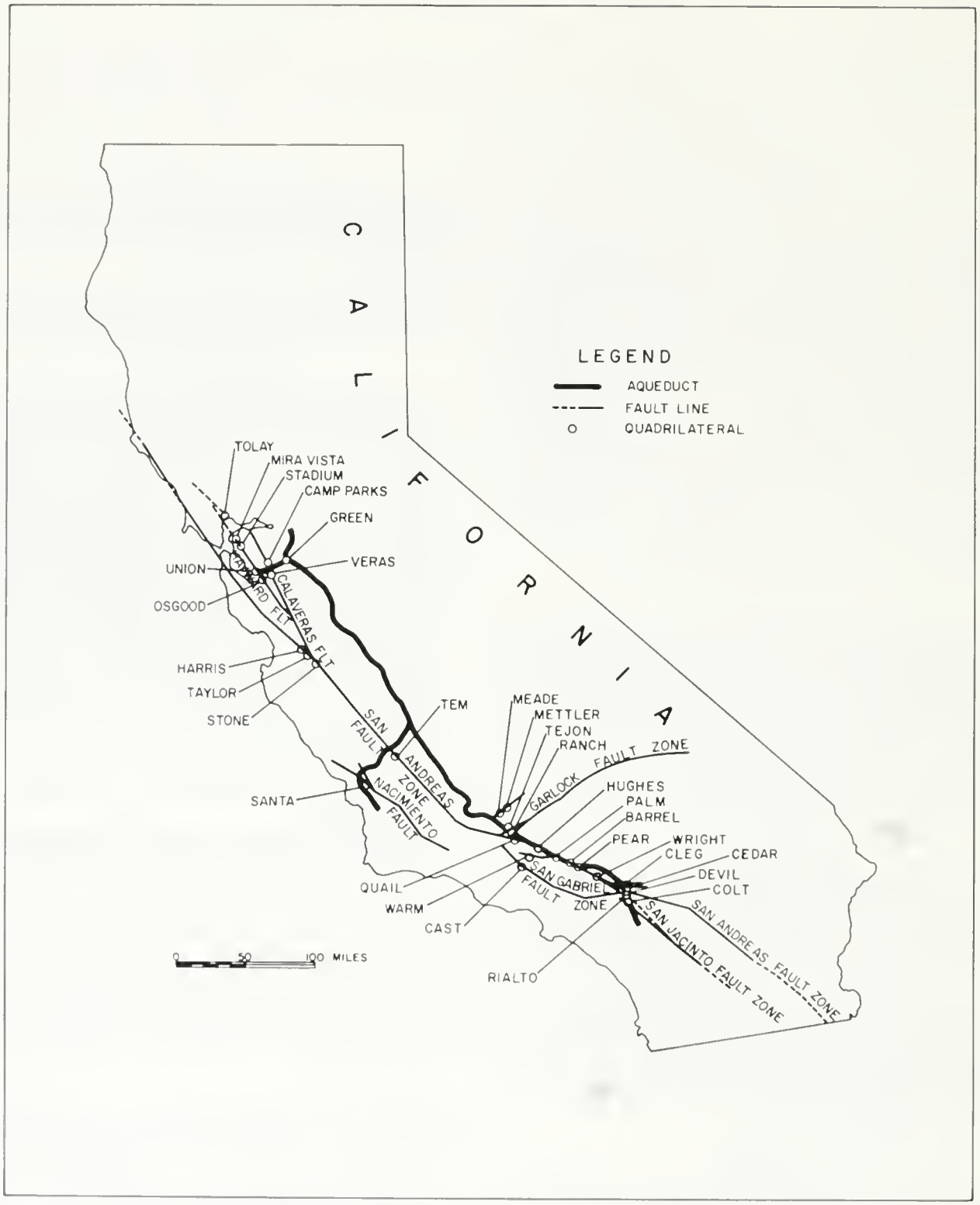

Figure B–1. Survey figures of aqueduct–fault crossing sites (modified from Greensfelder, 1972, p. 8).

GREEN

This site was established on the Greenville fault in 1965 and resurveyed in 1966. First–order levels were run at the site in 1965 and 1967. The astronomic azimuth of the line C–A remained essentially constant, but the taped length A–C changed by 1 cm. Miller (1966b) says that the change in length of A–C was not supported by any angle changes and thus is probably due to the difficulty of taping this line. Triangle closures and angle corrections were large, but they were within the specifications of the survey. There does not appear to be any consistent horizontal or vertical movement at this site.

UNION

This site on the Hayward fault (figure B–5) was established in 1965 and resurveyed in 1966, 1967, and 1969. Triangle closures and angle corrections were within first–order specifications. The astronomic azimuth of the base line, A–C, decreased by less than one second. The taped length A–C changed by 8 mm between 1966 and 1967. First–order levels were run in 1965 and 1967.

Changes in directions of the fault–crossing lines suggest a creep rate of about 8 mm/year on the Hayward fault (Miller, 1970a). Changes in elevation indicate stations west of the fault rose relative to stations east of the fault.

VERAS

This site was established in 1965 on the Calaveras fault (figure B–6) and resurveyed in 1966 and 1970. Miller (1970e) notes, "The triangle closures for the surveys of 1965 and 1966 are larger than normally expected, but within the accuracy limits of the specification..." The astronomic azimuth and taped length of the base C–E did not change significantly between the surveys. First– order levels were run in 1965 and 1967.

Again, the fault–crossing lines show a consistent change in direction that could be caused by right–lateral creep on the Calaveras fault. Miller (1970e) says, "Overall observed changes in the horizontal directions of lines approximately perpendicular to the fault showed an average right–lateral movement of 12 mm for the 5–year interval." The elevation differences indicate that marks east of the fault rose relative to marks west of the fault.

OSGOOD

This figure was established across the Hayward fault (figure B–7) in 1966 and resurveyed in 1968 and 1969. Triangle closures and angle corrections were within first–order specification. The taped length of A–C changed by 3 mm, but the astronomic azimuth of the line A–C changed nearly 4 seconds, which suggests that there may be some strain accumulation in the vicinity of the net.

Each of the lines crossing the fault trace shows a net increase in azimuth over four years. Resolving these angles into movement parallel to the fault, a creep rate of about 7 mm/year (Miller, 1970c) is obtained. This is consistent with the rate of 5 mm/year at STADIUM and 8 mm/year at UNION.

CIENEGA VALLEY (HARRIS, TAYLOR, STONE)

These figures have been established in Cienega Valley; the earliest was The resurveys at these sites indicate a creep rate of between 10 and 15 mm/year. Meade (1971 a,b) has discussed these figures, so no further discussion will be given here.

TEM

This figure was established across the San Andreas fault (figure B–8) in 1964 and resurveyed in 1965, 1966, 1968, and 1971. All the triangle closures and corrections were within the limits of the survey specifications. The astronomic azimuth of line B–D remained essentially constant, but the taped length of B–D changed by 12 mm between 1966 and 1971 (Miller, 1972a). Levels were run in 1968 and 1971.

There was no significant difference between the 1964 and 1965 surveys; but the 1966 survey, made after the 1966 Parkfield earthquakes, indicated a 25 mm right–lateral shift across the fault. The 1968 and 1971 surveys suggest continuing right–lateral movement at a rate of about 7 mm/year (Miller, 1972a). The elevation differences indicate that all the marks are sinking relative to mark F, but the three westernmost marks (B, C, and D) are sinking faster than the other marks.

Detailed mapping following the 1966 earthquakes indicated that ground surface rupture ended some 4.5 km northwest of TEM (Brown and Vedder, 1967). Eaton and others (1970) show that the aftershock zone of the 1966 earthquakes terminated abruptly about 5 km northwest of TEM. Thus, the observed azimuth changes at TEM in 1966 could reflect either movement on a fault plane that did not intersect the surface or the end effects due to a dislocation surface such as Chinnery (1961, 1963) discussed. The fact that the aftershock zone did not extend to the vicinity of TEM suggests that the azimuth changes are probably due to end effects rather than movement on a fault plane.

The two resurveys since 1966 suggest continuing fault movement after the 1966 earthquakes. However, data from the U.S. Geological Survey microearthquake net does not show any seismic activity south of the vicinity of Parkfield. The rather large change (12 mm) in the length of the base line B–D suggests strain accumulation rather than fault creep. Thus, the result of the TEM resurveys indicate either aseismic fault creep that probably does not intersect the ground surface or end effects due to the termination of surface creep between creepmeters XGH1 and XWT1 (Appendix A). Since the azimuth changes are large even for lines that do not cross the fault, neither hypothesis can be ruled out.

SANTA

This site was established on the Nacimiento fault (figure B–9) in 1964 and reobserved in 1965 and 1968. The triangle closures and angle corrections were large in all three surveys. Astronomic azimuths of the line A–C remained essentially constant, and the taped length of A–C lengthened by 4 mm between 1964 and 1965. The survey results do not indicate movement across the Nacimiento fault larger than the survey errors (Miller, 1968). A level survey was run in 1968, and the levels have not been rerun since then.

METTLER

This site was established in 1964 across the White Wolf fault and resurveyed in 1965, 1966, and 1969. There is good evidence that several of the marks in the figure were disturbed between the resurveys, and the site has been abandoned (Miller, 1970b). Due to the problems with the site, I feel that the results of the resurveys are of such poor quality that no further analysis is warranted.

MEADE

This site was established (figure B–10) in 1969 to replace METTLER and resurveyed in 1972. First–order levels were run on the site in 1969, 1970, and 1972. Triangle closures and angle corrections were within the specifications of the survey, and the non–fault–crossing taped lines (A–B and D–F) showed no significant changes. However, the astronomic azimuth of line A–F decreased by 3 seconds (Miller, 1972d).

The adjusted azimuth changes are dominated by a change in the astronomic azimuth of line A–F. Miller (1972d) states that the location of the White Wolf fault is not well known at this site. The counterclockwise rotation of line A–F and the depression of marks A and B relative to RON would be consistent with movement on the White Wolf fault if it passed through the northern part of the survey figure.

RANCH–TEJON

In 1964, RANCH and TEJON were established on the Garlock fault (figures B–11 and B–12). They were both resurveyed in 1965 and 1966; and RANCH was resurveyed in 1967, 1969, 1970, and 1972. In 1967, most of the marks at the TEJON site were destroyed by construction on the California Aqueduct. In 1970, a new set of marks was established near the original TEJON site, and RANCH and TEJON were connected by several longer lines.

RANCH

Levels were run at RANCH site in 1964, 1965, 1966, 1968, 1969, 1971, and 1972; and table B–1 shows the elevation differences. The elevation changes indicate that all marks were rising relative to D from 1964 to 1968; in the interval 1968 to 1969, all the marks subsided relative to D, and from 1969 to 1972, the marks generally moved up relative to D, but the amount of change was less than in earlier periods. The results of the horizontal surveys show that all lines crossing the fault except C–F lengthened, while C–F shortened by a small amount. The non–fault–crossing lines all shortened substantially, reflecting the shortening of the taped base line D–E. Thus, the adjusted line lengths suggest an expansion across the fault with some left–lateral movement. The observed directions from the survey indicate left–lateral movement at a rate of between 6 and 8 mm/year across the Garlock fault (Miller, 1970b, 1972d). If this is a real measure of fault creep, it indicates that the Garlock fault near this site is one of the most active faults in California.

However, a note of caution should be sounded. Between 1964 and 1968, a tunnel was being driven between RANCH and TEJON, and the south portal of the tunnel is in the middle of the RANCH figure. Thus, the horizontal and vertical changes noted above might be a result of the tunneling. However, the consistency of the observations argues against there being a large effect at the site due to the tunnel operation.

Table B–1. Elevation differences (mm) relative to RANCH–D.

Mark	*1964–65*	*1965–66*	*1966–68*	*1968–69*	*1969–71*	*1971–72*
A	+14	+1	+14	−21	+6	+2
B	+17	+5	+12	−9	+3	+2
C	+10	+4	+7	−12	+9	−1
E	−2	+7	−1	−	−4	+1
F	+20	−1	+19	−16	−1	+7

TEJON

Figure B–12a shows the TEJON (1964) survey figure. There was no evidence of consistent vertical movement. The observed horizontal direction changes between the three surveys suggest that there may have been some left–lateral movement at a rate of 1 to 2 mm/year across the Garlock fault (Parkin, 1966). The taped base A–B shortened, introducing some compression into the figure.

RANCH–TEJON COMBINED FIGURE

Figure B–13 shows the new RANCH–TEJON site. The level surveys suggest there may have been some subsidence of marks K and NO PORTAL TUN 3 relative to B, but more data are needed to establish trends. The results of the horizontal surveys indicate a general contraction of the figure between 1970 and 1972. The observed direction changes hint at small right–lateral movement across the North Garlock fault and larger left–lateral movement across the South Garlock fault. The position vectors of the stations north of PJW19 relative to PJW19 are well within their error ellipses, while the vectors for RANCH D and EMIL are barely within the error ellipses. These results suggest a continuing rate of 8 mm/year movement across the South Garlock fault (Miller, 1972d).

It should be pointed out that measurements on line 51 of the California Geodimeter Network, which crosses the Garlock fault near RANCH–TEJON, suggest a long–term left–lateral movement rate of 5 ± 2 mm/year (Savage and others, 1973, p. 48, figure 3). The Geodimeter results are consistent with the results from the RANCH–TEJON surveys. This indicates that the Garlock fault in this area may be more active than previously suspected.

QUAIL

This site was established on the San Andreas fault (figure B–14) in 1964 and resurveyed in 1965, 1968, and 1971. The triangle closures in 1964 and 1965 were somewhat larger than one would expect. The astronomic azimuth of line B–F changed by about 1.5 seconds between 1964 to 1965, and 1965 to 1968, but the value in 1971 was essentially the same as that in 1964. The taped base B–F changed by 4 mm over the course of the surveys. First–order levels were run in 1964, 1965, and 1968.

There does not appear to be any consistent pattern to the elevation differences. There is no indication of fault movement at this site based on the horizontal survey results (Miller, 1971b).

HUGHES

This site was established on the San Andreas fault (figure B–15) and was reobserved in 1965 and 1971. The survey results were within specifications, and the astronomic azimuths and taped distances remained essentially constant. First–order levels were run in 1964, 1965, and 1971.

There does not appear to be any consistent pattern in the elevation changes, and there is no evidence of fault movement in the vicinity of this site based on the survey results (Miller, 1972c).

PALM

This site was established on the San Andreas fault in 1964 and resurveyed in 1965 and 1966. First–order levels were run at the

site in 1964 and 1965. There was some evidence of rotation of the astronomic azimuth of the base line. The taped length of the base increased by 8 mm between 1964 and 1966. The triangle closures and angle corrections were quite large (Miller, 1966a).

The horizontal surveys revealed no displacement across the San Andreas fault larger than the survey errors (Miller, 1966a). The level survey revealed a general uplift of the figure.

WARM

This site was established in 1964 on the Clearwater fault and resurveyed in 1965. The 1965 results show no evidence of movement (Parkin, 1965b).

CAST

This site was established in 1964 and resurveyed in 1965, 1967, and 1970. It was supposed to cross the San Gabriel fault, but apparently the fault was missed when the figure was laid out (Miller, 1971a). Therefore, no further discussion will be presented.

BARREL

This site on the San Andreas fault was established in 1964 and reobserved in 1965, 1966, 1967, 1970, and early 1971. The 1970 survey was made between December 1970 and January 1971, and the 1971 surveys were made in February and May following the 1971 San Fernando earthquake. The astronomic azimuth of line B–D seems to be 3 to 6 seconds too large in 1964. The taped length of B–D varied by as much as 5 mm between the surveys. Triangle closures and corrections to angles were within specifications (Miller, 1971c).

Figure B–16 shows the survey figure and its relation to the San Andreas fault zone, and table B–2 shows the elevation changes relative to mark B. Note that the total net change in elevation shows that all the marks subsided relative to B. However, between 1965 and 1966, the marks all rose relative to B. The results of the horizontal surveys show that no fault movement larger than the survey error occurred on the San Andreas fault near this site (Miller 1971).

Table B-2. Elevation differences (mm) relative to BARREL-B.

Mark	1964–65	1965–66	1966–67	1967–71
A	−4	+3	−2	−1
C	−2	+3	−3	−3
D	−1	+5	−2	−2
E	−6	+4	−2	−1
F	−10	+6	−2	−2

PEAR

This survey figure was established across some minor faults associated the San Andreas fault zone in 1964 (figure B–17) and reobserved in 1965, 1966, 1967, and 1969. The astronomic azimuth of line A–G changed by about 4 seconds between 1964 and 1965, but it remained essentially constant after 1965. The taped length of A–G changed by 6 mm between 1964 and 1965. After that, changes were ± 2 to 4 mm in the length of A–G. The triangle closures and angle corrections were large in the first two surveys and much smaller in the last two surveys. The results of the horizontal and vertical surveys indicate that no systematic movement larger than the survey errors has occurred (Miller, 1969).

Table B-3. Elevation differences (mm) relative to PEAR-G.

Mark	1964–65	1965–66	1966–67	1967–69
A	+2	0	−2	+2
B	+4	−3	+3	0
C	+3	−1	0	0
D	+2	−3	+2	+1
F	+2	−3	+1	0
H	+1	−1	−1	0

WRIGHT

This site was established on the San Andreas fault in 1964 and resurveyed in 1965. The survey errors were somewhat larger than expected. There does not appear to be any systematic movement on the fault larger than the survey error (Parkin, 1965a).

CLEG

This figure was established on the Cleghorn fault in 1965 and resurveyed in 1966 and 1967. First–order levels were run in 1966 and 1967. Neither the horizontal nor the vertical surveys indicated any significant, systematic fault movement (Anonymous, 1967).

CEDAR

This site was established on the Cleghorn fault in 1964 and resurveyed in 1964 and 1967 (Miller, 1967b). The site has been destroyed since 1967 (Greensfelder, 1973). There was some movement of one of the marks in the figure. Measurements not involving that mark indicated no fault movement (Miller, 1967b).

DEVIL

This site was established on the San Andreas fault in 1964 (figure B–18) and resurveyed in 1965, 1966, 1968, 1970, and 1972. Levels were run in 1964, 1965, 1968, 1970, and 1971. There were large changes (± 4 seconds maximum) in the astronomic azimuth of line B–D between the surveys; the taped length of B–D has increased by 1 mm. The triangle closures and angle corrections were generally well within the specifications of the survey. The results of the horizontal surveys indicate no fault movement between 1970 and 1972 (Miller, 1972b). The vertical surveys indicate that the northeast side of the San Andreas fault is moving up relative to the southwest side. The vertical surveys will be discussed in more detail under "Survey Results Near San Bernardino".

RIALTO

This site was established in 1964 (figure B–19) on the San Jacinto fault and reobserved in 1965, 1967, 1968, 1970, and 1972. The astronomic azimuth of line B–D remained essentially constant until the survey of 1972, when it decreased about 3 seconds. The taped length of B–D varied over a range of 5 mm. Triangle closures and angle corrections were within the specifications of the surveys. There is reason to believe that mark C was disturbed by heavy equipment between 1968 and 1970 (Miller, 1972b).

Levels were run at this site in 1964, 1965, 1967, 1968, 1970, 1971, and 1972. A level line connecting RIALTO to COLT was established in 1971 and reobserved in 1972.

The results of the horizontal surveys showed a right–lateral creep rate of about 2 mm/year up until 1968. Between 1968 and 1970, there may have been some small amount of fault move-

ment; but the rate was not as large as the previous rate. From 1970 to 1972, there was no fault movement larger than the survey error. It is interesting to note that the elevation changes also changed trend in the period 1968 to 1970. This will be discussed in more detail under "Survey Results Near San Bernardino".

COLT

This site was established on the San Jacinto fault in 1964 (figure B–20) and reobserved in 1965, 1967, 1969, 1970, and 1972. The astronomic azimuth of line B–D decreased about 15 seconds from 1964 to 1972. The taped length B–D increased 3 mm between 1964 and 1972. There is some indication that mark F was disturbed between 1970 and 1972, and calculated position vectors suggest that marks F and D have been unstable since 1964 (Miller, 1972b). Levels were run at this site in 1964, 1965, 1967, 1968, 1969, 1971, and 1972. A level line connecting this site to RIALTO was established in 1971 and reobserved in 1972.

The results of the horizontal surveys indicate that, between 1964 and 1970, there was fault movement with a rate of about 1.5 mm/year on the San Jacinto fault. In 1972, all the marks moved southeast relative to mark A. The vertical surveys also indicate a substantial change in 1970. These results will be discussed in more detail under "Survey Results Near San Bernardino".

SURVEY RESULTS NEAR SAN BERNARDINO

In this section, the results from the three survey figures near San Bernardino will be discussed in more detail, and an attempt will be made to correlate these results with other data. First, let us recall the results mentioned previously.

At DEVIL, there was no indication of fault movement prior to 1970; while between 1970 and 1972, there was 15 mm of right–lateral movement at the site. At RIALTO, there was more or less steady right–lateral movement of 2 mm/year (total about 10 mm) between 1964 and 1968 with, perhaps, a slight bit of right–lateral movement between 1968 and 1970. After 1970, there was essentially no movement. At COLT, there was movement with a rate of about 1.5 mm/year (total about 9 to 10 mm) between 1964 and 1970, and there was no evidence of movement after 1970. The level data at DEVIL show a more or less steady uplift of the northeastern block relative to the southeastern block relative to the southwestern block, but the data are too sparse to draw firm conclusions about possible changes in rates. At RIALTO, the level data indicate a change in trend between the 1968 and 1970 surveys (figure B–20a); while at COLT, a change in trend occurs between the 1970 and 1972 surveys. Thus, both horizontal and vertical data at COLT and DEVIL suggest a major change in the strain field between 1970 and 1972.

Three Geodimeter lines of the California Geodimeter Network have been measured near this area; they are lines 66, 67, and 70 (Greensfelder and Bennett, 1973, figure 6). Lines 66 and 67 show length increases of 4 to 5 cm between 1968 and 1970 and length decreases of about 2 cm between 1970 and 1972 (figure B–21). Line 70 lengthens by about 10 cm between 1968 and 1972. Thus, the Geodimeter data also suggest a change in the strain field between 1970 and 1972. If the hypothesis of periodic fluctuations in line lengths proposed by Greensfelder and Bennett (1973) is valid, the data from these small survey figures may be reflecting this change. More data are needed to resolve this problem.

It is interesting to note that on September 12, 1970, a magnitude 5.4 earthquake occurred northwest of the San Bernardino area and that on February 9, 1971, the magnitude 6.6 San Fernando earthquake occurred 100 km east of the San Bernardino area (figures B–19b, B–20b, and B–21). It is possible that the change in the strain field between 1970 and 1972 was related to one or both of these two events, but the data are not adequate to resolve this question.

Finally, it is intriguing to note that Kanamori and Chung (1973) and Wu and others (1973) found changes in seismic velocities in the vicinity of Riverside between 1966 and 1971. They indicate that these changes might be related to future earthquake activity in the vicinity of Riverside. This leads us to the possibility that the small survey figures may be giving us information on dilatancy preceding an earthquake. More frequent measurements on somewhat expanded figures and level nets should be made to test this important possibility.

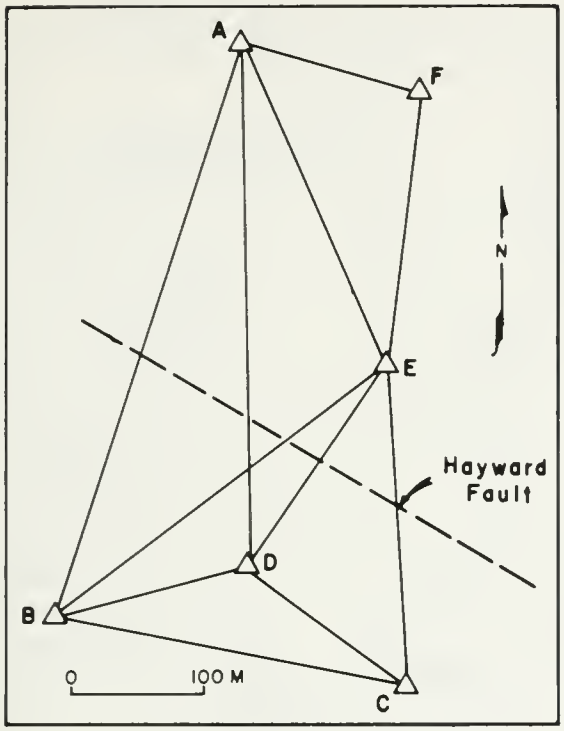

Figure B–2. Plan of the survey figure at the MAR site.

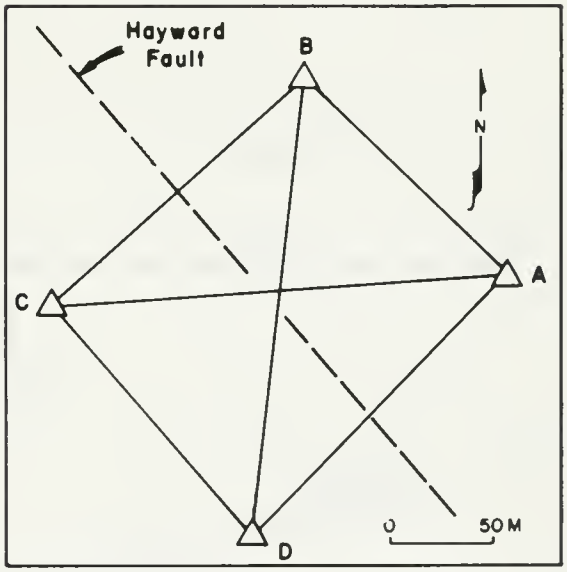

Figure B–3. Plan of the survey figure at the STADIUM site.

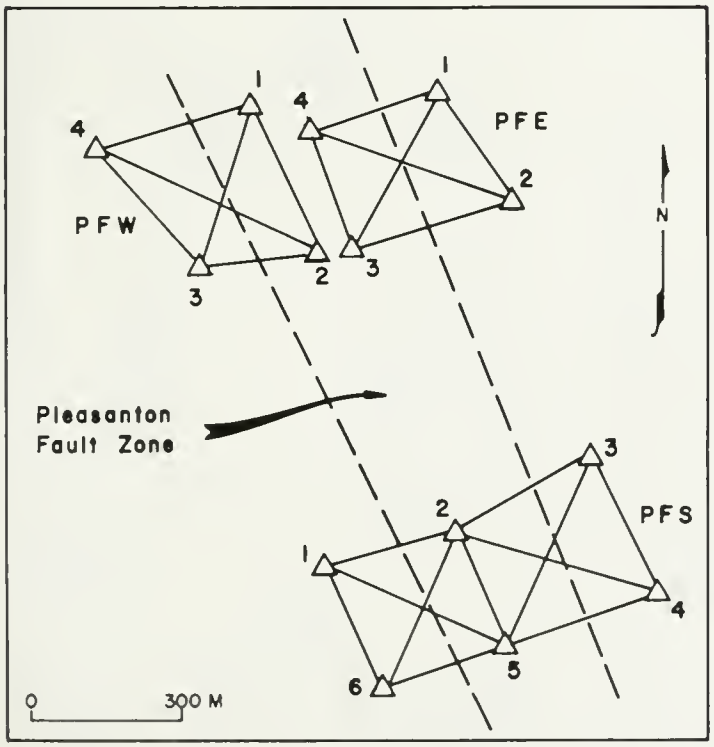

Figure B–4. Plan of the survey figure at the CAMP PARKS site.

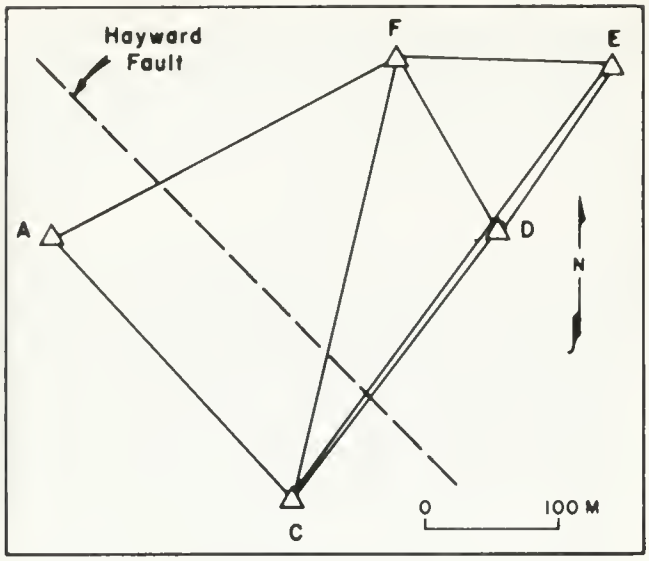

Figure B–5. Plan of the survey figure at the UNION site.

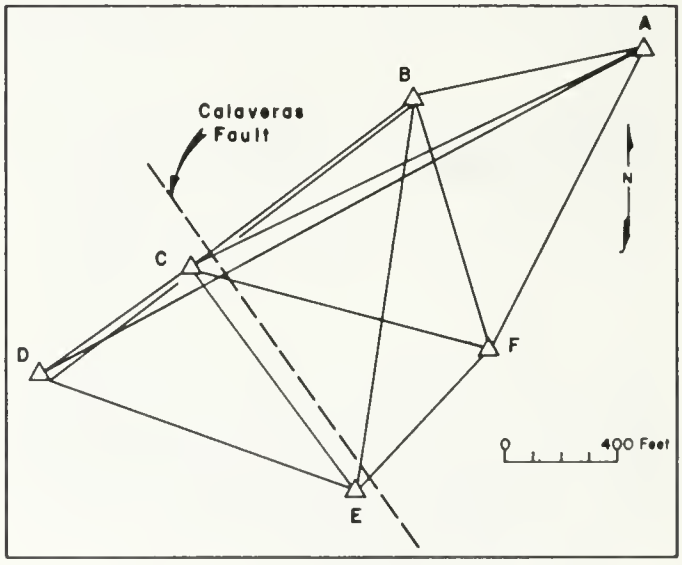

Figure B–6. Plan of the survey figure at the VERAS site.

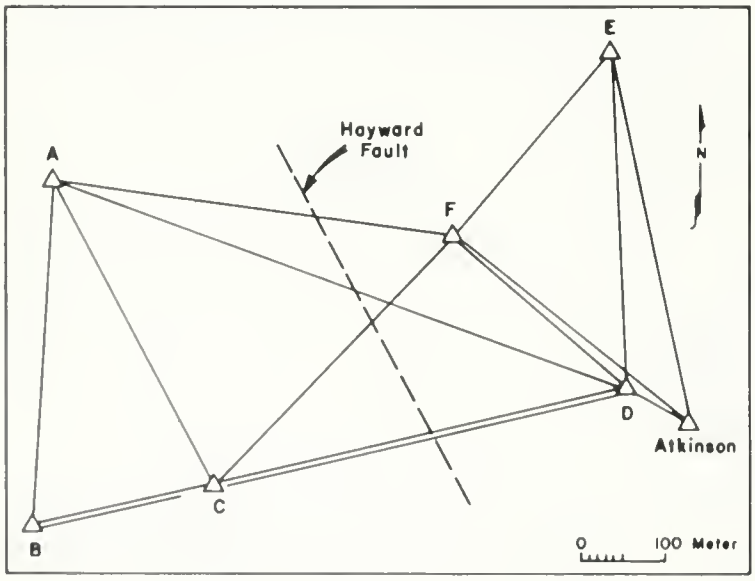

Figure B–7. Plan of the survey figure at the OS-GOOD site.

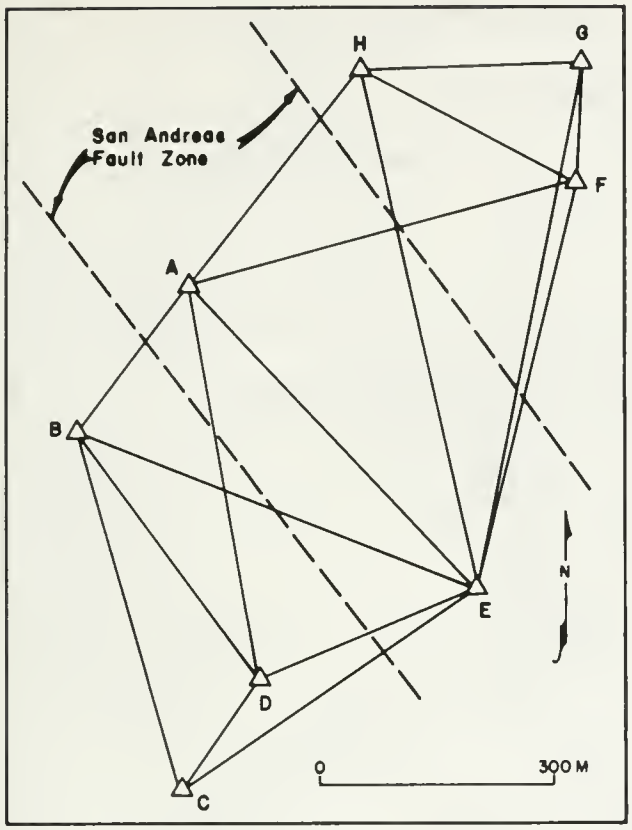

Figure B–8. Plan of the survey figure at the TEM site.

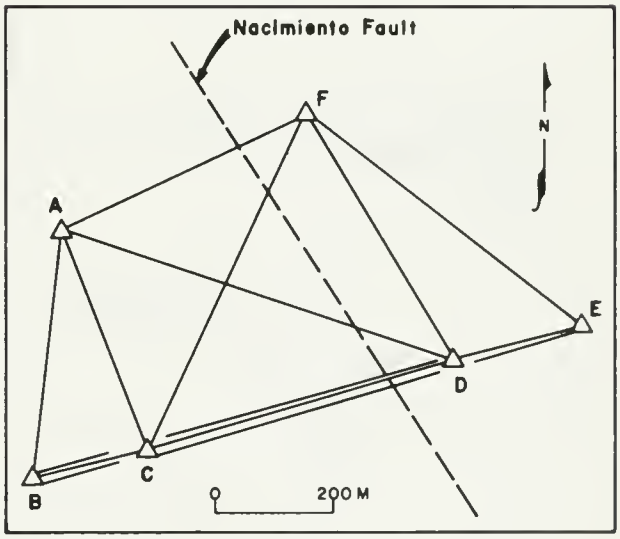

Figure B–9. Plan of the survey figure at the SANTA site.

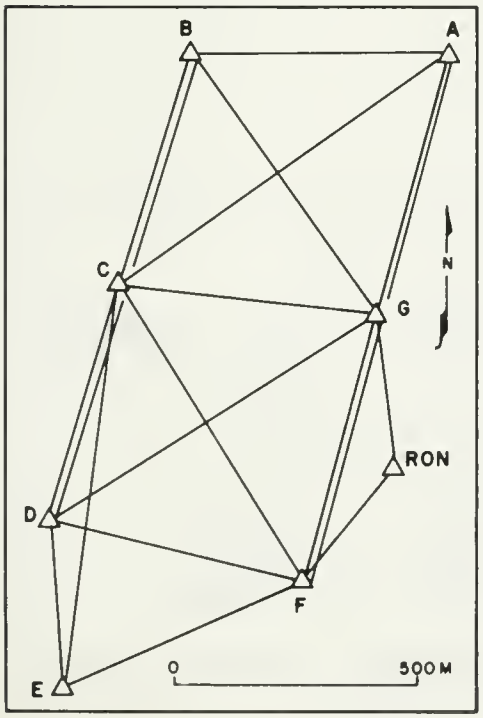

Figure B–10. Plan of the survey figure at the MEADE site.

Figure B–11. Plan of the survey figure at the RANCH site.

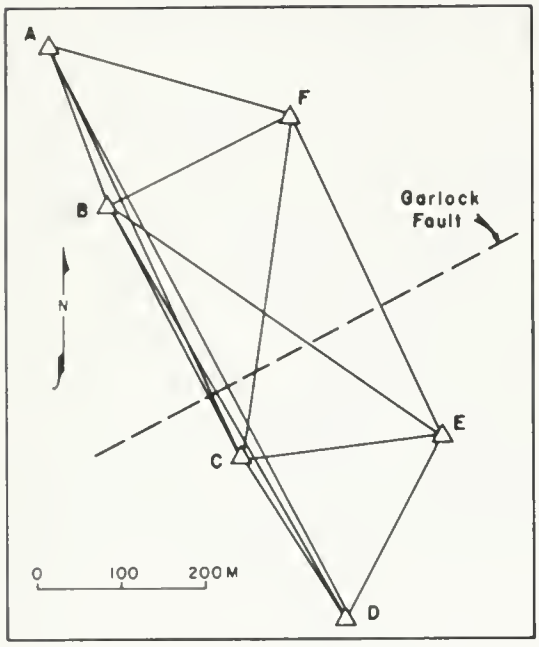

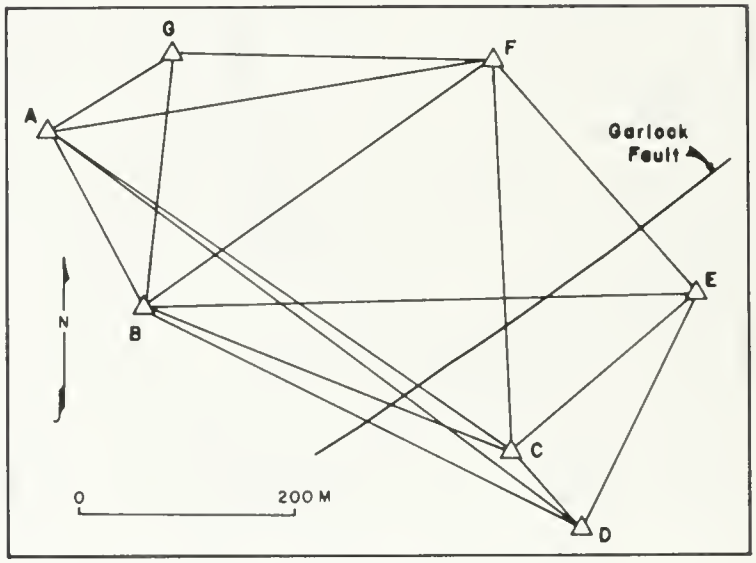

Figure B–12a. Plan of the survey figure at the original TEJON site (1964–66).

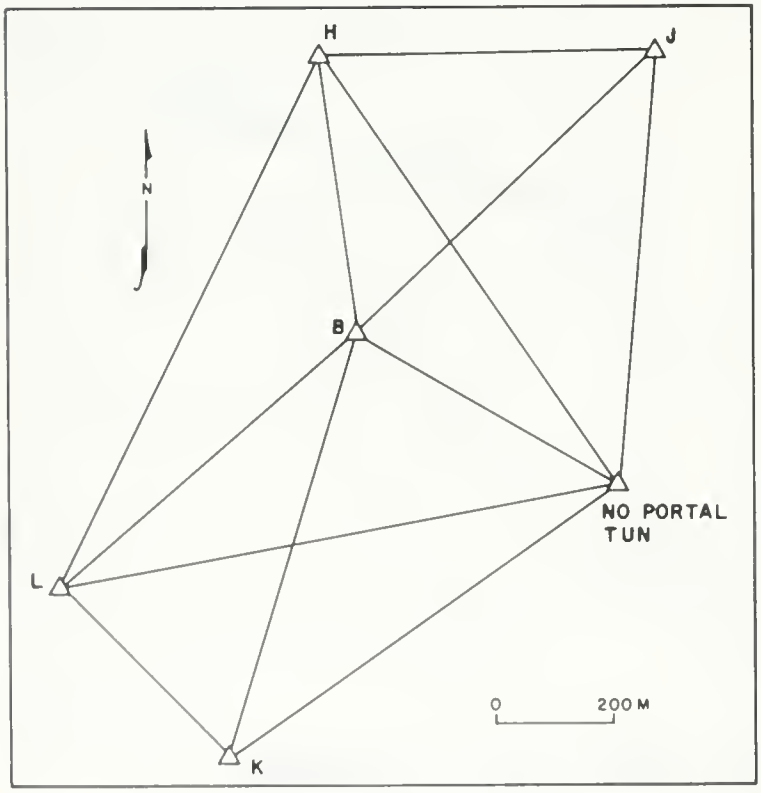

Figure B–12b. Plan of the survey figure at the new TEJON site (1970).

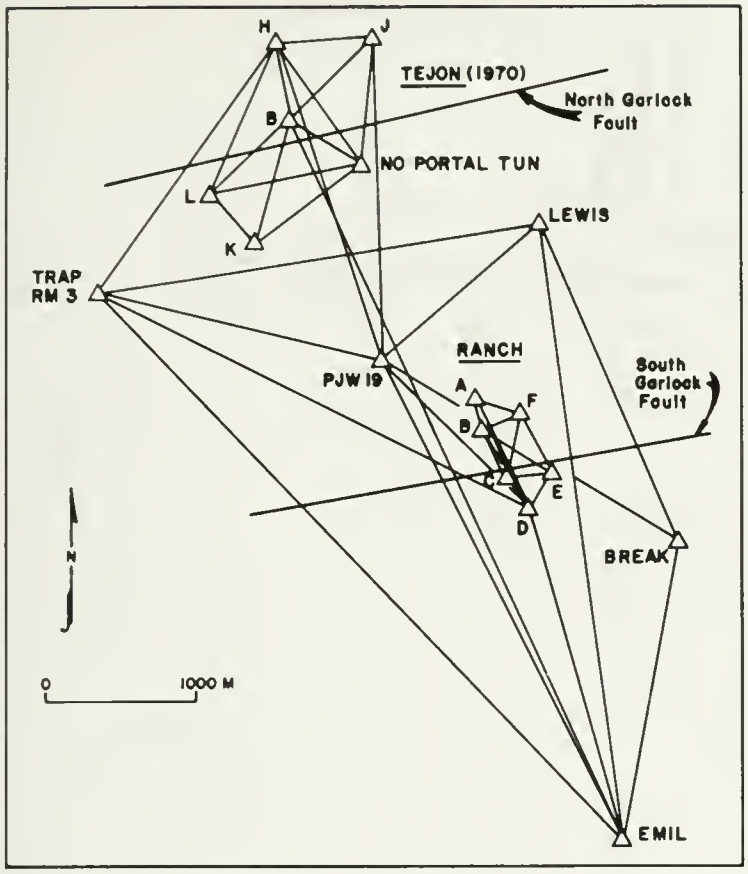

Figure B–13. Plan of the survey figure at the RANCH –TEJON site (1970).

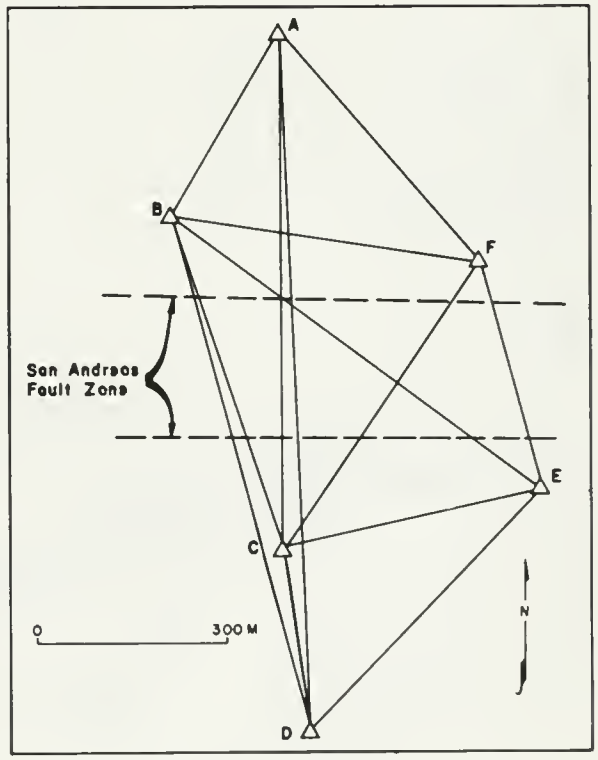

Figure B–14. Plan of the survey figure at the QUAIL site.

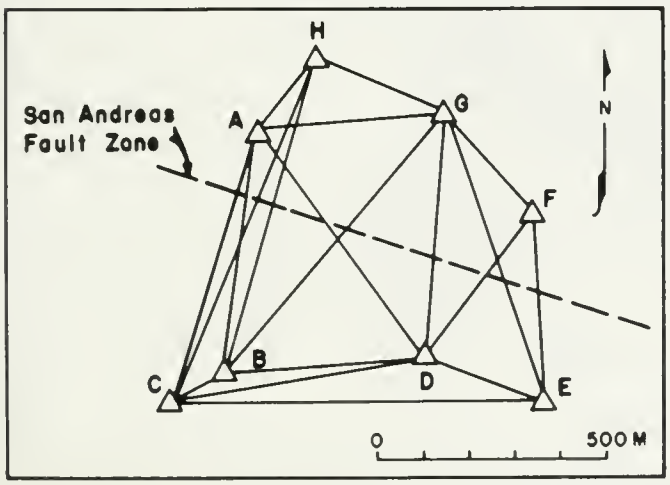

Figure B–15. Plan of the survey figure at the HUGHES site.

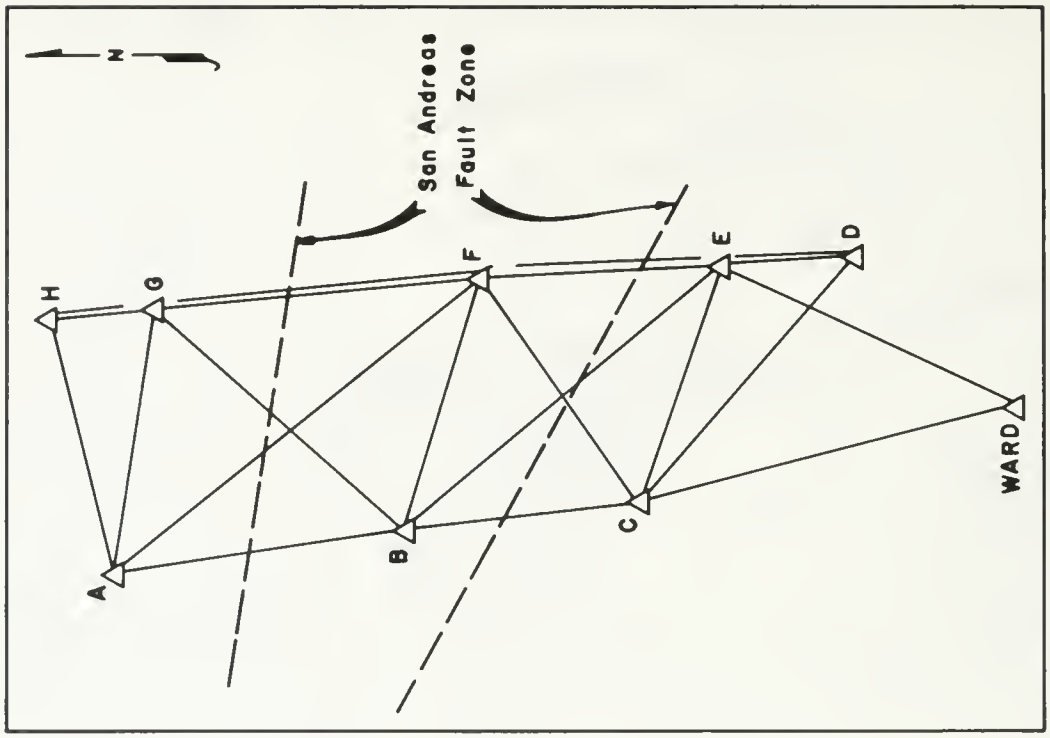

Figure B–16. Plan of the survey figure at the BARREL site.

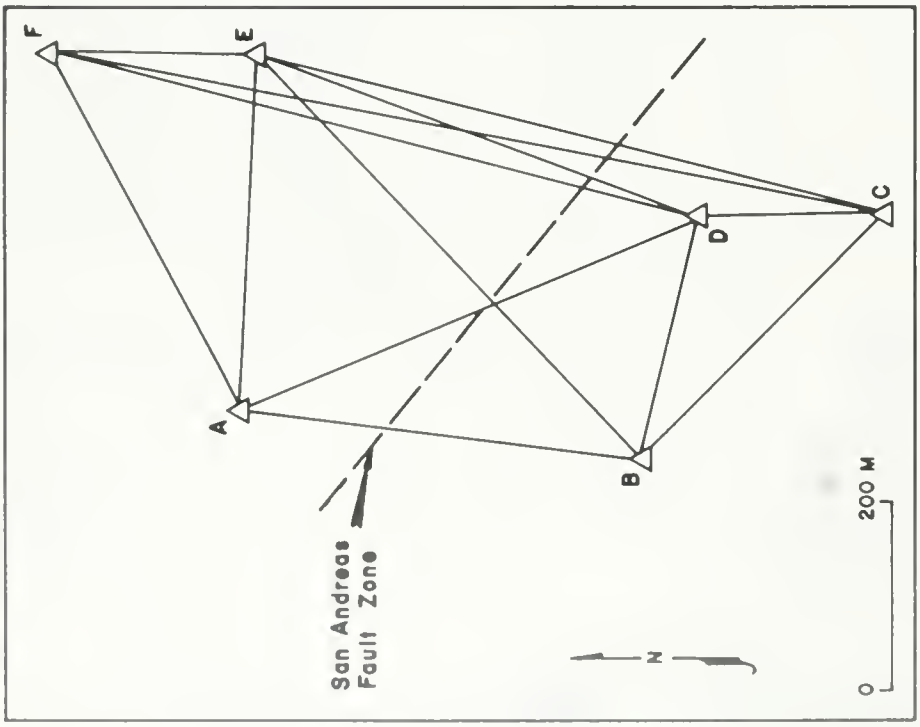

Figure B–17. Plan of the survey figure at the PEAR site.

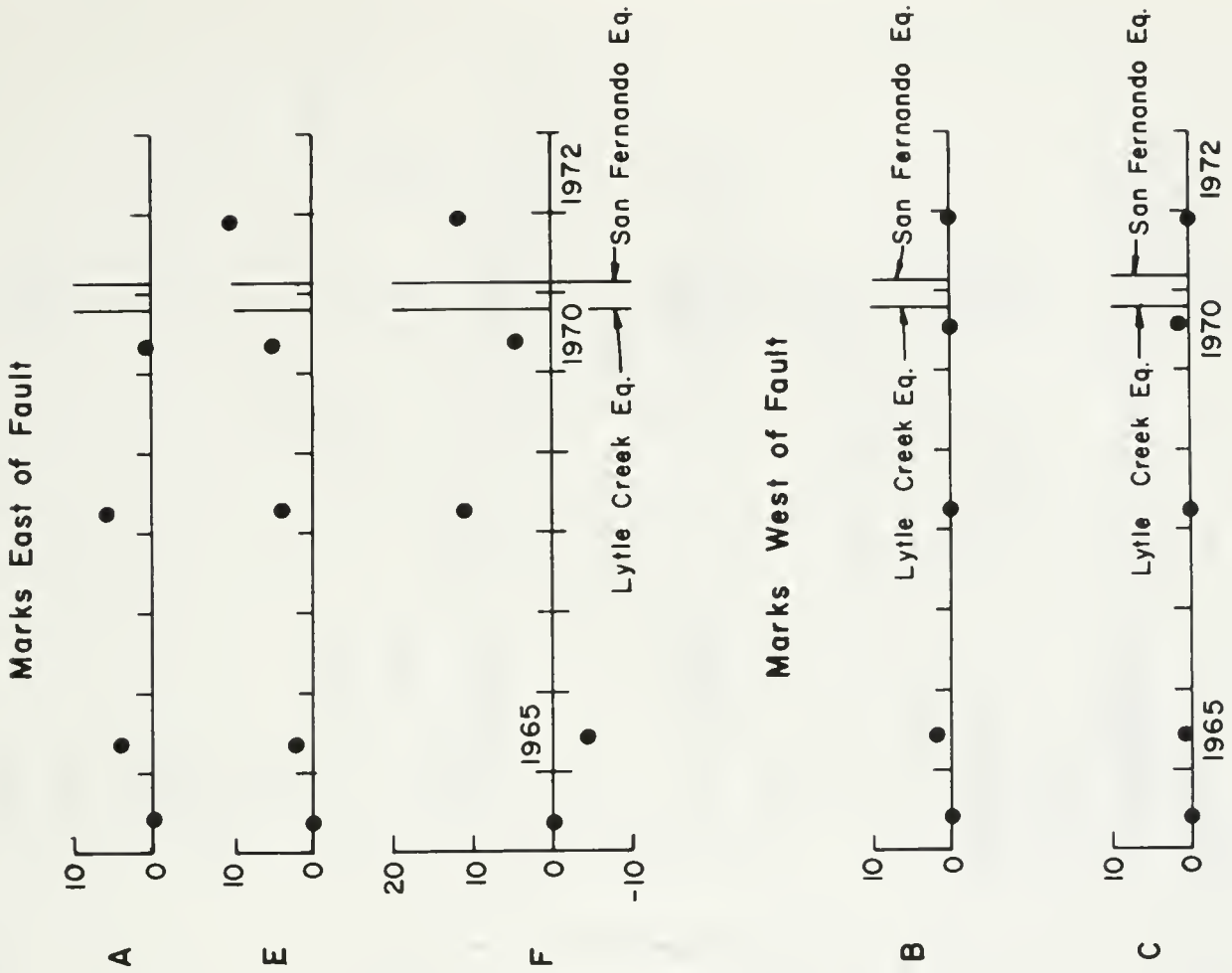

Figure B–18b. Elevation changes at the DEVIL site.

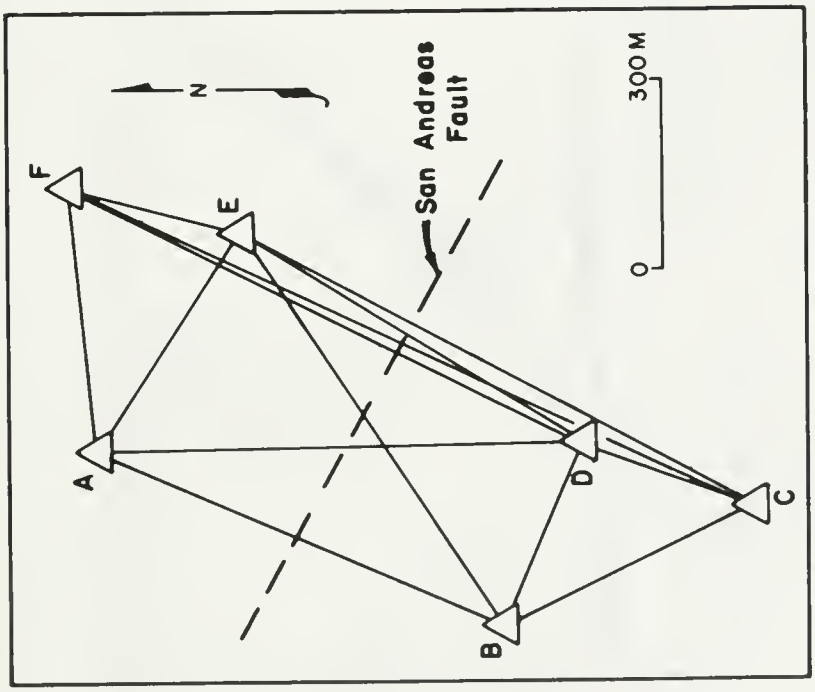

Figure B–18a. Plan of the survey figure at the DEVIL site.

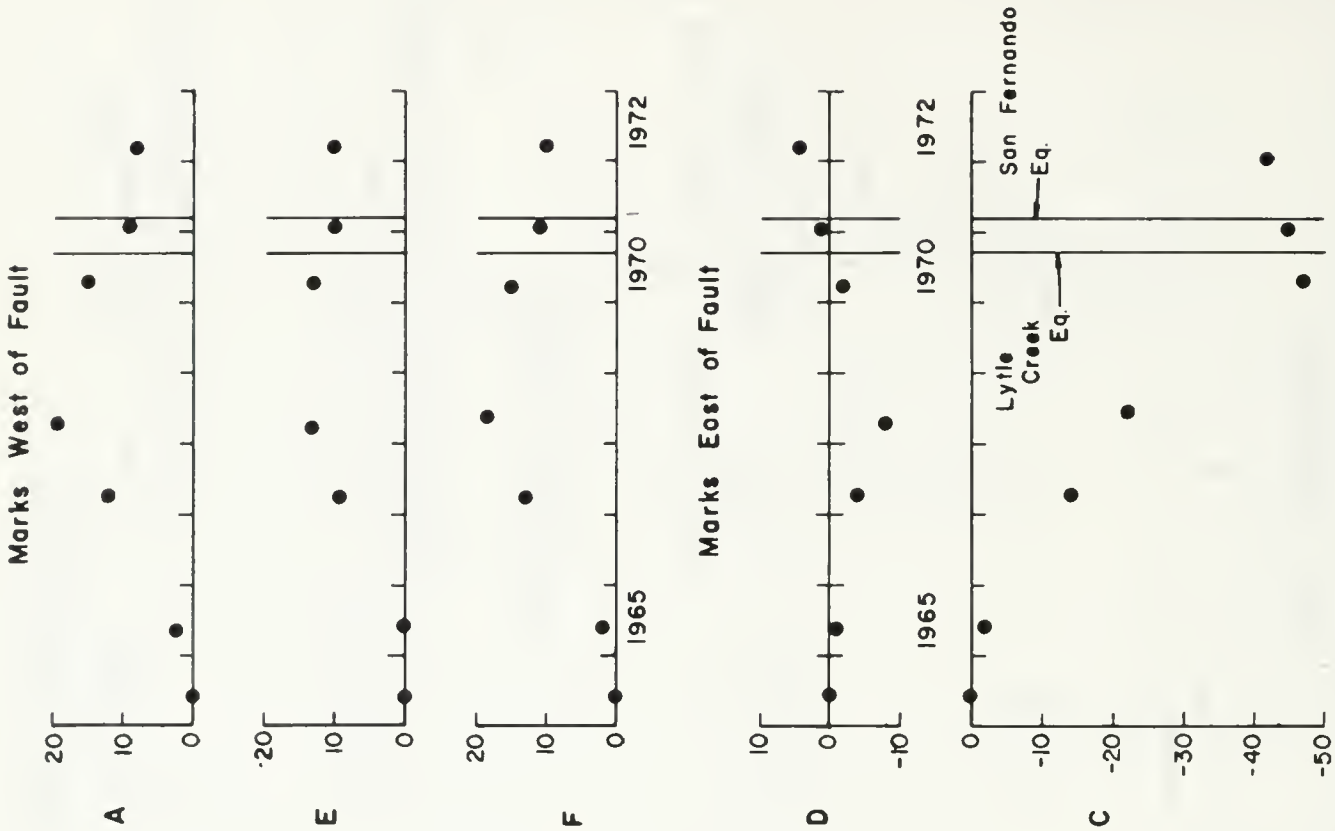

Figure B–19b. Elevation changes at the RIALTO site.

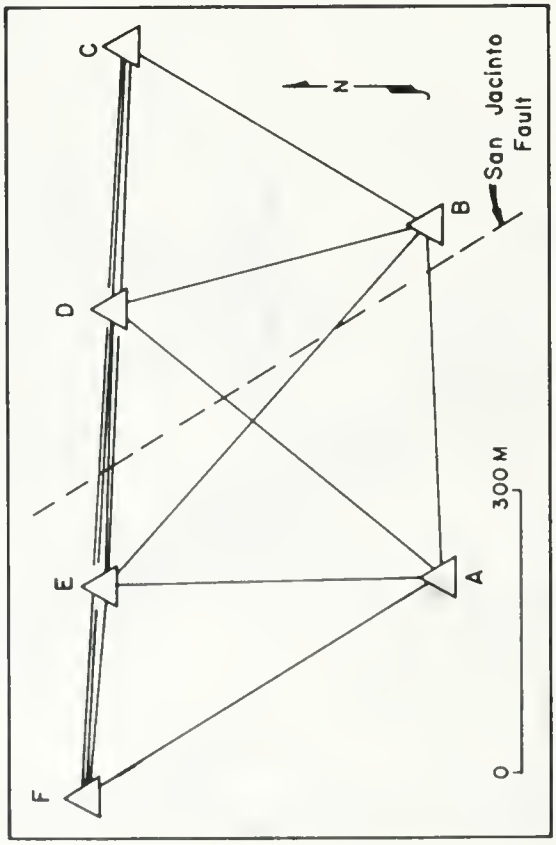

Figure B–19a. Plan of the survey figure at the RIALTO site.

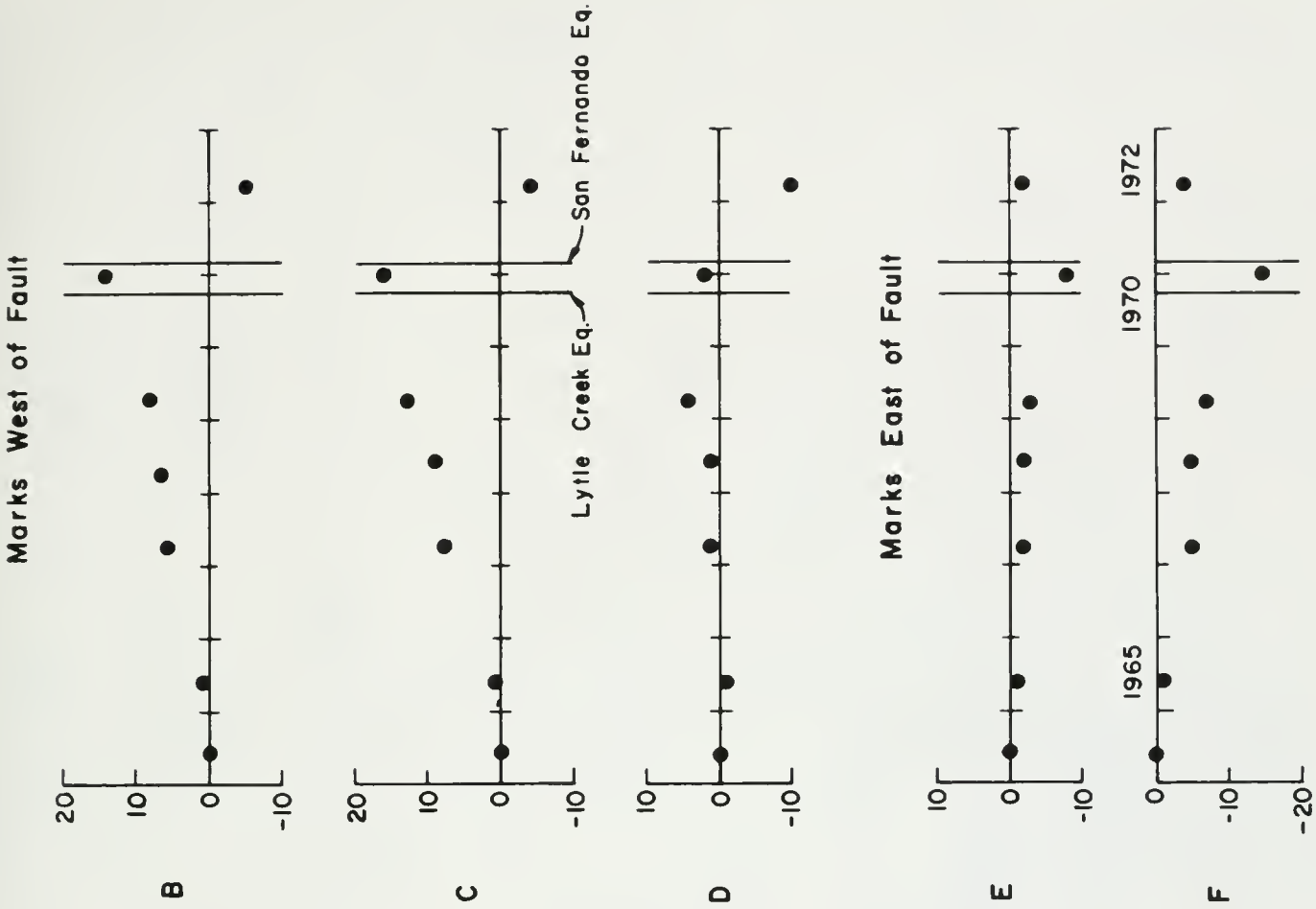

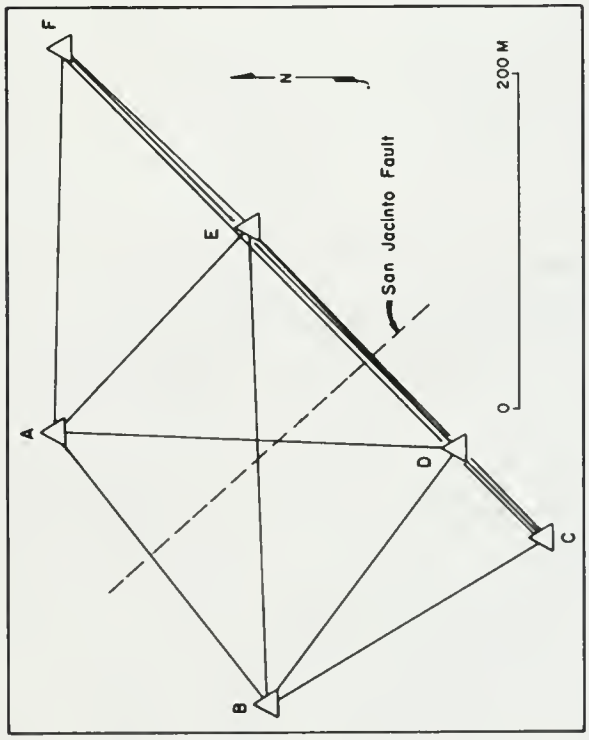

Figure B–20a. Elevation changes at the COLT site.

Figure B–20b. Plan of the survey figure at the COLT site.

FEB 28 '83
MAY 25 '83

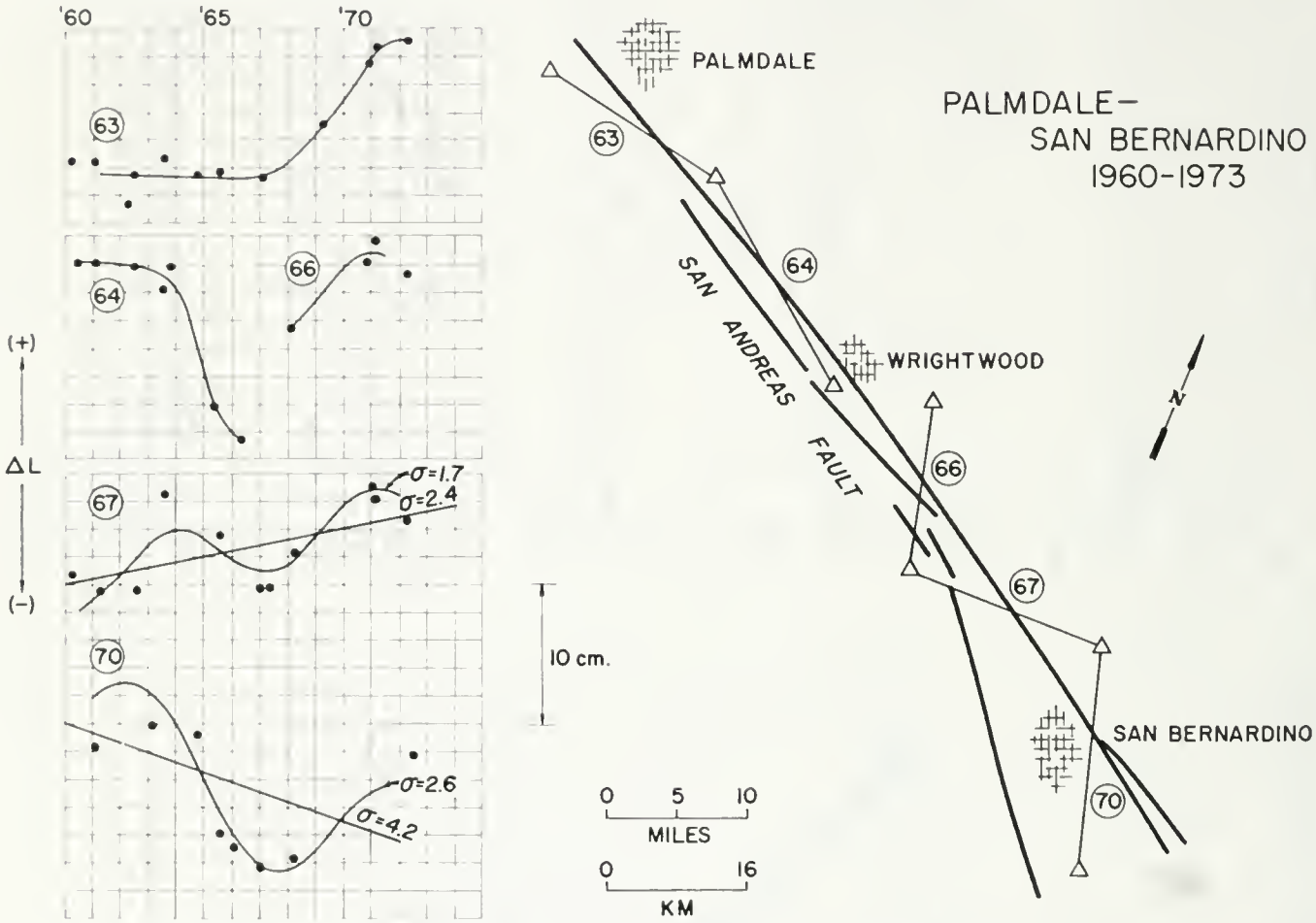

Figure B–21. Geodimeter line length changes, Palmdale to San Bernardino (from Greensfelder and Bennett, 1973).

79354-650 6-79 GSP 1225 LDA

DEC 14 '82

DEC 17

FEB 14

[redacted]

THIS BOOK IS DUE ON THE LAST DATE
STAMPED BELOW

BOOKS REQUESTED BY ANOTHER BORROWER
ARE SUBJECT TO IMMEDIATE RECALL

RECEIVED
MAR 16 1984
MAR

PHYS SCI LIBRARY

LIBRARY, UNIVERSITY OF CALIFORNIA, DAVIS

Book Slip–Series 458